

PARTITION DENSITY FUNCTIONAL THEORY

A Dissertation

Submitted to the Faculty

of

Purdue University

by

Jonathan Nafziger

In Partial Fulfillment of the

Requirements for the Degree

of

Doctor of Philosophy

May 2015

Purdue University

West Lafayette, Indiana

ACKNOWLEDGMENTS

I would like to thank all the members of the Suspenders who I have had a chance to work with over my years with the group. It has been a pleasure to learn and study DFT with a great group of people. Thanks to Daniel Jensen, Kaili Jiang, Martín Mosquera, Daniel Whitenack, Rougang Tang, Yu Zhang, Michael Mack, Carlos Borca, Kelsie Niffenegger, Ben Fasig, Alicia Hernández, and of course Adam Wasserman, our fearless leader. Also thanks to Qin Wu for hosting me at BNL and providing extremely helpful support with NWChem.

I also want to thank my housemates for providing excellent distraction from work over the years. I will always remember grad school for the broom ball, smoked meats and good friends. I would also like to thank Mathilde, my dog, for being a great sport about me being in grad school.

Finally, I would like to thank my parents and my siblings for tremendous support over my twenty three years of school. You have always been a rock.

TABLE OF CONTENTS

	Page
LIST OF TABLES	vi
LIST OF FIGURES	vii
ABSTRACT	xv
1 Introduction	1
2 Density-Functional Theory	5
2.1 Time-Independent Non-Relativistic Schrödinger Equation	6
2.2 Hohenberg-Kohn Theorems	8
2.3 N and v -representability	9
2.4 Density-Functional Approximations	10
2.5 Kohn-Sham Density-Functional Theory	11
2.6 Exchange-Correlation Functionals	14
3 Partition Density-Functional Theory	17
3.1 Fragment Equations	18
3.2 Partition Potential Optimization	21
3.3 Local- Q approximation	23
3.4 Occupation Number Optimization	24
3.5 Charge transfer between fragments	26
3.6 Singularities in the exact partition potential	29
4 Context in Fragment-Based DFT	33
4.1 Atoms-In-Molecules	33
4.2 Fragment-based density-functional methods	36

	Page
4.3 Fragment self-consistency within Subsystem-DFT and FDET	38
4.4 Non-uniqueness of solutions of the exact KSCED equations	39
4.5 Paths to Uniqueness	44
4.6 Connection to Subsystem-DFT	46
5 Algorithms	51
5.1 Inversion Algorithms	51
5.2 Algorithms using the Non-Additive Kinetic Energy	55
6 Non-Additive Kinetic Energy	57
6.1 Unambiguous Non-Additive Kinetic Energy Density	57
6.2 Implicit T_s^{nad} Functionals	59
6.3 Two-Orbital approximation	60
6.4 Rare-Gas Dimers	61
7 NWChem Implementation	65
7.1 Method	66
7.2 Results	69
7.2.1 Helium Dimer	70
7.2.2 Hydrogen Molecule	73
7.2.3 Lithium Hydride	74
7.3 Concluding Remarks	78
8 Near-Additivity and Non-Integer Occupations	81
8.1 Near-Additivity	82
8.2 Integers <i>vs.</i> Non-integers	86
8.3 Concluding Remarks	92
9 CADMium	95
9.1 Benchmark PDFPT calculations for Homo-nuclear Diatomic Molecules	95
9.2 Fractional Charges and Spins	100

	Page
10 Static-Correlation and Delocalization Errors	107
10.1 Ensembles in PDFT	108
10.2 Delocalization Error	111
10.3 Static Correlation Error	114
10.4 Peak and Step in XC potential	116
10.5 Concluding Remarks	117
REFERENCES	119
VITA	128

LIST OF TABLES

Table	Page
7.1 Comparison between molecular energies (a.u.) obtained from PDFT and from standard KS-DFT calculations using the same functional (B3LYP) and basis set (aug-cc-pvTz) for both.	70
7.2 Table of energies (in a.u.) for the two Lithium Hydride partitions. The molecular energy for LiH is -8.088129 and its HOMO is -0.1953916. . .	76
9.1 Energies and components of E_p , in atomic units. The LDA is used in all calculations (except in the first line corresponding to H_2^+ , where the exact functional for H_2^+ is used). Calculations are performed at equilibrium geometries, except for He_2	96
9.2 Table of PDFT energies in atomic units comparing ensemble (ENS) vs FOO treatment of fractional charges and spins. All calculations used the LDA.	101
10.1 Dissociation energies for H_2^+ and H_2 in units of milihartrees.	108
10.2 Comparison of total energies in hartree, for our PDFT code, and from benchmark KS-DFT calculations.	111

LIST OF FIGURES

Figure	Page
3.1 Numerically evaluated Q -functions, $Q_b(x', x) = \delta n_b(x')/\delta n_f(x)$, for one-dimensional non-interacting electrons (no ensembles are needed when calculating fragments for non-interacting electrons). The top row consists of calculations for the separation $R = 3$ and the bottom row is for separation $R = 10$. The left column shows the numerically exact Q -function, the right column is the local- Q approximation. Note that the local- Q approximation works well in both cases, but actually improves at the larger separation.	25
3.2 Charge transfer between fragments as a function of difference in chemical potential of the isolated fragments. The chemical potential difference is $\mu_b^0 - \mu_a^0$. When this difference is above one then charge transfers to fragment a , and when it is below negative one charge transfers in the opposite direction. Between about -1 and 1 no charge transfer takes place due to a cusp in G with respect to particle number.	27
3.3 Fragment densities with various occupation numbers. The left-hand column has plots of the density and the right hand column displays the log of the densities. The first row is for occupation values: $N_a = 3$ and $N_b = 1$ the second row is for occupation values $N_a = N_b = 2$. The last row uses occupation numbers of $N_a = 2.2469$ and $N_b = 1.7531$, the optimized PDF-T occupations. This illustrates that the optimized fragment occupations yield the most localized fragments. It also shows that when chemical potential equalization is reached, the fragments all have the same asymptotic behavior.	28
3.4 Plots of the partition potential along the bond axis for H_2^+, H_2 , He_2 , Li_2 , and Be_2 . The location of the nuclei can be identified from the small singularity features in the partition potential. This agrees with Eq. 3.35, as the equilibrium distances are larger for Li_2 and Be_2 , so the density from one fragment in those cases is very small at the location of the other nucleus. For the case of He_2 , the density of each fragment is so small at the location of the other nuclei that the corresponding singularity in the partition potential is not visible in this plot.	32

Figure	Page	
4.1	Exact embedding potentials for the helium dimer. The two helium atoms are placed at $x = \pm 3$ and labeled as left (nucleus at $x = -3$) and right (nucleus at $x = +3$). The top and bottom figures show different methods for converging the calculation. In the top frame the embedding potentials are iterated simultaneously while in the bottom frame freeze-and-thaw cycles are applied to reach self-consistency. For each of these sets of potentials the exact total energy and exact molecular density are recovered, although the fragment densities are different in each case.	41
4.2	Approximate embedding potentials for the Helium dimer using the Thomas-Fermi (TF) approximation of T_s^{nad} . The two monomers are placed at $x = \pm 3$ and labeled as left (nucleus at $x = -3$) and right (nucleus at $x = +3$). The left two plots show the solution to the KSCED equations which is unique for the TF approximation, but the potentials are not global meaning there is a different embedding potential for each fragment. The right two plots show results from PDFT using the local- Q approximation, where there is a global partition potential shared by each fragment. In each case the log of the fragment densities are plotted above the corresponding embedding potentials. Both cases are compared with the exact partition potential (solid black) which is unique and global.	42
4.3	Comparison of the components of an embedding potential in the region of the non-active fragment. The total is in solid black, the potential energy component is in dashed green, the kinetic energy component is in dot-dash blue and and the XC component is in dotted red. In the top figure the exact kinetic energy is used, while in the bottom the Thomas Fermi kinetic energy is used. In the top figure the kinetic energy has a positive singularity which cancels a large portion of the potential energies negative singularity so overall the embedding potential is fairly flat. In the bottom figure the Thomas Fermi kinetic energy does not cancel well with the negative singularity and as a result the embedding potential is not accurate in this region.	48

Figure	Page
4.4 Comparison of exact vs. Thomas-Fermi (TF) approximations for Subsystem-DFT and PDFT for the Helium dimer. The two monomers are placed at $x = \pm 3$ and we refer to these fragments as left (nucleus at $x = -3$) and right (nucleus at $x = +3$). The solid black line is both the exact partition potential and an exact embedding potential for the left monomer (they are slightly different but indistinguishable here, but may differ greatly as in Figure 4.1). The two dotted lines represent calculations using the Thomas-Fermi kinetic energy functional. The dash dotted line is the global TF partition potential and the dashed line is the TF embedding potential for the left monomer.	49
5.1 Flow diagram of simple PDFT SCF cycle used in inversion algorithms.	51
5.2 Comparison of convergence for simple 4-electron double-well 1-dimensional system using three different update procedures for the partition potential. The blue diamonds correspond to equation 5.2, the green triangles correspond to equation 5.3, red squares correspond to 5.4 and the cyan stars correspond to 5.7. The vertical axis shows the 1-norm of the error between the sum of fragment densities and the target density and the horizontal axis is the iteration number.	54
5.3 Flow diagram of PDFT SCF cycle with local-Q approximation and access to all functional derivatives of the partition energy.	56
6.1 Approximated (dashed red) and Inverted (solid black) orbital comparison for two different bond separations. The top shows a bond separation of 1 atomic unit and the bottom shows a separation of 2 atomic units. The approximation gets significantly better with increasing bond separation, but even at smaller separation it does well in the bonding region between the two wells.	61

Figure	Page
6.2 Binding energies for a variety of rare-gas dimers using the LDA. The solid black lines correspond to KS results. The other lines correspond to non-self consistent PDFT calculations performed on the isolated fragment densities fixed at various separations. The dotted and dashed lines correspond to using different non-additive kinetic energies. The dotted green line correspond to using the Thomas-Fermi kinetic energy functional. The cyan dot-dashed line corresponds to the two orbital approximation with $M = 1$. And the red dashed line corresponds to the two orbital approximation with optimally scaled M values. The optimal M values for each dimer are as follows: HeHe $M = 0.9249$, HeNe $M = 2.1187$, HeAr $M = 3.8641$, NeNe $M = 2.7930$, NeAr $M = 3.9959$, ArAr $M = 4.9287$	63
7.1 The Hartree-Fock energies for He_2 at different internuclear distances. .	71
7.2 The density differences in He_2 as compared to the original atoms along the line through both nuclei. The total difference (dashed line) is the sum of the deformation in each atom (solid line). The nuclei coordinates are $R = \pm 0.8 \text{ \AA}$	72
7.3 The partition potentials for He_2 at different internuclear distances. The nuclei are at $\pm R$	72
7.4 In each panel a different expansion is used for the partition potential of the Helium dimer (ng stands for n gaussians). The black curve is the difference between the sum of the densities and the molecular density from a standard DFT calculation (along the bond axis of the molecule). The red and blue curves are the differences between the PDFT fragments and the isolated fragments.	73
7.5 Top: The B3LYP energies for H_2 at different interatomic distances. The optimized bond length is $D = 0.743 \text{ \AA}$. Bottom: The partition potentials for H_2 at different internuclear distances.	75
7.6 The B3LYP partition potentials for LiH (constrained to fixed integer occupation numbers). The Li atom is at $x = 0$ and H at $x = 1.59 \text{ \AA}$	77
8.1 Comparison of the densities obtained for partitions I and II described in the text (Sec.8.1), for 3-site (left) and 6-site (right) linear chains, with 3 and 6 non-interacting electrons, respectively.	84

- 8.2 Change in the fragment occupations when one well of a two-electron tri-atomic system is separated from the other two. The variable R is the distance between the left well (A) and the central well (B). The distance between the center and right wells is 3.0a.u. The labels I and II indicate two different ways of partitioning. In I, each well has its own fragment, and in II the two rightmost wells share a fragment. The numbers 1→4 on the top horizontal axis correspond to the regions described in the text. Near-additivity can be observed by comparing the occupation of the first fragment from both partitioning schemes. 85
- 8.3 Two ways of fragmenting a 4-atom chain. *Left*: complete atomic fragmentation (partition I); *Center*: Binary fragmentation (partition II), where one fragment potential equals the sum of the two leftmost wells, and the other fragment potential equals the sum of the two wells on the right. The corresponding partition potentials are shown by thin solid lines; *Right*: Comparison of $n_C^I(x) + n_D^I(x)$ and $n_{CD}^{II}(x)$. They are identical within numerical accuracy. 86
- 8.4 *Top left*: Fragment energies and their sum versus constrained occupation number of fragment 1 for a homonuclear double-well potential with 4 non-interacting electrons. The correct PDFT occupation numbers are the ones which minimize the sum of the fragment energies. The cusp at $N_1 = 2$ forces the occupation numbers to be integers. *Bottom left*: Fragment chemical potentials versus constrained occupation number of fragment 1. The correct PDFT occupation numbers are the ones which equalize the fragment chemical potentials. The discontinuities in the chemical potentials for the homonuclear case are such that equalization can not be obtained, and instead the occupation numbers are forced to be integers. *Top right*: Same as top-left, but for a heteronuclear double-well, $v(x) = -Z_A \cosh^{-2}(x-1.5) - Z_B \cosh^{-2}(x+1.5)$, with $Z_A = 3$ and $Z_B = 1$. *Left*: The infimum is no longer a cusp, but a minimum near $N_B = 1.0$. *Bottom right*: The two chemical potentials cross near $N_B = 1.0$, where E_f is minimized. 89
- 8.5 The top right panel shows fragment occupations versus Z_A , for $v(x) = -Z_A \cosh^{-2}(x-1.5) - \cosh^{-2}(x+1.5)$. For $Z_A < 2$, the cusp in E_f forces the occupation numbers into integer values as seen in the upper left panel of figure 8.4. Above this value the occupation numbers take on non-integer values as seen in the top right panel of figure 8.4. The other panels show the fragment densities at the various Z_A values indicated in the top right panel. 90

Figure	Page
8.6 Occupation number of the shallower well versus separation (R) for a heteronuclear double well $v(x) = -Z_A \cosh^{-2}(x - R/2) - Z_B \cosh^{-2}(x + R/2)$ populated with 2 electrons (left panel), and 4 electrons (right panel). Various values of $\Delta Z = Z_A - Z_B$ are shown. <i>Left:</i> As the separation grows to infinity, the occupation numbers approach integers and for certain ΔZ at close separations the occupations are strictly integers. <i>Right:</i> The vertical axis on the right panel corresponds to the occupation of the deeper well (A) minus the occupation of the shallower well (B). The shallower well is fixed at a strength of 1.0 and the deeper well has a strength of Z_A which varies from 2.1 to 2.5. We can again observe that as the separation goes to infinity the occupation numbers approach integers and for certain ΔZ at close separations the occupations are integers. We also note that compared to the 2-electron case, the occupation numbers are much stiffer and require much larger heteronuclear differences to cause transfer.	92
9.1 PDFT(LDA) calculations on H_2^+ and H_2 . The left column displays the difference between the left fragment density and the isolated atomic density while the right column displays the corresponding partition potential. The density for the fragment in the molecule sits in the same potential but with the addition of the partition potential. Thus, the partition potential is responsible for deformations of the isolated density into the fragment density in the molecule. In both plots, the partition potential is depressed in the bonding region (see also Figure 3.4), increasing the density in that region.	97
9.2 PDFT(LDA) calculations on He_2 , Li_2 , and Be_2 . The left column displays the difference between the left fragment density and the isolated atomic density while the right column displays the corresponding partition potential. In all three plots, the partition potential is depressed in the bonding region (see also Figure 3.4), increasing the density in that region. In the case of Be_2 , the partition potential squeezes each fragment and elongates it along the bond axis. In the case of Li_2 , the partition potential displays distinct plateau structures surrounding both nuclei. The edges of this plateau correspond to the transition between regions where the lowest occupied orbital contributes the most density and regions where the HOMO contributes the most density.	98
9.3 Components of the partition potential for H_2 , He_2 , Li_2 and Be_2 using the LDA. The total partition potential is solid black, the Hartree plus external potential component is in brown, the kinetic energy component is in blue and the XC component is in green.	99

Figure	Page
9.4 Left: Components of the partition potential for H_2^+ using the LDA. Right: The hartree and XC components of the partition potential, along with their sum. In the exact case, the XC component precisely cancels with the hartree component, which is shown in solid black. However, the LDA XC component does not exactly cancel with the hartree component.	100
9.5 Left: One of the Li fragments within a Li_2 molecule as compared to an isolated Li atom and the density for the Li_2 molecule. Right: Each Li fragment has 3 electrons and come from an open shell calculation, however the Li_2 molecule is closed shell. This figure displays the ensemble spin up component with one electron and the ensemble spin up component with two electrons which combine to give a fragment density corresponding to a fractional spin up density.	100
9.6 Energies of the hydrogen atom with fractional charge (left) and fractional spin(right). In both cases the exact is linear and is shown in solid black. PBE is shown in the dashed line and the LDA is shown in dot dashed line.	103
9.7 Kinetic energies of the hydrogen atom with fractional charge (left) and fractional spin(right). In both cases the exact is linear and is shown in black. Thomas Fermi is shown in the dot dashed line and the LC94 (PW91k) is shown in dashed line. These energies were evaluated for the exact densities.	103
10.1 Plots on the left: Energies of a hydrogen atom with fractional number of electron. Exact energies are plotted in solid black along with DFA and ensemble-DFA results. Note that ensemble-PBE and the exact curve are indistinguishable. The origin of the self interaction error of stretched H_2^+ is indicated in both frames. Plots on the right: The exact dissociation energy of H_2^+ is plotted in solid black along with standard KS-DFT results and PDFT results using Eq.(10.4).	112
10.2 Top: H_2 Dissociation energies for: standard functionals (red), eq.10.5 with standard functionals for E_f (green) and exact [124] (solid black) Middle: H_2 Dissociation energies for OWA functionals and exact [124] (solid black) Bottom: The H_2 overlap, S , for a PDFT-LDA calculation in comparison to an OWA-LDA calculation. We see that the OWA slightly suppresses the overlap.	115

10.3	Effective XC-potentials for two PDFT H_2 calculations with $R = 10$ bohr. The top two plots show an entire 2D plane along the bonding axis while the bottom plot compares the effective XC-potential in a 1D slice along the bond axis. Nuclei are at $+5$ and -5 on the bond axis.	117
------	--	-----

ABSTRACT

Nafziger, Jonathan PhD, Purdue University, May 2015. Partition Density Functional Theory. Major Professor: Adam Wasserman.

Partition density functional theory (PDFT) is a method for dividing a molecular electronic structure calculation into fragment calculations. The molecular density and energy corresponding to Kohn Sham density-functional theory (KS-DFT) may be exactly recovered from these fragments. Each fragment acts as an isolated system except for the influence of a global one-body 'partition' potential which deforms the fragment densities. In this work, the developments of PDFT are put into the context of other fragment-based density functional methods. We developed three numerical implementations of PDFT: One within the NWChem computational chemistry package using basis sets, and the other two developed from scratch using real-space grids. It is shown that all three of these programs can exactly reproduce a KS-DFT calculation via fragment calculations. The first of our in-house codes handles non-interacting electrons in arbitrary one-dimensional potentials with any number of fragments. This code is used to explore how the exact partition potential changes for different partitionings of the same system and also to study features which determine which systems yield non-integer PDFT occupations and which systems are locked into integer PDFT occupations. The second in-house code, **CADMium**, performs real-space calculations of diatomic molecules. Features of the exact partition potential are studied for a variety of cases and an analytical formula determining singularities in the partition potential is derived. We introduce an approximation for the non-additive kinetic energy and show how this quantity can be computed exactly. Finally a PDFT functional is developed to address the issues of static correlation and delocalization errors in

approximations within DFT. The functional is applied to the dissociation of H_2^+ and H_2 .

1. Introduction

Partition-density functional theory (PDFT) is a method for dividing a molecule into fragments. There are three primary benefits for such a division. First, calculations may be performed in smaller, and more manageable chunks leading to improved computational efficiency. Second, there is the possibility of improving the accuracy of density functional approximations. Lastly there is the possibility of improved chemical understanding of the behavior of atoms within molecules. This dissertation concerns the development and exploration of PDFT. Here we provide an outline of the Chapters of the thesis.

- **Density-Functional Theory** This chapter outlines the formalism of Density Functional Theory and the Kohn Sham equations. This theory provides the important backdrop for PDFT.
- **Partition Density-Functional Theory** This chapter outlines the PDFT formalism and derives the equations which determine the fragment densities in analogy with the derivation of the Kohn-Sham equations in KS-DFT. This section contains work from the review article entitled ‘Density-Based Partitioning Methods for Ground-State Molecular Calculations’, written by the author and Adam Wasserman published in the Journal of Physical Chemistry A.
- **Context in Fragment-Based DFT** This chapter establishes some of the context for PDFT in relation to other fragment-based density functional theory. This section contains work from the review article entitled ‘Density-Based Partitioning Methods for Ground-State Molecular Calculations’, written by the author and Adam Wasserman published in the Journal of Physical Chemistry A. [1]

- **Algorithms** This chapter goes over several algorithms used in various PDFT calculations used throughout the rest of the dissertation.
- **Non-Additive Kinetic Energy** This chapter looks at the Non-Additive Kinetic Energy, which is a critical quantity in PDFT calculations.
- **NWChem Implementation** This section describes work done in collaboration with Qin Wu to develop a proof of concept program in the computational chemistry package NWChem. This section contains work from an article entitled ‘Molecular binding energies from partition density functional theory’ written by the author, Qin Wu and Adam Wasserman, published in the Journal of Chemical Physics [2].
- **Near-Additivity and Non-Integer Occupations** This chapter describes work done in collaboration with Rougang Tang to explore the behavior of various partitionings in simple one-dimensional toy models. In particular we explore the concept of chemical equilibration between fragments and fractionally occupied fragments. This section contains work from an article entitled ‘Fragment occupations in partition density functional theory’, written by Rougang Tang, the author, and Adam Wasserman, published in Physical Chemistry Chemical Physics. [3]
- **Chemical Atoms in Diatomic Molecules** This chapter describes results from the custom built PDFT software we built called CADMium (Chemical Atoms in Diatomic Molecules). This software is capable of performing, all-electron KS-DFT, PDFT and sDFT calculations on diatomic molecules up to the size of the Krypton dimer (72 electrons). This section contains work from the review article entitled ‘Density-Based Partitioning Methods for Ground-State Molecular Calculations’, written by the author and Adam Wasserman published in the Journal of Physical Chemistry A. [1]

- **Towards fixing Static Correlation and Delocalization Errors** This chapter presents a possible solution to the KS-DFT issue of static correlation and delocalization errors through the framework of PDFT. This work may also be found on the arxiv. [4]

2. Density-Functional Theory

Matter is composed of atoms consisting of negatively charged electrons orbiting heavier positively charged nuclei. The interactions of these atoms determine a large part of the behavior of the world around us. While the idea that matter is composed of atoms dates back to antiquity, it has only been a little over a century since the scientific community has completely accepted this fact. And yet already in 1929 Dirac stated “The fundamental laws necessary for the mathematical treatment of a large part of physics and the whole of chemistry are thus completely known, and the difficulty lies only in the fact that application of these laws leads to equations that are too complex to be solved. [5]” This bold statement was possible due to the enormous progress made by Dirac and other pioneers in the field of quantum mechanics during the first decades of the twentieth century. In the 85 years since his statement, enormous progress has been made in solving and approximating the solution to these fiendishly complex equations.

The goal of DFT [6] is to provide an alternative framework in which to look at these difficult equations. DFT is formally exact and essentially provides a reformulation of the Schrödinger equation. This reformulation is interesting and merits study on its own right, but its real value comes from its ability to construct useful approximations which are computationally inexpensive. There are many excellent review articles and books which provide introduction to DFT [7–11]. Here we will attempt to give a brief derivation of important points which emphasize the similarities with the derivation of PDMFT. We will start this introduction to DFT with a look at the Schrödinger equation.

2.1 Time-Independent Non-Relativistic Schrödinger Equation

The primary equation of interest to chemists is the non-relativistic Schrödinger equation. The time-independent version of this equation is sufficient to capture the behavior of many molecular systems studied by chemists, biologists and materials scientists. In most cases the Born-Oppenheimer approximation may be used to obtain any properties of interest, meaning we can fix the location of all nuclei of the system and consider only the electronic degrees of freedom.

As is typical in chemistry, the Hamiltonian for a system of N electrons is written as the sum of three operators, the kinetic energy operator, the electron-electron repulsion operator and the one-body potential operator.

$$\hat{H} = \hat{T} + \hat{V}_{ee} + \hat{V} \quad (2.1)$$

Throughout this report we make use of atomic units, meaning that the mass and charge of the electron, and Planck's constant are equal to one ($m_e = e^2 = \hbar = 1$). This means that distances will be measured in bohr ($1 a_0 = 0.529\text{\AA}$) and energy in hartree ($1 \text{ Ha} = 27.2 \text{ eV}$). The kinetic energy operator is then given by:

$$\hat{T} = -\frac{1}{2} \sum_{i=1}^N \nabla_i^2 \quad (2.2)$$

where the index, i , ranges over all the electrons from 1 to N . The electron-electron repulsion is simply the Coulomb interaction between electrons:

$$\hat{V}_{ee} = \sum_{i < j} \frac{1}{|\mathbf{r}_i - \mathbf{r}_j|} \quad (2.3)$$

The indices, i and j , run over the N electrons. The one-body potential operator takes care of the interaction between electrons and the nuclei (which are fixed within the Born-Oppenheimer approximation):

$$\hat{V} = \sum_i^N v_{\text{nuc}}(\mathbf{r}_i) \quad (2.4)$$

For Coulomb systems this potential is given by

$$v_{\text{nuc}}(\mathbf{r}) = \sum_j \frac{1}{|\mathbf{r} - \mathbf{R}_j|} \quad (2.5)$$

where the $\{\mathbf{R}_j\}$ are the locations of nuclei.

The goal of electronic structure calculations is to find the ground state energy of N electrons in the presence of some nuclei. The energy as well as all other observables can be found from the wavefunction. That is the anti-symmetric wavefunction which satisfies the time-independent schrödinger equation.

$$\hat{H}\Psi(\mathbf{r}_1, \mathbf{r}_2, \dots, \mathbf{r}_N) = E\Psi(\mathbf{r}_1, \mathbf{r}_2, \dots, \mathbf{r}_N) \quad (2.6)$$

The wavefunction, Ψ , is a $3N$ -dimensional function (ignoring spin coordinates), where N is number of electrons in the system. This makes a direct computer representation of Ψ completely infeasible for all but the simplest of systems. Without the electron-electron interaction the Schrödinger equation can be solved by writing the wavefunction as a single Slater determinant of one-electron functions, yielding a set of much simpler one-body equations. This avoids the problems with multidimensionality. However, the electron-electron interaction term prevents this separation.

The approach of DFT is to replace the many-body wavefunction with the much simpler one-body electronic density:

$$n(\mathbf{r}) = N \int d^3r_2 \dots \int d^3r_N \Psi^*(\mathbf{r}, \mathbf{r}_2, \dots, \mathbf{r}_N) \Psi(\mathbf{r}, \mathbf{r}_2, \dots, \mathbf{r}_N) \quad (2.7)$$

Here the integration runs over all the electrons except for one. The resulting quantity is defined so that $n(\mathbf{r})d^3r$ yields the expectation value of the number particles found in the volume d^3r . Clearly this quantity which depends on just 3 spatial coordinates will be much easier to handle numerically than a quantity that has $3N$ spatial coordinates. However it is not immediately clear that this change preserves all the necessary information needed to model the system, or if this change will fundamentally oversimplify things. This question was answered in 1964 by Hohenberg and Kohn who proved two theorems which are considered foundational to DFT [6].

2.2 Hohenberg-Kohn Theorems

The first theorem establishes a one-to-one mapping between the ground state many-body wavefunction and the ground state one-body density. Upon reflection it is quite remarkable that there exists a one-to-one mapping between these two objects. The complicated many-body wavefunction is a function of $3N$ coordinates while the density is just a function of the 3 spatial coordinates. However from an information theory perspective a one-to-one mapping implies that these two objects contain the same amount of information.

As a result of this theorem the ground state wavefunction and therefore all observables of the ground state can be written as a functional of the density. Perhaps the most important observable is the energy:

$$\begin{aligned} E[n] &= T[n] + V_{ee}[n] + \int v_{\text{nuc}}(\mathbf{r})n(\mathbf{r})d^3r \\ &= F[n] + \int v_{\text{nuc}}(\mathbf{r})n(\mathbf{r})d^3r \end{aligned} \tag{2.8}$$

Here the energy is broken up into a kinetic energy functional, $T[n]$, an electron-electron energy functional, $V_{ee}[n]$, and an external potential energy, $\int v_{\text{nuc}}(\mathbf{r})n(\mathbf{r})d^3r$, coming from interaction with the nuclei. Neither of the first two of these functionals depend directly on the system, and therefore are often grouped together into what

is called the universal functional, $F[n]$. In contrast, the remaining term, depends completely on the system, and is determined by the position of the nuclei. Once the system is known, this part of the energy functional is known exactly, however, the exact form of $F[n]$ is not known and must be approximated.

The second Hohenberg and Kohn theorem establishes a variational principle:

$$E[\tilde{n}] > E[n_0] \quad (2.9)$$

The ground state density is the one which minimizes the energy functional. Any trial density, \tilde{n} , not equal to the ground state density, n_0 , will have a higher energy. This gives us a recipe for DFT calculations. We simply need to search over all densities and find the one which minimizes the energy functional subject to the constraint that the density must integrate to N electrons. Equivalently we can solve the corresponding euler equation:

$$\frac{\delta F[n]}{\delta n(\mathbf{r})} + v_{\text{nuc}}(\mathbf{r}) - \mu = 0 \quad (2.10)$$

Here μ is the lagrange multiplier which enforces the constraint. It is also known as the chemical potential.

2.3 N and v -representability

The Hohenberg-Kohn theorems establish this one-to-one correspondance between ground-state densities and ground-state wavefunctions, however there are other related questions to consider. For example, can an arbitrarily function $n(\mathbf{r})$ integrating to N electrons be represented by a N -electron antisymmetric wavefunction as in equation 2.7? In other words, ground-state densities have a one-to-one correspondence with ground-state wavefunctions, but what about other densities. Is it possible that our search over all densities will lead us to a minimizing density which cannot be represented by a wavefunction? If so this density will be non-physical, and the

result useless. This is known as the N -representability problem and is fortunately solved [7, 12]. Any arbitrary density is N -representable provided that $n(\mathbf{r}) \geq 0$ and $\int n(\mathbf{r}) d\mathbf{r} = N$.

Another important representability question known as v -representability tries to establish whether for a given N -representable density there exists a potential $v(\mathbf{r})$ for which that density is the ground-state [7]. The Hohenberg-Kohn theorem proves the uniqueness of such a potential, but doesn't arbitrarily prove its existence. Work on this question has been less conclusive. It has been shown that under some restrictions v -representability can be established (ensembles, discretized systems), but in the general case it has also been shown that there exist continuous densities that are not *pure-state* v -representable [13, 14]. However, v -representability of the interacting system is not required for the Hohenberg-Kohn Theorems thanks to the constrained search formalism of Levy and Lieb [7, 15, 16].

2.4 Density-Functional Approximations

The biggest problem with attempting to solve equation 2.10 directly is that the universal functional, $F[n]$ is not a *simple* functional of the density. Despite the first Hohenberg-Kohn Theorem's statement of the existence of the energy as a functional of the density it gives no indication of how to construct the energy as an explicit functional of the density. We do not know how to write either the kinetic energy nor the electron-electron repulsion energy as an explicit functional of the density. Particularly problematic is that no sufficiently accurate approximation has been found for the kinetic energy density functional (KEDF).

The very first density functional predates the Hohenberg-Kohn theorems and was a KEDF developed by Thomas and Fermi [17, 18].

$$T^{\text{TF}}[n] = A_s \int n^{\frac{5}{3}}(\mathbf{r}) d^3r, \quad A_s = 3(4\pi^2)^{\frac{2}{3}}/10 \quad (2.11)$$

This local functional is defined to give the exact result for the kinetic energy of the homogeneous electron gas. When applied to systems with non-uniform density the Thomas-Fermi functional gives surprisingly good results, however the results are not of sufficient accuracy for practical electronic structure calculations.

2.5 Kohn-Sham Density-Functional Theory

A method to bypass the poor performance of KEDFs was proposed by Kohn and Sham in 1965 [19]. They proposed that the ground state of an auxiliary system of non-interacting electrons should be considered. The kinetic energy of this system of non-interacting electrons will in most cases be a good approximation for the fully-interacting kinetic energy. We simply constrain the density of this auxiliary system to be equal to density we are interested in. The kinetic energy of this non-interacting system forms an implicit density functional.

$$T_s[n] = \min_{\Psi \rightarrow n} \langle \Psi | \hat{T} | \Psi \rangle \quad (2.12)$$

The subscript s denotes that this is the non-interacting kinetic energy. This recipe for the KEDF can be described as searching over all non-interacting wavefunctions which yield a particular density $n(\mathbf{r})$ and then choosing the one which yields the lowest kinetic energy. This constrained minimization can be transformed into a corresponding unconstrained minimization,

$$W[n] = \min_{\Psi} \langle \Psi | \hat{T} | \Psi \rangle + \int v_s(\mathbf{r}) (\langle \Psi | \hat{n} | \Psi \rangle - n(\mathbf{r})) \quad (2.13)$$

where the lagrange multiplier, $v_s(\mathbf{r})$, must be chosen such that that the density of the non-interacting wavefunction is equal to the target density $n(\mathbf{r})$. Because in this case there is no electron-electron interaction, the ground-state wavefunction of this system can be exactly represented as a single Slater determinant. Optimization of

the lagrangian with respect to the orbitals of the determinant yield a set of orbital equations known as the Kohn-Sham equations.

$$\left(-\frac{1}{2}\nabla^2 + v_s(\mathbf{r})\right)\phi_i = \epsilon_i\phi_i \quad (2.14)$$

The lagrange multiplier $v_s(\mathbf{r})$ can be interpreted as an effective potential for this auxiliary system of non-interacting electrons, which must ensure that its density corresponds to some arbitrary density $n(\mathbf{r})$. The density of the non-interacting system can easily be constructed from the orbitals.

$$n(\mathbf{r}) = \sum_i f_i |\phi_i(\mathbf{r})|^2 \quad (2.15)$$

Here, the occupation numbers, f_i , are either zero or one depending on whether the corresponding eigenvalue ϵ_i is greater ($f_i = 0$) or less than ($f_i = 1$) the chemical potential, μ . Solution of Eqs. 2.14 and 2.15 is equivalent to solution of the euler equation:

$$\frac{\delta T_s[n]}{\delta n(\mathbf{r})} + v_s(\mathbf{r}) - \mu = 0 \quad (2.16)$$

Now we must find a way to choose the lagrange multiplier, $v_s(\mathbf{r})$, such that density of this auxiliary system of electrons reproduces the density of the interacting system. To do this we begin by rewriting the total energy functional of the interacting system.

$$E[n] = T_s[n] + V_H[n] + E_{xc}[n] + \int n(\mathbf{r})v(\mathbf{r})d^3r \quad (2.17)$$

The first term is the non-interacting kinetic energy, defined in Eq. 2.12. The second is the hartree energy:

$$V_H[n] = \frac{1}{2} \int \frac{n(\mathbf{r}_1)n(\mathbf{r}_2)}{|\mathbf{r}_1 - \mathbf{r}_2|} d^3r_1 d^3r_2 \quad (2.18)$$

which is simply the classical self-repulsion of a distribution of charge $n(\mathbf{r})$. The third term, $E_{\text{xc}}[n]$ is an important functional called the exchange correlation energy, which is defined to make Eq. 2.17 exact.

$$E_{\text{xc}}[n] = T[n] - T_s[n] + V_{ee}[n] - V_{\text{H}}[n] \quad (2.19)$$

This term accounts for both the difference between the true interacting kinetic energy and the non-interacting kinetic energy as well as the difference between the true electron-electron repulsion energy and the hartree energy. While all the other terms in Eq. 2.17 can be calculated exactly the exchange correlation energy, must be approximated in practice. This is the most convenient term in Eq. 2.17 to approximate, because $T_s[n] \approx T[n]$ and $V_{\text{H}}[n] \approx V_{ee}[n]$, and therefore $E_{\text{xc}}[n]$ is relatively small.

From Eq. 2.14 and Eq. 2.15 it is clear that the non-interacting density is a functional of the lagrange multiplier $v_s(\mathbf{r})$. Therefore we can write Eq. 2.17 using potential functionals of $v_s(\mathbf{r})$.

$$E[v_s] = T_s[v_s] + V_{\text{H}}[v_s] + E_{\text{xc}}[v_s] + \int n[v_s](\mathbf{r})v_{\text{nuc}}(\mathbf{r})d^3r \quad (2.20)$$

Then if we simply choose the lagrange multiplier, $v_s(\mathbf{r})$, such that the total energy is minimized then from the Hohenberg-Kohn theorems we must have achieved our constraint that the non-interacting density is equal to the fully-interacting ground state density. To accomplish this task we solve the euler equation:

$$\frac{\delta E[v_s]}{\delta v_s(\mathbf{r})} = 0 \quad (2.21)$$

The solution to this equation reveals that we must choose $v_s(\mathbf{r})$ such that:

$$v_s(\mathbf{r}) = v_{\text{nuc}}(\mathbf{r}) + \frac{\delta V_{\text{H}}[n]}{\delta n(\mathbf{r})} + \frac{\delta E_{\text{xc}}[n]}{\delta n(\mathbf{r})} \quad (2.22)$$

It is important to note that this procedure is formally exact. That is to say, if we knew the exact form of $E_{\text{xc}}[n]$ then solution of Eq. 2.14 along with Eq. 2.22 would yield exactly the correct ground state density (ignoring any questions of representability). Of course given the definition of $E_{\text{xc}}[n]$ as the term which makes Eq. 2.17 exact this perhaps not terribly surprising. What is surprising is that even fairly crude local approximations of $E_{\text{xc}}[n]$ can give quite reasonable results.

2.6 Exchange-Correlation Functionals

The simplest approximation for $E_{\text{xc}}[n]$ is called the local density approximation (LDA) [19].

$$E_{\text{XC}}^{\text{LDA}}[n] = \int n(\mathbf{r}) \epsilon_{\text{XC}}^{\text{HEG}}(n(\mathbf{r})) d^3r \quad (2.23)$$

Here the XC energy per particle, $\epsilon_{\text{XC}}^{\text{HEG}}$, for the homogeneous electron gas (HEG) is calculated as a *function* of the density such that this expression is exact for homogeneous densities. Then this same expression is simply applied to the inhomogeneous density of any system of interest. More advanced functionals use more advanced forms for the XC energy in which the XC energy density is allowed to depend on not only the density but its gradients. For example generalized gradient approximations (GGAs) [20] have the form:

$$E_{\text{XC}}^{\text{GGA}}[n] = \int n(\mathbf{r}) \epsilon_{\text{XC}}^{\text{GGA}}(n(\mathbf{r}), \nabla n(\mathbf{r})) d^3r \quad (2.24)$$

The development of new and more accurate density functional approximations is a large area of research. A hierarchy of approximations has emerged which is referred to by John Perdew as Jacob's ladder (see the first chapter of [8]). The lowest rung is the LDA and the second rung consists of the GGA's. The next rung consists of functionals which may depend on the Kohn-Sham kinetic energy density (meta-

GGAs). Functionals higher up on the ladder give better accuracy, but are also more computationally demanding.

Calculations based on KS-DFT using these exchange-correlation functionals fill a critical role in the context of other electronic structure methods, by providing unparalleled compromise between speed and accuracy. While other more accurate electronic structure methods rely on more accurate treatment of the wavefunction, DFT fundamentally uses the electronic density as the primary variable. Increased accuracy in DFT calculations is only achieved through improved XC functionals. This allows for far more favorable scaling with system size resulting in superior computational efficiency.

KS-DFT calculations have proved useful in solid-state physics calculations over the last forty years and have come to dominate quantum chemistry calculations in the last twenty years. The number of papers involving DFT calculations has grown almost exponentially since the 1998 Nobel prize of Kohn and Pople for their pioneering work in the field. The applications of DFT calculations continue to grow.

3. Partition Density-Functional Theory

This section contains work from the review article entitled ‘Density-Based Partitioning Methods for Ground-State Molecular Calculations’ written by the author and Adam Wasserman published in the Journal of Physical Chemistry A. [1]

We now turn to the derivation of PDFT, which is analogous to the derivation of Kohn-Sham theory given above. A system of non-interacting fragments will be glued together with a one-body potential much like the non-interacting electrons of Kohn-Sham theory are glued together by the Kohn-Sham potential. These non-interacting fragments are the auxiliary system of PDFT. Our derivation starts with the definition of the energy $E_\alpha[n_\alpha]$ of each fictitious fragment.

In order to make this definition the external potential, $v_{\text{nuc}}(\mathbf{r})$, is divided into fragments $v_{\text{nuc}}^\alpha(\mathbf{r})$. This can be done arbitrarily as long as the fragment potentials sum to the total potential.

$$v_{\text{nuc}}(\mathbf{r}) = \sum_{\alpha} v_{\text{nuc}}^{\alpha}(\mathbf{r}) \quad (3.1)$$

The energy of a fragment is then defined as the energy of N_α electrons in an external potential $v_{\text{nuc}}^\alpha(\mathbf{r})$.

The sum of fragment energies is the energy of a fictitious system of non-interacting fragments constrained to have the same total density, $n(\mathbf{r})$, as the interacting system of electrons. Systems of truly non-interacting fragments do not exist in nature except as a limit with increasing separation between fragments. In this limit, we can consider that each fragment may still exchange electrons with other fragments and thus may have a non-integer number of electrons. Density functional theory for open systems with fluctuating numbers of electrons was studied by Perdew, Parr, Levy and Balduz [21]. These systems are described as a statistical mixture of pure states also known as

an ensemble. Perdew, Parr, Levy and Balduz extended the Hohenberg-Kohn theorem to include ensembles and they showed that the ground state energy of such a system versus the number of electrons, N , is a series of straight lines between integer values of N . The fragment energies of PDFT are also defined as ensembles. In cases where N_α is not an integer the fragment energy, $E_\alpha[n_\alpha]$ is defined through an ensemble of two states, each containing an integer number of particles:

$$E_\alpha[n_\alpha] = \nu_\alpha E_{v_\alpha}[n_{p_\alpha+1}] + (1 - \nu_\alpha) E_{v_\alpha}[n_{p_\alpha}] \quad (3.2)$$

Here, ν_α is the non-integer portion of N_α and p_α is the lower bounding integer of N_α . These fragment energies are defined as:

$$E_{v_\alpha}[n_{p_\alpha}] = T_s[n_{p_\alpha}] + E_H[n_{p_\alpha}] + E_{xc}[n_{p_\alpha}] + \int v_{\text{nuc}}^\alpha(\mathbf{r}) n_{p_\alpha}(\mathbf{r}) d^3\mathbf{r} \quad (3.3)$$

This definition gives PDFT fragments behavior which agrees with that of a real system in the limit that fragments are well separated. With these definitions, the non-interacting kinetic energy, the hartree, and exchange-correlation energy functionals only ever act on densities with integral numbers of electrons ($n_{p_\alpha}(\mathbf{r})$ and $n_{p_\alpha+1}(\mathbf{r})$), even while the fragment density as a whole, $n_\alpha(\mathbf{r})$, may contain non-integer numbers of electrons.

3.1 Fragment Equations

The densities $n_{p_\alpha}(\mathbf{r})$ and $n_{p_\alpha+1}(\mathbf{r})$ are defined as those which minimize the sum of fragment energies,

$$E_f[\{n_\alpha\}] \equiv \sum_\alpha E_\alpha[n_\alpha] \quad (3.4)$$

and simultaneously satisfy two constraints. First, that the sum of fragment densities, $n_f(\mathbf{r}) \equiv \sum_{\alpha} n_{\alpha}(\mathbf{r})$, is equal to the molecular density,

$$n_f(\mathbf{r}) = n_m(\mathbf{r}) \quad (3.5)$$

where each fragment density is calculated from the ensemble as:

$$n_{\alpha}(\mathbf{r}) = \nu_{\alpha} n_{p_{\alpha}+1}(\mathbf{r}) + (1 - \nu_{\alpha}) n_{p_{\alpha}}(\mathbf{r}) \quad (3.6)$$

Second, that the total fragment density integrates to N , the total number of electrons in the system.

$$N = \int n_f(\mathbf{r}) d^3\mathbf{r} = \sum_{\alpha} N_{\alpha} \quad (3.7)$$

In other words we have a definition for the non-interacting fragment energy functional which is analogous to the definition of the non-interacting kinetic energy functional of Eq. 2.12.

$$E_f[n] = \min_{\{n_{\alpha}\} \rightarrow n} E_f[\{n_{\alpha}\}] \quad (3.8)$$

Overall, this constrained minimization of E_f is transformed into an unconstrained optimization of G through the introduction of two lagrange multipliers: the *partition potential*, $v_p(\mathbf{r})$, and the molecular chemical potential, μ_m .

$$G[n] = \min_{\{n_{\alpha}\}} [E_f[\{n_{\alpha}\}] + \int v_p(\mathbf{r}) (n_f(\mathbf{r}) - n(\mathbf{r})) d^3\mathbf{r} - \mu_m (\int n_f(\mathbf{r}) d^3\mathbf{r} - N)] \quad (3.9)$$

The molecular chemical potential, μ_m , controls the total number of electrons in the system and the partition potential, $v_p(\mathbf{r})$ must be chosen so that the resulting fragment densities sum to the correct total density $n(\mathbf{r})$. This lagrangian must then be

minimized with respect to every element of each fragment ensemble, yielding the euler equations:

$$\begin{aligned} 0 &= \frac{\delta G}{\delta n_{p_\alpha}(\mathbf{r})} \\ &= (1 - \nu_\alpha) \frac{\delta E_\alpha[n_{p_\alpha}]}{\delta n_{p_\alpha}(\mathbf{r})} + (1 - \nu_\alpha) v_p(\mathbf{r}) - (1 - \nu_\alpha) \mu_m \end{aligned} \quad (3.10)$$

$$\begin{aligned} &= \frac{\delta E_\alpha[n_{p_\alpha}]}{\delta n_{p_\alpha}(\mathbf{r})} + v_p(\mathbf{r}) - \mu_m \\ &= \frac{\delta T_s[n_{p_\alpha}]}{\delta n_{p_\alpha}(\mathbf{r})} + v_H[n_{p_\alpha}](\mathbf{r}) + v_{XC}[n_{p_\alpha}](\mathbf{r}) + v_\alpha(\mathbf{r}) + v_p(\mathbf{r}) - \mu_m \end{aligned} \quad (3.11)$$

In order to solve Eq.(3.10) we use a KS systems of p_α electrons in the external potential $v_\alpha(\mathbf{r}) + v_p(\mathbf{r})$ to obtain the density $n_{p_\alpha}(\mathbf{r}) = \sum_{i_{p_\alpha}}^{p_\alpha} |\phi_{i_{p_\alpha}}(\mathbf{r})|^2$, where the fragment orbitals are determined by the fragment KS equations:

$$\left\{ -\frac{1}{2} \nabla^2 + v_\alpha^{\text{eff}}[n_{p_\alpha}](\mathbf{r}) + v_p(\mathbf{r}) \right\} \phi_{i,p_\alpha}(\mathbf{r}) = \epsilon_{i,\alpha} \phi_{i,p_\alpha}(\mathbf{r}) \quad (3.12)$$

where the fragment effective potential is given by:

$$v_\alpha^{\text{eff}}[n_{p_\alpha}](\mathbf{r}) = v_H[n_{p_\alpha}](\mathbf{r}) + v_{XC}[n_{p_\alpha}](\mathbf{r}) + v_\alpha(\mathbf{r}) \quad (3.13)$$

Through these equations we see that each fragment density may be written as a functional of the partition potential and the occupation number $N_\alpha = p_\alpha + \nu_\alpha$.

$$n_\alpha = n_\alpha[v_p, N_\alpha](\mathbf{r}) \quad (3.14)$$

Our next step is then to find how the partition potential and occupation numbers may be found such that E_f is minimized and both constraints are satisfied.

3.2 Partition Potential Optimization

We must choose the lagrange multiplier, $v_p(\mathbf{r})$, such that it correctly enforces its constraint. To do this, we write the total molecular energy (corresponding to $n_f(\mathbf{r})$) as the sum of fragment energies, E_f , and the partition energy, E_p . The partition energy is defined exactly through this equation but may be approximated in practical calculations:

$$E[\{n_\alpha\}] = E_f[\{n_\alpha\}] + E_p[\{n_\alpha\}] \quad (3.15)$$

As mentioned in the previous section, we can write the fragment densities as functionals of the partition potential and therefore we can also write all the energy components of Eq. 3.15 as functionals of the partition potential:

$$E[v_p] = E_f[v_p] + E_p[v_p] \quad (3.16)$$

Assuming that the density is ensemble v -representable, the Hohenberg-Kohn theorem indicates that if we find the minimum of the total energy with respect to $v_p(\mathbf{r})$ then the corresponding density $n_f(\mathbf{r})$ must be equal to the correct total density of the fully-interacting system, $n(\mathbf{r})$.

Variation of the total energy with respect to the partition potential gives us a new Euler equation:

$$\begin{aligned} 0 &= \frac{\delta E}{\delta v_p(\mathbf{r})} \\ &= \sum_{\alpha} \frac{\delta E_{\alpha}}{\delta v_p(\mathbf{r})} + \frac{\delta E_p}{\delta v_p(\mathbf{r})} \end{aligned} \quad (3.17)$$

Let us consider first the first term, which we expand by using the chain rule:

$$\sum_{\alpha} \frac{\delta E_{\alpha}}{\delta v_p(\mathbf{r})} = \sum_{\alpha} \int \left((1 - \nu_{\alpha}) \frac{\delta E_{v_{\alpha}}}{\delta n_{p_{\alpha}}(\mathbf{r}')} \frac{\delta n_{p_{\alpha}}(\mathbf{r}')}{\delta v_p(\mathbf{r})} + \nu_{\alpha} \frac{\delta E_{v_{\alpha}}}{\delta n_{p_{\alpha+1}}(\mathbf{r}')} \frac{\delta n_{p_{\alpha+1}}(\mathbf{r}')}{\delta v_p(\mathbf{r})} \right) d^3 \mathbf{r}' \quad (3.18)$$

Because each of the n_{p_α} comes from the solution to Eq.(3.10) we can write Eq. (3.18) as:

$$\sum_{\alpha} \frac{\delta E_{\alpha}}{\delta v_p(\mathbf{r})} = \int (\mu_m - v_p(\mathbf{r}')) \sum_{\alpha} \left((1 - \nu_{\alpha}) \frac{\delta n_{p_{\alpha}}(\mathbf{r}')}{\delta v_p(\mathbf{r})} + \nu_{\alpha} \frac{\delta n_{p_{\alpha}+1}(\mathbf{r}')}{\delta v_p(\mathbf{r})} \right) d^3 \mathbf{r}' \quad (3.19)$$

Using our definition of $n_f(\mathbf{r})$ we find that the first term becomes $\int (\mu - v_p(\mathbf{r}')) \frac{\delta n_f(\mathbf{r}')}{\delta v_p(\mathbf{r})} d^3 \mathbf{r}'$. Because variation of the partition potential will only induce norm-conserving changes in $n_f(\mathbf{r})$, the integral over the constant term μ vanishes, and therefore:

$$\sum_{\alpha} \frac{\delta E_{\alpha}}{\delta v_p(\mathbf{r})} = - \int v_p(\mathbf{r}') \frac{\delta n_f(\mathbf{r}')}{\delta v_p(\mathbf{r})} d^3 \mathbf{r}' \quad (3.20)$$

Now we may consider the second term of Eq. 3.17. Cohen and Wasserman established that there is a one-to-one mapping between $n_f(\mathbf{r})$, the sum of fragment densities minimizing $E_f[\{n_{\alpha}\}]$, and the partition potential, $v_p(\mathbf{r})$ [22]. This indicates that $n_f(\mathbf{r})$ is a functional of $v_p(\mathbf{r})$ allowing us to use the chain rule to expand the functional derivative of E_p :

$$\frac{\delta E_p}{\delta v_p(\mathbf{r})} = \int \int \sum_{\alpha} \sum_{x=0,1} \frac{\delta E_p}{\delta n_{p_{\alpha}+x}(\mathbf{r}'')} \frac{\delta n_{p_{\alpha}+x}(\mathbf{r}'')}{\delta n_f(\mathbf{r}')} \frac{\delta n_f(\mathbf{r}')}{\delta v_p(\mathbf{r})} d^3 \mathbf{r}' d^3 \mathbf{r}'' \quad (3.21)$$

Combining Eqs. 3.20 and 3.21, we see that the only way to ensure the Euler equation will always be satisfied for arbitrary $\delta v_p(\mathbf{r})$ is if:

$$v_p(\mathbf{r}) = \int \sum_{\alpha} \sum_{x=0,1} \frac{\delta E_p}{\delta n_{p_{\alpha}+x}(\mathbf{r}')} \frac{\delta n_{p_{\alpha}+x}(\mathbf{r}')}{\delta n_f(\mathbf{r})} d^3 \mathbf{r}' \quad (3.22)$$

or,

$$v_p(\mathbf{r}) = \int \sum_{\alpha} \sum_{x=0,1} v_{p,\alpha,x}(\mathbf{r}') Q_{\alpha,x}(\mathbf{r}', \mathbf{r}) d^3 \mathbf{r}' \quad (3.23)$$

where the fragment-dependent partition potential and Q -functions are given by:

$$v_{p,\alpha,x}(\mathbf{r}) = \frac{\delta E_p}{\delta n_{p_{\alpha}+x}(\mathbf{r})} \quad (3.24)$$

$$Q_{\alpha,x}(\mathbf{r}', \mathbf{r}) = \frac{\delta n_{p_{\alpha}+x}(\mathbf{r}')}{\delta n_f(\mathbf{r})} \quad (3.25)$$

The Q -functions must satisfy the sum-rule:

$$\sum_{\alpha} \sum_{x=0,1} Q_{\alpha,x}(\mathbf{r}', \mathbf{r}) = \delta(\mathbf{r}' - \mathbf{r}) \quad (3.26)$$

3.3 Local- Q approximation

The Q -functions represent the way in which the fragment densities respond when a small variation, δn_f , is made to the molecular density. Some of this variation in density will be distributed to each component of each fragment ensemble. These functions are not known as explicit density functionals and in practical calculations these functions may be approximated using the local- Q approximation [23]:

$$Q_{p_{\alpha},x}^{\text{local}}(\mathbf{r}', \mathbf{r}) = \frac{n_{p_{\alpha},x}(\mathbf{r})}{n_f(\mathbf{r})} \delta(\mathbf{r} - \mathbf{r}') \quad (3.27)$$

However, it is important to note that when the exact E_p functional is used, either through inversion [2] or through use of the exact kinetic energy density functional (known only in limiting cases), then the choice of Q -function approximation is irrelevant as long as the sum rule of Eq.(3.26) is satisfied. This is due to the interesting fact that in these cases, at convergence, the functional derivative of the partition energy with respect to any of the fragment densities is exactly the same.

In cases where approximate non-additive functionals are used to construct the partition energy functional then using the local- Q approximation may restrict the partition potential, leading to densities that are not necessarily optimal with respect to the total energy. A potential functional formalism such as the one described by Huang and Carter [24] will avoid this issue and yield the optimal global partition potential.

We can use simple numerical models to check the validity of the local- Q approximation, Eq.(3.27). For example, we use a double well potential with $N = N_a + N_b$ non-interacting electrons:

$$v(x) = -Z_a \cosh(x + R/2)^2 - Z_b \cosh(x - R/2)^2, \quad (3.28)$$

placing N_a electrons on the left (a) and N_b electrons on the right (b). In these cases we calculate a target molecular density and corresponding chemical potential ahead of time using a one-dimensional real-space grid. We then make a search over partition potentials and directly optimize Eq. 3.9 as discussed in chapter 5.

For this model system we can easily find the numerically exact Q -functions in order to compare with the local- Q approximation. In the following, we chose the values of $Z_a = Z_b = 3$ and $N_a = N_b = 3$ and considered two values of the separation between the wells, $R = 3, 10$. We found the corresponding molecular density and the resulting fragment densities. Then, for small changes in the molecular density we re-optimized the fragment densities and occupations. The results of these variations yield the exact Q -functions. The exact Q -functions along with the corresponding local- Q approximation are displayed in Figure 3.1. We note that at both separations the local- Q approximation accounts for nearly all of the exact Q -function. For $R = 10$, the only non-local contribution resides close to the bond-midpoint where the fragment densities are both very small.

3.4 Occupation Number Optimization

The occupation numbers are also be optimized to satisfy the PDFPT requirement that the sum of fragment energies is minimized. In general there are two possibilities that may occur when Eq.(3.9) is optimized with respect to the occupations numbers, $\{N_\alpha\}$. The first possibility is that there will be a minimum of G at a non-integer value of one or more of the N_α . In this case we can find the stationarity condition

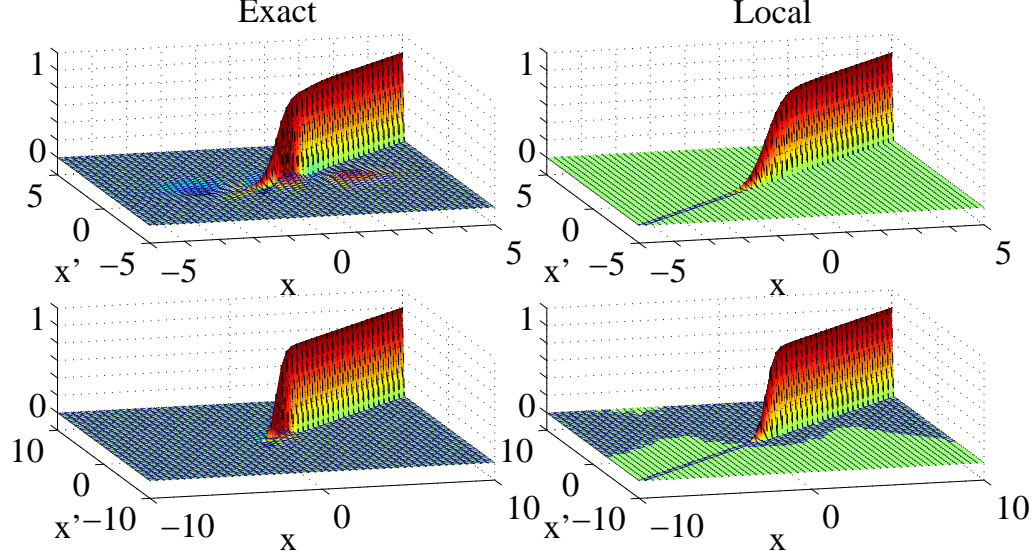


Figure 3.1. Numerically evaluated Q -functions, $Q_b(x', x) = \delta n_b(x') / \delta n_f(x)$, for one-dimensional non-interacting electrons (no ensembles are needed when calculating fragments for non-interacting electrons). The top row consists of calculations for the separation $R = 3$ and the bottom row is for separation $R = 10$. The left column shows the numerically exact Q -function, the right column is the local- Q approximation. Note that the local- Q approximation works well in both cases, but actually improves at the larger separation.

by taking the derivative of G with respect to the non-integer part of the occupation number, ν_α .

$$\begin{aligned}
 0 &= \frac{\partial G}{\partial \nu_\alpha} \\
 &= E_\alpha[n_{p_\alpha+1}] - E_\alpha[n_{p_\alpha}] + \int v_p(\mathbf{r})(n_{p_\alpha+1} - n_{p_\alpha}) - \mu_m \\
 &= \mu_\alpha - \mu_m
 \end{aligned} \tag{3.29}$$

Here we have defined a chemical potential for each fragment in a molecule and we see that because μ_m is a global quantity, all of these fragment chemical potentials must be equal [22]. It is important to note that the chemical potential derived from PDFT fragment energies will be different from those defined by Subsystem-DFT

and FDET, where fragment energies may be defined differently than in PDFT. The notable difference is that in Subsystem-DFT and FDET the electron-nuclear energy is not split into fragment and non-additive pieces, and instead each fragment energy includes the interaction between the fragment density and all of the nuclei, rather than just a subset of nuclei assigned to a fragment. This difference in fragment energy has the effect that, in general, chemical potentials within Subsystem-DFT and FDET are equalized even at fixed integer occupation numbers [25–27].

Within PDFT it is also possible for there to be no minimum at non-integer values. In this case the occupation numbers will be locked into integer values and there will not necessarily be chemical potential equalization between the fragments. We will explore these two possibilities in the next section.

The partition potential and occupation numbers may be simultaneously optimized to find the extrema of the functional of Eq. 3.9. The first derivative with respect to the occupation numbers is given in Eq. 3.29, and its second derivative is zero. The cross derivatives with respect to occupation numbers and the partition potential are identified as the fragment Fukui functions:

$$\frac{\partial}{\partial \nu_\alpha} \frac{\delta G}{\delta v_p(\mathbf{r})} = f_\alpha(\mathbf{r}) = n_{p_\alpha+1}(\mathbf{r}) - n_{p_\alpha}(\mathbf{r}) \quad (3.30)$$

3.5 Charge transfer between fragments

In cases where the optimized occupation numbers are not integers, some charge has transferred from one fragment to another. The PDFT occupation numbers can then serve as a method of population analysis. We use our one-dimensional PDFT solver to study how electrons are transferred between fragments. Placing a total of $N_a + N_b = 4$ electrons in the potential of Eq.(3.28), we vary the strength of the well in fragment a from $Z_a = 1$ to $Z_a = 6$ while fixing $Z_b = 3$. This effectively tunes the electronegativity

of fragment a . As we make the well deeper, some of the charge transfers from fragment b to fragment a .

As a measure of the difference in electronegativity we look at the difference in the chemical potential of the isolated fragments. The negative of the chemical potential has been identified with the electronegativity [28, 29]. We can then observe how this difference in chemical potential in the isolated fragments affects charge transfer between fragments in the molecule.

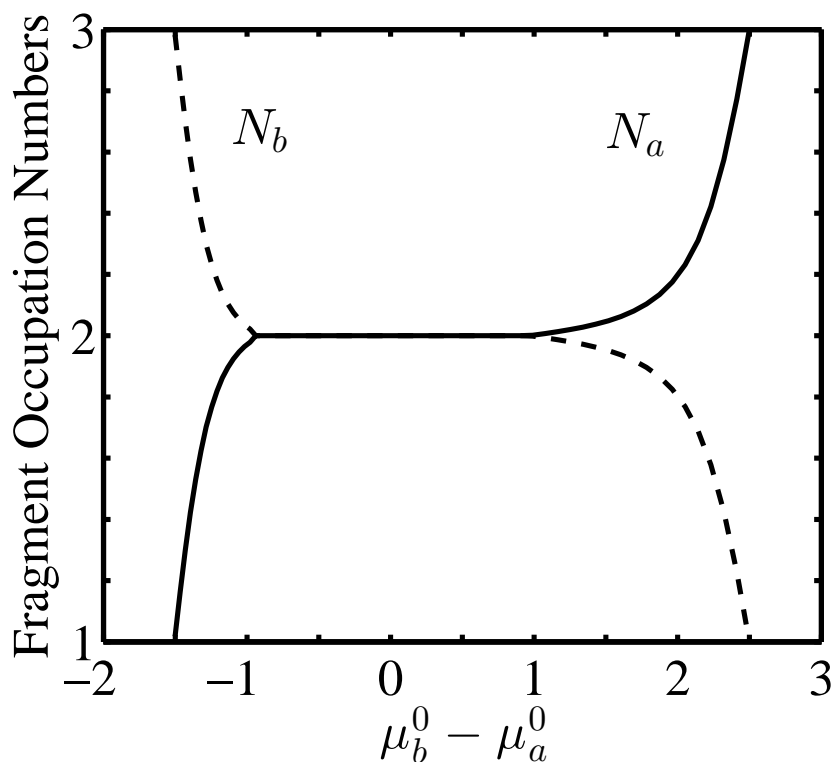


Figure 3.2. Charge transfer between fragments as a function of difference in chemical potential of the isolated fragments. The chemical potential difference is $\mu_b^0 - \mu_a^0$. When this difference is above one then charge transfers to fragment a , and when it is below negative one charge transfers in the opposite direction. Between about -1 and 1 no charge transfer takes place due to a cusp in G with respect to particle number.

The results, displayed in Figure 3.2, indicate that the fragment occupations are locked into integers until the absolute difference in chemical potential is greater than a value

close to $\mu_b^0 - \mu_a^0 = 1$. In this region the infimum of G has a cusp at $N_a = 2$ and $N_b = 2$ which means that there is no minimum in between integers and the fragment chemical potentials cannot equalize. In the two outer regions, charge is transferred between the fragments and the fragment chemical potentials *are* equalized. See reference [3] or chapter 8 of this dissertation for further discussion of chemical potential equalization in PDFT.

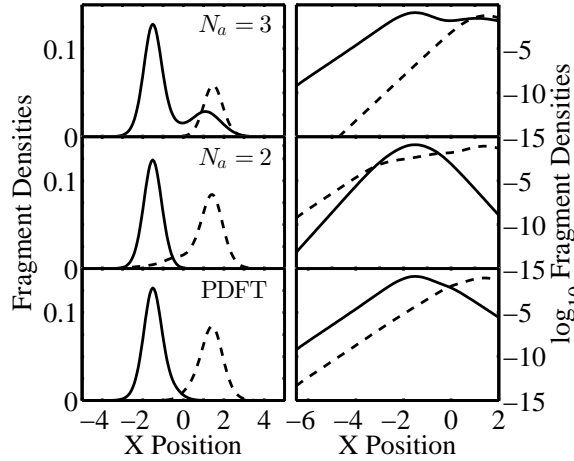


Figure 3.3. Fragment densities with various occupation numbers. The left-hand column has plots of the density and the right hand column displays the log of the densities. The first row is for occupation values: $N_a = 3$ and $N_b = 1$ the second row is for occupation values $N_a = N_b = 2$. The last row uses occupation numbers of $N_a = 2.2469$ and $N_b = 1.7531$, the optimized PDFT occupations. This illustrates that the optimized fragment occupations yield the most localized fragments. It also shows that when chemical potential equalization is reached, the fragments all have the same asymptotic behavior.

For any of these potentials we can also fix the occupation numbers to arbitrary values, provided $N_a + N_b = N$. In Figure 3.3 we compare occupation numbers fixed at integers with the optimized PDFT occupation numbers. We considered the cases where $Z_a = 5.5$ and $Z_a = 3.0$ with two choices for fixed occupation numbers ($N_a = 3$ and $N_b = 1$ as well as $N_a = N_b = 2$). The optimized PDFT occupation numbers are $N_a = 2.2469$ and $N_b = 1.7531$. As in previous studies of PDFT [30], regardless

of the choice for occupation numbers we were always able to find a global partition potential satisfying the constraint $n_f(\mathbf{r}) = n(\mathbf{r})$. When the PDFT occupation numbers are used, the chemical potentials of all fragments are identical, but when occupation numbers are fixed, the chemical potentials do not equalize. Because the PDFT chemical potentials control the exponential tails of the fragment densities, this equalization (or lack of) can be seen in the log of the density (plotted in the second column of Figure 3.3). In the first two rows of plots, which correspond to fixed occupation numbers, the fragment densities decay at different rates while the PDFT occupation numbers lead to densities that decay at exactly the same rate. This differs from fragment chemical potentials in Subsystem-DFT and FDET which, due to differences in definition for the fragment energy, do not control the exponential tails of the corresponding fragment densities [27].

We also see that the PDFT occupation numbers lead to fragment densities that are much more localized, resulting in a smaller overlap between fragments. This has important implications for calculations using approximate non-additive kinetic energy functionals, when it is preferable to have as little overlap as possible, as large errors are associated with regions of large overlap [31]. By reducing the regions of overlap between fragments, we reduce the dependence on these approximate (non-interacting) kinetic energy functionals.

3.6 Singularities in the exact partition potential

We now derive an exact condition that the partition potentials must satisfy. The presence of singularities in the external potential leads to cusps in the molecular density. These cusps in turn lead to singularities in the partition potential at the location of the singularities of the external potential. If we consider Coulomb potentials, $-Z/r$, then the strength, $Z_{v_p}^a$, of the singularity in the partition potential at the point \mathbf{r}_a is proportional to the ratio of fragment densities at the same point.

To derive the condition we start with Kato's cusp condition [32] for the molecular density due to a singularity in the external potential Z_{ext}^a at the point \mathbf{r}_a :

$$\frac{\partial}{\partial r}[\bar{n}_f(r)]|_{r=0} = -2Z_{\text{ext}}^a n_f(\mathbf{r})|_{\mathbf{r}=\mathbf{r}_a} \quad (3.31)$$

Here, $\bar{n}_f(r)$ is the spherical average of the density a distance r away from \mathbf{r}_a . In PDFT the total density, $n_f(\mathbf{r})$, is the sum of the fragment density, $n_a(\mathbf{r})$, and all the other fragments, $n_{\text{other}}(\mathbf{r})$. The fragment a is the fragment whose potential $v_a(\mathbf{r})$ contains the singularity from the external potential. Because the partition potential is global, both $n_a(\mathbf{r})$ and $n_{\text{other}}(\mathbf{r})$ must also satisfy cusp conditions with their effective potentials at point \mathbf{r}_a . Fragment a contains the singularity in question plus any singularity from the partition potential:

$$\frac{\partial}{\partial r}[\bar{n}_a(r)]|_{r=0} = -2(Z_{\text{ext}}^a + Z_{v_p}^a)n_a(\mathbf{r})|_{\mathbf{r}=\mathbf{r}_a} \quad (3.32)$$

The other fragments live in an effective potential which, at the point \mathbf{r}_a , only contains singularities due to the partition potential:

$$\frac{\partial}{\partial r}[\bar{n}_{\text{other}}(r)]|_{r=0} = -2Z_{v_p}^a n_{\text{other}}(\mathbf{r})|_{\mathbf{r}=\mathbf{r}_a} \quad (3.33)$$

Since the derivatives and spherical averaging are linear operations, we can combine Eqs. 3.31-3.33 to get:

$$Z_{\text{ext}}^a [n_a(\mathbf{r}) + n_{\text{other}}(\mathbf{r})]|_{\mathbf{r}=\mathbf{r}_a} = Z_{v_p}^a n_{\text{other}}(\mathbf{r})|_{\mathbf{r}=\mathbf{r}_a} + (Z_{\text{ext}}^a + Z_{v_p}^a)n_a(\mathbf{r})|_{\mathbf{r}=\mathbf{r}_a} \quad (3.34)$$

which leads directly to:

$$Z_{v_p}^a = Z_{\text{ext}}^a \frac{n_f(\mathbf{r}) - n_a(\mathbf{r})}{n_f(\mathbf{r})}|_{\mathbf{r}=\mathbf{r}_a} = Z_{\text{ext}}^a \frac{n_{\text{other}}(\mathbf{r})}{n_f(\mathbf{r})}|_{\mathbf{r}=\mathbf{r}_a} \quad (3.35)$$

It can be shown that this singularity is contained entirely in the potential-energy contribution to the partition potential when using the local- Q approximation. The potential energy component of the partition energy is:

$$V_{\text{nuc}}^{\text{nad}} = \int n_f(\mathbf{r})v_{\text{ext}}(\mathbf{r})d\mathbf{r} - \sum_{\alpha} \int n_{\alpha}(\mathbf{r})v_{\alpha}(\mathbf{r})d\mathbf{r} = \sum_{\alpha \neq \beta} \int n_{\alpha}(\mathbf{r})v_{\beta}(\mathbf{r})d\mathbf{r} \quad (3.36)$$

The functional derivative of this quantity with respect to a fragment n_{α} is simply $\sum_{\beta \neq \alpha} v_{\beta}(\mathbf{r})$, so the contribution to the partition potential due to this portion of the partition energy is:

$$v_{\text{nuc}}^{\text{nad}}(\mathbf{r}) = \int \sum_{\alpha} \sum_{\beta \neq \alpha} v_{\beta}(\mathbf{r}')Q_{\alpha}(\mathbf{r}', \mathbf{r})d^3\mathbf{r}' \quad (3.37)$$

Plugging this result into the local- Q approximation of Eq.(3.27), we find

$$v_{\text{nuc}}^{\text{nad}}(\mathbf{r}) = \sum_{\alpha} \sum_{\beta \neq \alpha} v_{\beta}(\mathbf{r})n_{\alpha}(\mathbf{r})/n_f(\mathbf{r}) \quad (3.38)$$

If we consider the contribution from a single fragment potential which contains a singularity, we can see that the local- Q approximation satisfies Eq.(3.35). This effect can be seen in the partition potentials of Figure 3.4, most notably in the cases of H_2^+ and H_2 where the fragments are relatively close together, and thus the ratio of $n_{\text{other}}(\mathbf{r})$ to $n_f(\mathbf{r})$ is larger.

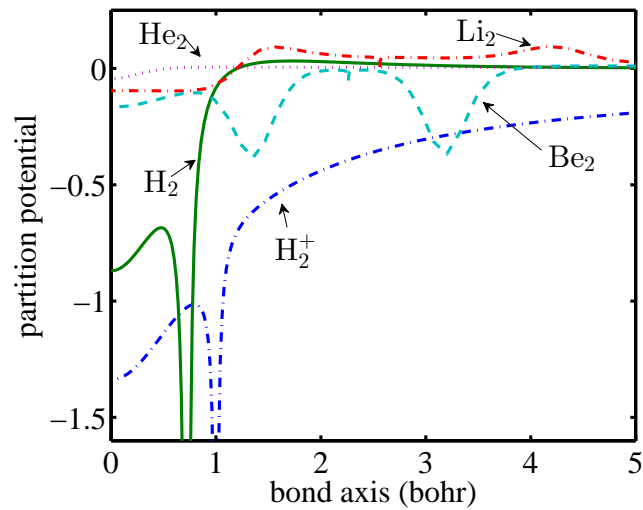


Figure 3.4. Plots of the partition potential along the bond axis for H_2^+ , H_2 , He_2 , Li_2 , and Be_2 . The location of the nuclei can be identified from the small singularity features in the partition potential. This agrees with Eq. 3.35, as the equilibrium distances are larger for Li_2 and Be_2 , so the density from one fragment in those cases is very small at the location of the other nucleus. For the case of He_2 , the density of each fragment is so small at the location of the other nuclei that the corresponding singularity in the partition potential is not visible in this plot.

4. Context in Fragment-Based DFT

This section contains work from the review article entitled ‘Density-Based Partitioning Methods for Ground-State Molecular Calculations’ written by the author and Adam Wasserman published in the Journal of Physical Chemistry A. [1]

4.1 Atoms-In-Molecules

Chemistry relies heavily on the idea that atoms do not entirely lose their identity when they come together to form molecules. Atoms and functional groups within different molecules behave in similar ways. However, quantum mechanics provides no convenient demarcation to establish which electrons belong to which fragment within a molecular context. In order to build chemical models we would very much like to know how we can expect atoms and functional groups within molecules to behave in different chemical contexts, and how the molecular environment changes and deforms them. In order to pursue this question it is helpful to provide a definition of what is meant by an atom within a molecule. Density-Functional Theory (DFT) gives us one possibility for keeping track of such changes. For a given molecular system we can divide its total electronic density, $n(\mathbf{r})$, into atomic or fragment densities, $n_\alpha(\mathbf{r})$. The question is then how to define the density of each fragment such that the fragment densities sum to the total electronic density,

$$\sum_{\alpha} n_{\alpha}(\mathbf{r}) = n(\mathbf{r}) \quad (4.1)$$

There are obviously many sets of fragment densities that may satisfy this equation, but is there an optimal way to choose them? We certainly have some intuition about

how we would like atoms-in-molecules to behave. Some features of isolated atomic densities should be shared. We would expect the fragments to be well localized spatially, and we would like them to decay monotonically with distance from the nuclei. These ideas suggest a definition that looks for similarities to the density of the isolated species.

Many possibilities exist, and as pointed out by Parr, Ayers and Nalewajski [33] the choice is necessarily ambiguous since no experiment can distinguish one choice as more correct than any other. In that paper they advocated for the use of the Hirshfeld or stockholder partitioning [34] of atoms-in-molecules, but they pointed out that various other choices may be better suited in certain circumstances. The Hirshfeld or stockholder fragment densities are given by:

$$n_{\alpha}(\mathbf{r}) = \frac{n_{\alpha}^0(\mathbf{r})}{\sum_{\alpha} n_{\alpha}^0(\mathbf{r})} n(\mathbf{r}) , \quad (4.2)$$

where $n_{\alpha}^0(\mathbf{r})$ is the density of the isolated α -fragment. Nalewajski and Parr showed that this definition of atoms-in-molecules yields fragments that are most similar to the isolated atoms according to an information theory measurement called the Kulback Liebler information distance [35].

Another way to achieve similarity with the isolated atomic species is to follow the suggestion by Parr et al. [28, 36], that atoms-in-molecules be defined as the set of fragment densities which have equal chemical potential and minimum *promotion energy* from their ground state. They defined the promotion energy as the difference in energy of the atomic fragments when they are in the molecule as compared to when they are isolated. Thus, the promotion energy is a measure of the extent to which the isolated atomic densities must be deformed in order to satisfy the condition that all of the fragment densities add up to the correct molecular density. This minimization of fragment energies is also used in the Partition Theory of Cohen and Wasserman [37], forming a basis for Partition Density-Functional Theory (PDFT) [23, 38]. Palke [39] and Guse [40] both developed algorithms and performed calculations to find the

atoms-in-molecules defined by Parr et al. for the hydrogen molecule and its positive ion. Guse’s method has some similarities with the algorithms of PDFT (the details of which are explained in chapters 3 and 5).

The Hirshfeld or stockholder definition of atoms-in-molecules has strong parallels with the definition of Parr et al., since both are based on a minimization principle. Rather than minimizing the energy difference between isolated atoms and the atoms in their molecular environment, the Hirschfeld partitioning minimizes the information distance between the two.

Also well known are Bader’s atoms-in-molecules [41, 42]. These are based on the topology of the molecular density. The fragments are non-overlapping pieces of the total density, divided by boundaries where the gradient of the density normal to the boundary surface is zero. Bader’s quantum theory of atoms-in-molecules (QTAIM) contrasts strongly with the proposed definition of both Hirschfeld and Parr et al. because Bader’s QTAIM fragments have sharp discontinuities and are non-overlapping, whereas the other two fragment definitions lead to smooth fragment densities that may overlap one another. From a density-functional viewpoint, the fragments of Parr et al. are attractive because, as can be shown, each fragment density is v -representable. Zhang and Wasserman studied the transferability of these fragment definitions and found that the method based on energy minimization led to the best transferability, at least in simple model systems [43].

On the other hand, Bader severely critiqued the promotion-energy definition of atoms-in-molecules. He argued that QTAIM fragments are based on firm foundations of quantum mechanics and Schwinger’s principle of stationary action, while the atoms of Parr et al. are based on an arbitrary definition for the minimum promotion energy [44, 45]. The energies of each fragment in Bader’s method add directly to the energy of the system, while with the atoms of Parr et al. only the densities are additive while the energy contains non-additive contributions. In other words, Parr et al. use fragments that are fictitious systems, not actually tied to the reality of quantum mechanics.

Nevertheless, DFT regularly makes use of another equally fictitious system with great success (KS electrons), so we see little merit in Bader’s argument.

4.2 Fragment-based density-functional methods

In addition to its use as an interpretive tool in chemistry, the division of the density into fragments has also been used as a practical tool in electronic structure calculations. Gordon and Kim in 1972 [46] essentially used Eq. 4.1 to construct the molecular density of rare-gas dimers from isolated atomic Hartree-Fock densities. They made non-self-consistent calculations based on the assumption that the density of the dimer was not significantly changed from superimposed atomic densities. They then used density functionals based on the electron gas to estimate the relevant binding energy curves. Other workers added corrections to account for self-interaction errors [47, 48] and to include induction effects and dispersion forces [49]. For an early review on the Gordon-Kim model see ref [50]. Vela, Cedilla, and Gazquez [51] made the connection between calculations of Gordon and Kim and the atoms-in-molecules of Parr et al.

Self-consistent versions of the Gordon-Kim model were not far behind. Senatore and Subbaswamy were the first in 1986 [52] and in the early 1990’s several general methods were developed which can be seen as self-consistent versions of the Gordon-Kim model. Cortona [53], Wesolowski and Warshel [54] and Boyer and Mehl [55] all developed formalisms for fragment-based DFT calculations. The starting point is the same for all these methods. The total electronic energy, E , is understood as a functional of the set of fragment densities $\{n_\alpha(\mathbf{r})\}$. It is divided into fragment contributions as:

$$E[\{n_\alpha\}] = V_{\text{nuc}}[n] + E_{\text{H}}[n] + E_{\text{xc}}[n] + \sum_{\alpha} T_s[n_\alpha] + T_s^{\text{nad}}[\{n_\alpha\}] \quad (4.3)$$

In Eq.(4.3), V_{nuc} , is the electron-nuclear energy, E_{H} is the Hartree energy, E_{xc} is the exchange-correlation energy, T_s is the non-interacting kinetic energy, and T_s^{nad} is the

non-additive non-interacting kinetic energy. This last term is simply the difference between the kinetic energy functional evaluated for the sum of fragment densities and the sum of energy functionals evaluated for each of the fragment densities:

$$T_s^{\text{nad}}[\{n_\alpha\}] = T_s[n] - \sum_\alpha T_s[n_\alpha] \quad (4.4)$$

This rewriting of the total energy is of course still in principle exact as long as Eq.(4.1) is satisfied. However, in practical calculations, the non-additive kinetic energy term may be evaluated using approximate functionals while fragment kinetic energies may be calculated using KS orbitals. This is precisely the method of Gordon and Kim, except that the fragment densities were not calculated self-consistently. Allowing the calculations to be done self-consistently was an important step forwards.

Cortona in 1991 [53] performed calculations for a non-magnetic crystal with fragment densities centered at each lattice point. The non-additive kinetic energy was approximated using the Thomas-Fermi functional, and the fragments were approximated as spherically symmetric. Cortona used the method to perform calculations for NaCl and KCl, treating all the atoms in the crystal lattice as separate fragments, and finding the total energy by minimizing it with respect to each of the fragment densities. All of the fragments in Cortona’s calculation reach self-consistency and subsequent calculations in which all fragments are fully relaxed and self-consistent are commonly referred to as Subsystem-DFT [56].

In 1993 Wesolowski and Warshel [54] developed frozen-density embedding theory (FDET). They considered initially a two-fragment system where one fragment was a solute molecule and the other fragment was its solvent. Rather than self-consistently relaxing both fragment densities, the larger solvent fragment was frozen as an approximation, and allowed to create an effective potential for the solute, which was found self-consistently. FDET may also be made completely self-consistent by using freeze-thaw cycles in which the fragment being held frozen is alternated. In this case Subsystem-DFT and FDET become equivalent because they use the same underlying

equations, the Kohn Sham equations for constrained electron density (KSCED, see Sec. 4.3 below). These methods have been used for studying many systems including spectroscopy of complex systems and solvatochromatic shifts [57–60]. For recent reviews of Subsystem-DFT and FDET calculations there are several excellent reviews available [56, 61, 62].

Govind et al. in 1998 [63] developed a method to embed different levels of calculation into a DFT calculation. The method uses the ideas of Wesolowski and Warshel and Cortona, except that one of the subsystems may be treated with a more accurate wavefunction method. The wavefunction method is used to calculate the energy and density of a chosen subsystem in the presence of the *embedding* potential that is generated from DFT calculations on the other fragments. This allows specific parts of a larger DFT calculation to be treated with higher accuracy. This method is usually referred to as Embedding-DFT. See the review of Huang and Carter for a more in depth account of this method [64].

The self-consistent atomic deformation theory (SCAD) of Boyer, Mehl and coworkers [55, 65–69], which was also developed in 1993, can be viewed as a version of Subsystem-DFT requiring that fragment densities be written as atomic densities. Also, although it is not the focus of the present article, there are also time-dependent versions of fragment-based DFT [70–75].

4.3 Fragment self-consistency within Subsystem-DFT and FDET

In order to calculate fragment densities in within Subsystem-DFT and FDET mentioned in the previous section, the total energy of Eq. 4.3 is minimized by allowing each fragment density to vary subject to the constraint that it is normalized to an integer number of electrons, which are then said to belong to that fragment. As we shall see, this leads to an embedding potential for each fragment. In FDET this potential is updated for one fragment at a time leaving the other fragments frozen, while in

Subsystem-DFT all fragment embedding potentials are updated simultaneously. The minimization leads to an Euler equation for each fragment:

$$0 = \frac{\delta E[\{n_\alpha\}]}{\delta n_\alpha(\mathbf{r})} - \mu_\alpha \quad (4.5)$$

$$\mu_\alpha = \frac{\delta T_s[n_\alpha]}{\delta n_\alpha(\mathbf{r})} + \frac{\delta T_s^{\text{nad}}[\{n_\alpha\}]}{\delta n_\alpha(\mathbf{r})} + v_{\text{nuc}}[n](\mathbf{r}) + v_{\text{H}}[n](\mathbf{r}) + v_{\text{XC}}[n](\mathbf{r}) \quad (4.6)$$

where the potentials are the functional derivatives of the energy terms in Eq.(4.3). The lagrange multiplier, μ_α , enforces the constraint that fragment α has N_α electrons. It is also referred to as the chemical potential of fragment α .

We then assume that each fragment density has an auxiliary Kohn-Sham system of non-interacting electrons with identical density [19]. This leads directly to the fragment Kohn-Sham equations with constrained electron density (KSCED) [53, 54, 76]:

$$\left\{-\frac{1}{2}\nabla^2 + v_\alpha^{\text{KSCED}}[n_\alpha](\mathbf{r})\right\}\phi_{i,\alpha}(\mathbf{r}) = \epsilon_{i,\alpha}\phi_{i,\alpha}(\mathbf{r}) \quad (4.7)$$

where the KSCED potential, v_α^{KSCED} , is given by

$$v_\alpha^{\text{KSCED}}[n_\alpha](\mathbf{r}) = \frac{\delta T_s^{\text{nad}}[\{n_\alpha\}]}{\delta n_\alpha(\mathbf{r})} + v_{\text{nuc}}[n](\mathbf{r}) + v_{\text{H}}[n](\mathbf{r}) + v_{\text{XC}}[n](\mathbf{r}) \quad (4.8)$$

The last three potential terms simply constitute the KS potential for the entire molecular system. These equations form the basis for both FDET and Subsystem-DFT. The KSCED potential may be divided further into fragment and non-additive terms as will be explored in Sec. 4.5.

4.4 Non-uniqueness of solutions of the exact KSCED equations

If T_s^{nad} and its functional derivatives are calculated exactly, these equations will exactly reproduce a given KS calculation performed on the whole system. We refer to this as an “exact solution to the KSCED equations”, but it should be noted that this

does not mean that the results would exactly reproduce the fully interacting system, unless of course the exact XC functional is used.

It is known that the exact solution to the KSCED equations is not unique. We show below that in fact *any* set of non-interacting v -representable densities, $\{n_\alpha\}$, satisfying Eq. 4.1, will necessarily be a solution to the KSCED equations. This indicates that with the exact functional for T_s^{nad} , a self-consistent solution to Eqs. 4.7-4.8 yields different results dependent on the choice of initial fragment densities and the method of convergence.

Interestingly, this non-uniqueness disappears when employing an approximation for T_s^{nad} . In such case, sets of fragment densities summing to the same total density will not have the same total energy, and because the total energy is minimized, the KSCED equations will yield the set of fragment densities that minimizes the error due to the approximate non-additive kinetic energy functional employed. It has been observed that local and semi-local approximations for the non-additive kinetic energy lead to fragments that reduce their mutual overlap [77, 78]. Each approximation to T_s^{nad} results in a unique set of fragment densities and fragment potentials which together satisfy the KSCED equations.

Non-unique potentials corresponding to the exact T_s^{nad} are illustrated in Figure 4.1, where we compare the embedding potentials and densities obtained for the helium dimer using two different methods of convergence, the freeze-and-thaw cycle [76] and simultaneous relaxation [53]. In both cases the densities of the isolated fragments were used as the initial guess, but the fragment densities at convergence are clearly different for the two convergence methods. The total energy and density from both is the same, despite ending with differing sets of fragment densities. This occurs whenever the non-additive terms match exactly the corresponding fragment energy terms. In this case, the total energy will be identical for any set of fragment densities that add up to the same total density.

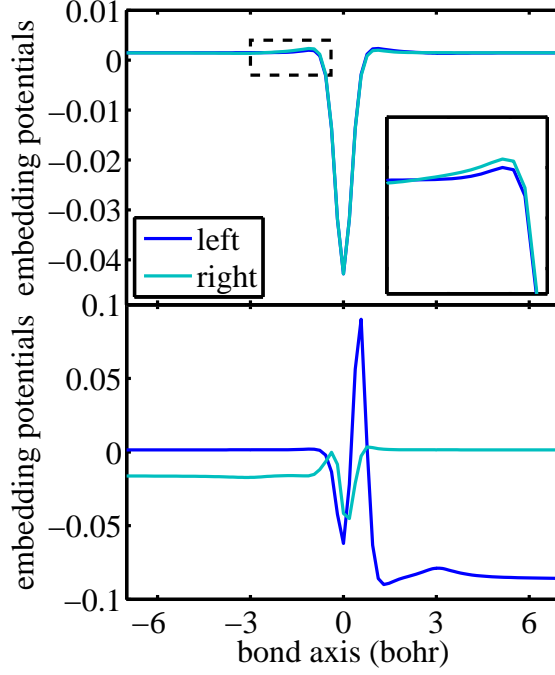


Figure 4.1. Exact embedding potentials for the helium dimer. The two helium atoms are placed at $x = \pm 3$ and labeled as left (nucleus at $x = -3$) and right (nucleus at $x = +3$). The top and bottom figures show different methods for converging the calculation. In the top frame the embedding potentials are iterated simultaneously while in the bottom frame freeze-and-thaw cycles are applied to reach self-consistency. For each of these sets of potentials the exact total energy and exact molecular density are recovered, although the fragment densities are different in each case.

Unique potentials from approximate T_s^{nad} can be seen in Figure 4.2, where the simplest approximation for T_s^{nad} , the Thomas-Fermi approximation [17,18], is used. In this case both freeze-and-thaw and simultaneous relaxation yield the same fragment densities and fragment embedding potentials, whereas in the exact case (Figure 4.1) they gave different results. We plot the log of the density to show that the fragment densities have very small cusps at the location of the other nuclei.

To show the non-uniqueness of the exact KSCED equations we start by identifying the functional derivative of the non-additive kinetic energy. If the fragment densities are

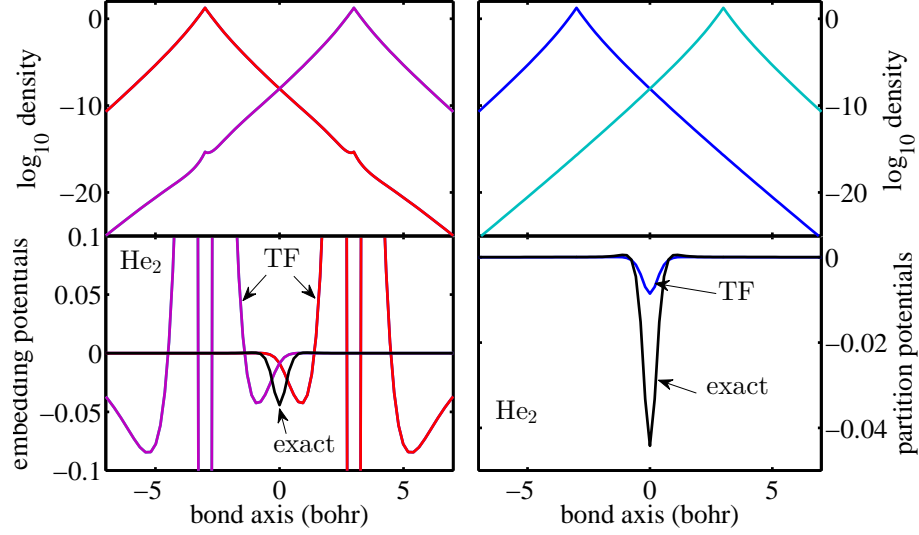


Figure 4.2. Approximate embedding potentials for the Helium dimer using the Thomas-Fermi (TF) approximation of T_s^{nad} . The two monomers are placed at $x = \pm 3$ and labeled as left (nucleus at $x = -3$) and right (nucleus at $x = +3$). The left two plots show the solution to the KSCED equations which is unique for the TF approximation, but the potentials are not global meaning there is a different embedding potential for each fragment. The right two plots show results from PDFT using the local- Q approximation, where there is a global partition potential shared by each fragment. In each case the log of the fragment densities are plotted above the corresponding embedding potentials. Both cases are compared with the exact partition potential (solid black) which is unique and global.

non-interacting v -representable (n_α is a ground-state density for N_α non-interacting electrons in the potential v_{n_α}) then we write down the Euler equation for a system of non-interacting electrons corresponding to density n_α :

$$\frac{\delta T_s[n_\alpha]}{\delta n_\alpha(\mathbf{r})} + v_{n_\alpha}(\mathbf{r}) = \mu_\alpha \quad (4.9)$$

Also, the molecular Euler equation with chemical potential μ_m reads:

$$\frac{\delta T_s[n]}{\delta n(\mathbf{r})} + v_{\text{nuc}}[n](\mathbf{r}) + v_{\text{H}}[n](\mathbf{r}) + v_{\text{xc}}[n](\mathbf{r}) = \mu_m \quad (4.10)$$

These two expressions can be combined to find the functional derivative of the non-additive kinetic energy:

$$\frac{\delta T_s^{\text{nad}}[\{n_\alpha\}]}{\delta n_\alpha(\mathbf{r})} = \mu_m - \mu_\alpha + v_{n_\alpha}(\mathbf{r}) - v_{\text{nuc}}[n](\mathbf{r}) - v_{\text{H}}[n](\mathbf{r}) - v_{\text{XC}}[n](\mathbf{r}) \quad (4.11)$$

Note that for approximate T_s^{nad} this equality does not hold, but for the exact case we can plug Eq.(4.11) into Eq.(4.8) to obtain:

$$v_\alpha^{\text{KSCED}}[n_\alpha](\mathbf{r}) = \mu_m - \mu_\alpha + v_{n_\alpha}(\mathbf{r}) \quad (4.12)$$

Since $\mu_m - \mu_\alpha$ is just a constant, the new KSCED potential for fragment α is equivalent to $v_{n_\alpha}(\mathbf{r})$ which is exactly the potential needed to produce the fragment density n_α . Thus, provided T_s^{nad} is exact, we have shown that *any arbitrary set of non-interacting v -representable densities that satisfy $\sum_\alpha n_\alpha(\mathbf{r}) = n(\mathbf{r})$ is a solution to the KSCED equations.*

In this way we see that the nature of the KSCED equations with approximate non-additive functionals differs qualitatively from that of exact non-additive functionals; in the first case there is a unique solution, while in the second there are many. Non-uniqueness in the exact case is an important consideration because several methods have been developed to perform calculations with the *exact* KSCED equations using OEP-like techniques. [2, 24, 25, 61, 79–82]. While computationally expensive, these techniques can be used as a benchmark to compare with calculations using approximate T_s^{nad} functionals. To this end it would be ideal to have a method known to provide a unique solution when using the exact non-additive functionals. In the next section we explore how to achieve unique solutions, even in the exact case.

4.5 Paths to Uniqueness

Uniqueness has been achieved from two directions. First, through the development of Partition Density-Functional Theory (PDFT) [23, 38] in 2010, based on the earlier Partition Theory [37], and second through a reformulation of Embedding-DFT by Huang, Pavone and Carter in 2011 [24, 82]. In both cases the key to ensuring uniqueness of the fragment densities is a global embedding potential. While each fragment density in standard Subsystem-DFT is independently varied to minimize the total energy, the requirement that some portion of each fragment's effective potential is global (i.e. the same for all fragments) constrains the solution to be unique. This does not mean that each fragment KS system sits in the same potential (although this would clearly lead the unique set of fragment densities that are all identical), but instead just the part of each fragment's effective potential which depends on other fragment's densities is identical for all fragments. Cohen and Wasserman proved that there is a one-to-one mapping between this type of global one-body potential, shared by all fragments, and the corresponding set of fragment densities [22]. Both PDFT and the method of Huang, Pavone and Carter rely on this theorem to ensure the uniqueness of the fragment densities.

The first step in both of these developments is to define the energy associated with each fragment. In other words, each piece of the energy in Eq. 4.3 must be divided into additive contributions from the fragments and non-additive contributions from the interaction:

$$E[\{n_\alpha\}] = \sum_{\alpha} E_{\alpha}[n_{\alpha}] + E_{\text{int}}[\{n_{\alpha}\}] \quad (4.13)$$

This partitioning leads to a definition of fragment energies and a corresponding interaction energy. The interaction energy is defined as the quantity which makes Eq. 4.13 exact, but it can also be written as a sum of non-additive functionals:

$$E_{\text{int}}[\{n_{\alpha}\}] = T_s^{\text{nad}}[\{n_{\alpha}\}] + E_{\text{H}}^{\text{nad}}[\{n_{\alpha}\}] + E_{\text{xc}}^{\text{nad}}[\{n_{\alpha}\}] + V_{\text{nuc}}^{\text{nad}}[\{n_{\alpha}\}] \quad (4.14)$$

In order to do make this division the external potential, $v_{\text{nuc}}(\mathbf{r})$, is divided into fragments $v_{\text{nuc}}^{\alpha}(\mathbf{r})$. This can be done arbitrarily as long as the fragment potentials sum to the total external potential. There are a few subtle differences between the PDFT and Huang-Pavone-Carter definition of fragment energies, as we will mention later.

Huang, Pavone and Carter continue the derivation along the same lines as Subsystem-DFT, by minimizing the total energy with respect to fragment densities. The corresponding KSCED potentials are then divided into contributions from the local fragment and a term arising from the interactions between the fragments:

$$v_{\alpha}^{\text{KSCED}}[n_{\alpha}](\mathbf{r}) = v_{\text{eff}}^{\alpha}[n_{\alpha}](\mathbf{r}) + v_{\text{emb}}^{\alpha}[\{n_{\alpha}\}](\mathbf{r}) \quad (4.15)$$

The first potential, v_{eff}^{α} , depends just on the fragment density,

$$v_{\text{eff}}^{\alpha}[n_{\alpha}](\mathbf{r}) = v_{\text{nuc}}^{\alpha}(\mathbf{r}) + v_{\text{coul}}^{\alpha}[n_{\alpha}](\mathbf{r}) + v_{\text{xc}}^{\alpha}[n_{\alpha}](\mathbf{r}) \quad (4.16)$$

while the embedding potential, v_{emb}^{α} , depends on all the other fragment densities:

$$v_{\text{emb}}^{\alpha}[\{n_{\alpha}\}](\mathbf{r}) = \sum_{\beta \neq \alpha} (v_{\text{nuc}}^{\beta}(\mathbf{r}) + v_{\text{H}}^{\beta}[n_{\beta}](\mathbf{r})) + v_{\text{xc}}^{\text{nad}}[\{n_{\alpha}\}](\mathbf{r}) + v_{\text{kin}}^{\text{nad}}[\{n_{\alpha}\}](\mathbf{r}) \quad (4.17)$$

Huang, Pavone and Carter then impose the additional constraint that this embedding potential must be the same for all fragments [82]. In a later paper, they formulate the embedding problem as a potential functional of this global embedding potential [24]. The globality of the embedding potential ensures that the fragments are unique through the theorem of Cohen and Wasserman [22].

PDFT [23, 38, 83] takes a slightly different route. Rather than directly minimizing the total energy, the sum of fragment energies (first term of equation 4.13), is minimized subject to the constraint that the sum of fragment densities is equal to the molecular density. This minimization of fragment energies guarantees the uniqueness of the

fragment densities and the globality of the embedding potential, due to the same theorem [22].

This slightly different route will still lead to the exact ground state energy of the molecular system given the same assumptions made in the more general case of Subsystem-DFT. The KSCED equations will lead to fragments which sum to the exact molecular density as long as the molecular density is non-interacting pure state v-representable and it is decomposable into fragment densities which are non-interacting pure state v-representable [84]. These requirements apply to PDFT as well, except that the fragment densities in PDFT need only be non-interacting ensemble v-representable. Additionally, in both the formulation of reference [24] and in PDFT there is the requirement that there exists a global embedding potential which is added to the external potential of all fragments. The proof of Cohen and Wasserman establishes the existence and uniqueness of this global potential [22].

4.6 Connection to Subsystem-DFT

In the formalism of Huang, Pavone, and Carter [82], the connection to Subsystem-DFT is clear: an additional constraint forces the fragment embedding potentials to be identical. In PDFT, it is the Q -functions which allow us to connect to Subsystem-DFT calculations. The fragment contributions to the partition potential, $v_{p,\alpha,x}(\mathbf{r})$, given in Eq.(3.22), are closely related to the embedding potentials of Subsystem-DFT or FDET. However in PDFT calculations these fragment contributions to the partition potential are averaged together using the Q -functions to obtain a global v_p . In this way any code capable of performing Subsystem-DFT calculations could use the local- Q functions to average the embedding potentials for each fragment and obtain the unique partition potential for a PDFT calculation. Thus the Q -functions provide a bridge between Subsystem-DFT calculations and PDFT calculations. This

averaging has interesting features that may help address some issues encountered with approximate Subsystem-DFT embedding potentials, as indicated next.

Examining Eq. 4.17, we see that the embedding potential for a given fragment has attractive Coulomb singularities at the nuclei belonging to all other fragments. Jacob et al. showed in 2007 that the exact non-additive kinetic energy potential cancels these contributions in the limit of large separation between fragments [85]. However, approximate non-additive kinetic energy potentials do not cancel these singularities and leave significant Coulomb attraction near nuclei from other fragments. This is illustrated in Figure 4.3 for the helium dimer by decomposing the embedding potential for one fragment into its kinetic, nuclear, hartree, and exchange-correlation components. The figure shows the components of the embedding potential for the left fragment centered at $x = -3$ bohr, but it shows them near the *right* fragment, centered at $x = +3$ bohr. In the top frame, the components of the embedding potential are calculated exactly while in the bottom frame the Thomas-Fermi functional is used for the kinetic component. In the exact case, the large components of the embedding potential nearly cancel out leaving an embedding potential which in the case of He_2 varies on the order of 10^{-2} hartree. On the other hand, the potential from the approximate kinetic energy functional cannot balance the other components in the region of the non-active fragment, and as a result there is a relatively large singularity in the embedding potential at the location of the non-active nuclei.

In purely electrostatic embedding this can lead to orbitals from fragment α localizing at the nuclei from other fragments (known as the electron leak problem), but it has been shown that this does not happen in Subsystem-DFT [86]. In Subsystem-DFT, the non-additive kinetic energy potential provides enough repulsion at these nuclei so that occupied orbitals do not localize. However, unoccupied orbitals could localize at those points, with implications for fragment-based linear response [73].

Jacob et al. [85] and Lastra et al. [87] both proposed non-decomposable approximations to the embedding potential to correct this problem. These non-decomposable

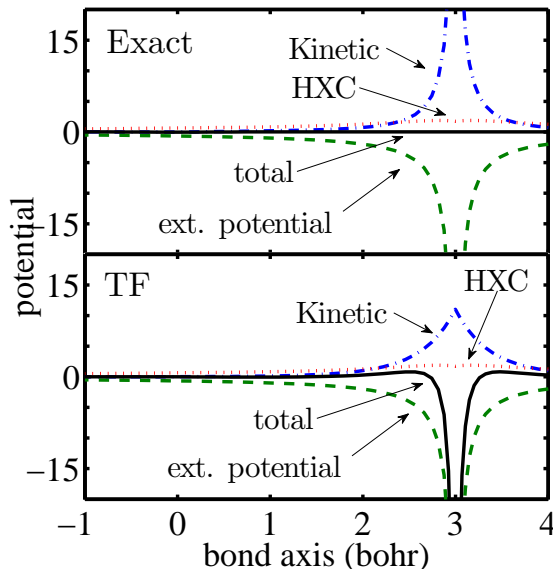


Figure 4.3. Comparison of the components of an embedding potential in the region of the non-active fragment. The total is in solid black, the potential energy component is in dashed green, the kinetic energy component is in dot-dash blue and the XC component is in dotted red. In the top figure the exact kinetic energy is used, while in the bottom the Thomas Fermi kinetic energy is used. In the top figure the kinetic energy has a positive singularity which cancels a large portion of the potential energies negative singularity so overall the embedding potential is fairly flat. In the bottom figure the Thomas Fermi kinetic energy does not cancel well with the negative singularity and as a result the embedding potential is not accurate in this region.

approximations are ones for which the embedding potential can not be directly split into two pieces, one coming from the molecule and the other coming from the fragment. Jacob et al. proposed such an approximation that switches off the embedding potential near the frozen nuclei in order to fulfill the exact limit they found [85], and Fux et al. used this correction to improve the description of coordination bonds in FDET calculations [88]. Lastra et al. also proposed an approximation based on switching, but instead focused correcting just the kinetic contribution to the embedding potential in two-fragment cases where one fragment is negligible and the other fragment contains two electrons [87]. An attractive feature of PDF-T is that the Q -

function averaging of Eq.(3.22), even within the local- Q approximation of Eq.(3.27), leads to fragment effective potentials that have the correct behavior at the location of nuclei in other fragments, according to the formula derived in Sec. 3.6.

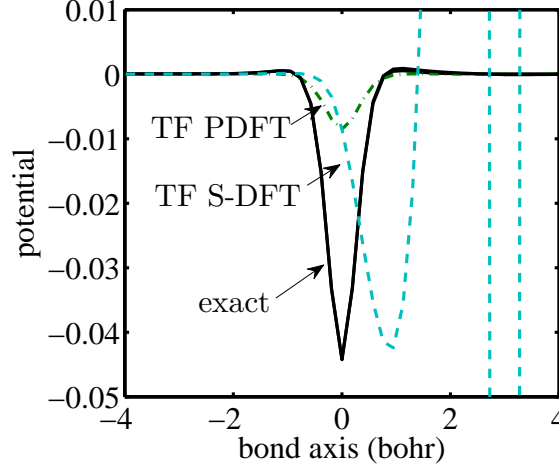


Figure 4.4. Comparison of exact vs. Thomas-Fermi (TF) approximations for Subsystem-DFT and PDFT for the Helium dimer. The two monomers are placed at $x = \pm 3$ and we refer to these fragments as left (nucleus at $x = -3$) and right (nucleus at $x = +3$). The solid black line is both the exact partition potential and an exact embedding potential for the left monomer (they are slightly different but indistinguishable here, but may differ greatly as in Figure 4.1). The two dotted lines represent calculations using the Thomas-Fermi kinetic energy functional. The dash dotted line is the global TF partition potential and the dashed line is the TF embedding potential for the left monomer.

Figure 4.4 compares partition and embedding potentials for the helium dimer. The solid line shows the potentials obtained with the *exact* $T_s[n]$. When the exact functional is used the partition potential is virtually indistinguishable from the two embedding potentials of Subsystem-DFT (however, the embedding potentials are not unique as discussed in Sec. 4.4). Figure 4.4 makes it clear that when the Thomas-Fermi functional is used, the partition potential and the embedding potentials differ significantly. The partition potential is global and therefore the same for both fragments, while the embedding potential is different for both (Figure 4.4 shows it for the left fragment, centered at $x = -3$ bohr).

5. Algorithms

Several algorithms have been developed to perform PDFT calculations. Some these algorithms are designed to yield the exact partition potential which reproduces a given KS-DFT calculation. In general these algorithms involve solving an inverse problem and are in general less computationally efficient than a standard KS-DFT calculation. However they can provide useful insight into the behavior of the exact partition potential and the exact fragment densities for comparison with approximations. In this chapter we will discuss the various algorithms used for PDFT calculations in this dissertation. We will start with the inversion-based algorithms which yield exact partition potentials and then discuss the algorithms for use with approximations to the partition energy.

5.1 Inversion Algorithms

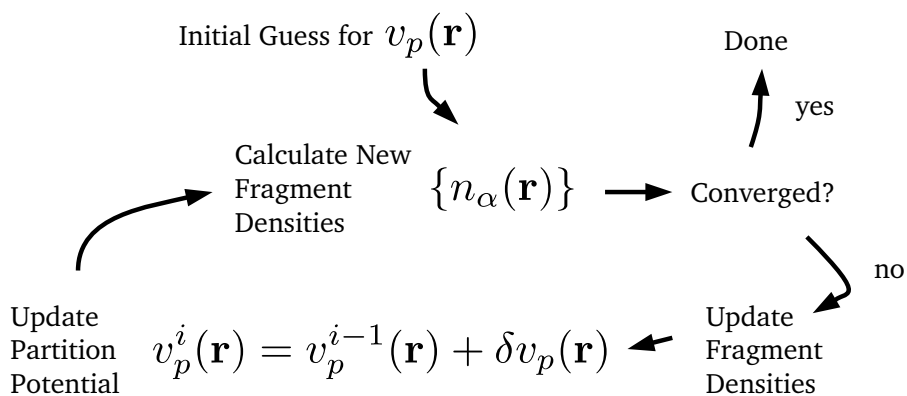


Figure 5.1. Flow diagram of simple PDFT SCF cycle used in inversion algorithms.

All the algorithms described here use a basic SCF algorithm or at least a variation of it as shown in figure 5.1. In many calculations in this dissertation simple linear mixing is used between newly calculated fragment densities and the fragment densities from the previous iterations.

$$n_{\alpha}^i(\mathbf{r}) = \beta n_{\alpha}(\mathbf{r}) + (1 - \beta)n_{\alpha}^{i-1}(\mathbf{r}) \quad (5.1)$$

Where β is a chosen parameter between 0 and 1. The primary difference between the algorithms described here is in the 'Update Partition Potential' step, where each algorithm specifies a different choice for the $\delta v_p(\mathbf{r})$.

The conceptually simplest methods are achieved in cases where the molecular density may be precomputed. This precomputed molecular density, $n_m(\mathbf{r})$, provides a target density for the fragment densities. The partition potential is updated at each iteration by simply comparing the sum of fragment densities with the target molecular density.

$$\delta v_p(\mathbf{r}) = \gamma \left(\sum_{\alpha} n_{\alpha}(\mathbf{r}) - n_m(\mathbf{r}) \right) \quad (5.2)$$

Here, γ must be a carefully chosen positive number. This algorithm may be understood in very simple terms. In regions of space where the sum of fragments has higher density than the target density the partition potential will increase and therefore push density away from these areas in the next iterations and similarly in regions where the fragment densities are less than the target density the partition potential will decrease, thereby pulling more electron density into that region. As expected this algorithm is slow and may not converge if γ is not well chosen. In particular, regions with small density may converge extremely slowly.

An alternative update procedure is to use a scaled error:

$$\delta v_p(\mathbf{r}) = \gamma \frac{(\sum_{\alpha} n_{\alpha}(\mathbf{r}) - n_m(\mathbf{r}))}{n_m(\mathbf{r})} \quad (5.3)$$

This works in a similar fashion to 5.2 but the asymptotic regions are given more importance. This update procedure works better than the previous update procedure, but still requires a carefully chosen parameter.

A more sophisticated update procedure is essentially a newton gradient-descent algorithm and uses the linear response of the fragments to determine the update to the partition potential.

$$\delta v_p(\mathbf{r}) = \int \chi_f^{-1}(\mathbf{r}, \mathbf{r}') (\sum_{\alpha} n_{\alpha}(\mathbf{r}') - n_m(\mathbf{r}')) d\mathbf{r}' \quad (5.4)$$

Where, χ is the response of the fragments to changes in the partition potential:

$$\chi_p(\mathbf{r}, \mathbf{r}') = \sum_{\alpha} \frac{n_{\alpha}(\mathbf{r})}{v_p(\mathbf{r}')} \quad (5.5)$$

These fragment responses may be calculated from first order perturbation theory using the occupied and unoccupied fragment orbitals [89]:

$$\frac{n_{\alpha}(\mathbf{r})}{v_p(\mathbf{r}')} = 2 \sum_i^{occ.} \sum_j^{unocc.} \frac{\phi_i^*(\mathbf{r}) \phi_a(\mathbf{r}) \phi_a^*(\mathbf{r}') \phi_i(\mathbf{r}')}{\epsilon_i - \epsilon_j} + c.c. \quad (5.6)$$

An alternative update procedure is used by Elliot et al. in 2010 [38] and Nafziger et al. in 2011 [2] (also Chapter 7). Unlike the previous update procedures this one does not rely on a precomputed density. The full derivation of the update formula can be found in Elliot et al., but we briefly describe how it works. At each step, k , the current guess for the partition potential is used to determine each fragment density. Then the sum of fragment densities is inverted to obtain its corresponding potential, $v[n_f^k(\mathbf{r})](\mathbf{r})$. This potential is compared to the molecular potential (which is the potential that produces the correct molecular density) in order to update the partition potential according to:

$$\delta v_p(\mathbf{r}) = (v(\mathbf{r}) - v[n_f](\mathbf{r})) \quad (5.7)$$

We can see that this update will only have a fixed point when $v(\mathbf{r}) - v[n_f(\mathbf{r})](\mathbf{r}) = 0$. The Hohenberg Kohn theorem ensures that this can only occur when the sum of fragment densities is equal to the molecular density.

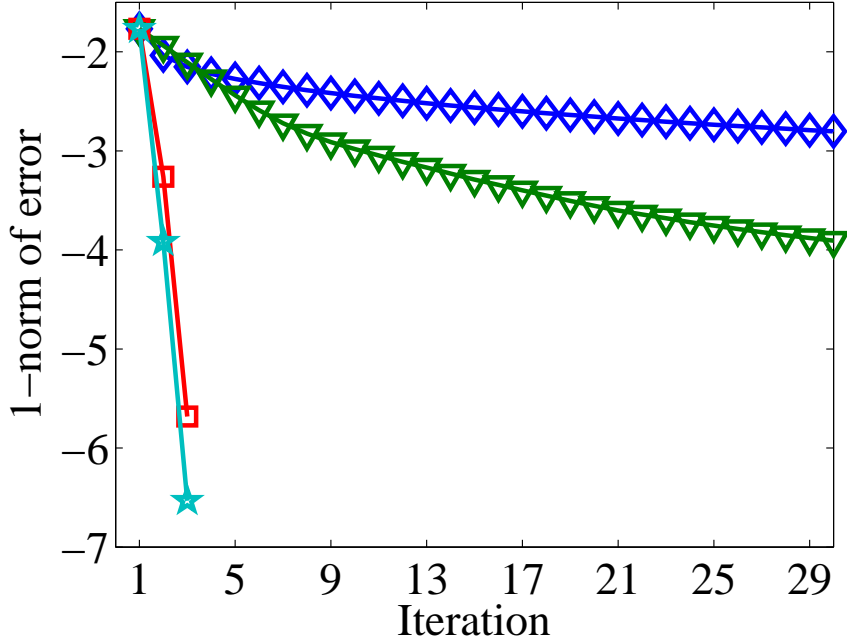


Figure 5.2. Comparison of convergence for simple 4-electron double-well 1-dimensional system using three different update procedures for the partition potential. The blue diamonds correspond to equation 5.2, the green triangles correspond to equation 5.3, red squares correspond to 5.4 and the cyan stars correspond to 5.7. The vertical axis shows the 1-norm of the error between the sum of fragment densities and the target density and the horizontal axis is the iteration number.

All these update equations are compared in figure 5.2. It is clear that the response update (equation 5.4) and the update from Elliot et al. [38] converge much faster than the other two update methods. However, the downside is that in the case of equation 5.4 the responses of each fragment must be calculated at each iteration and in the case of equation 5.7 the sum of the fragment densities must be inverted. Inverting the sum of fragment densities is a rather expensive procedure and so even though this procedure converges faster the calculation overall is slower. This method does have

the nice property that the molecular density does not need to be calculated ahead of time.

A final option for these inversion based algorithms is to use a pre-made constrained optimizer to directly minimize the fragment energy subject to the density constraint. This will generally be more robust than fixed update equations and may also be integrated directly with the optimization of fragment occupations.

A number of other methods have been developed that use inversion techniques to calculate embedding potentials exactly [2, 24, 25, 61, 79–82] within other fragment-based DFT methods. The inversion calculations used in these algorithms can have added difficulties when used with basis sets. We use a real-space grid and thus avoid many of the problems associated with inversions using basis sets. While inversions with basis sets are possible, greater care must be taken to ensure that the result is unambiguous [90].

5.2 Algorithms using the Non-Additive Kinetic Energy

If a model for the non-additive kinetic energy, T_s^{nad} , is available then it is possible to calculate all the functional derivatives of the partition energy with respect to the fragments. In this case equation 3.23 indicates how to calculate a new partition potential based on a set of fragment densities. Figure 5.3 displays a flow diagram indicating an SCF procedure that may be used.

This algorithm requires the calculation of functional derivative of all components of the partition energy as given in equation 3.3. Typically the hartree and exchange-correlation partition energy components are chosen to exactly reproduce KS-DFT calculations on the molecular system. In chapter 10 we will explore different approximation for these components which will reduce static-correlation and delocalization error. The most difficult component to calculate is the T_s^{nad} term. Exact calculation of this term as well as approximations to it will be discussed in the next chapter.

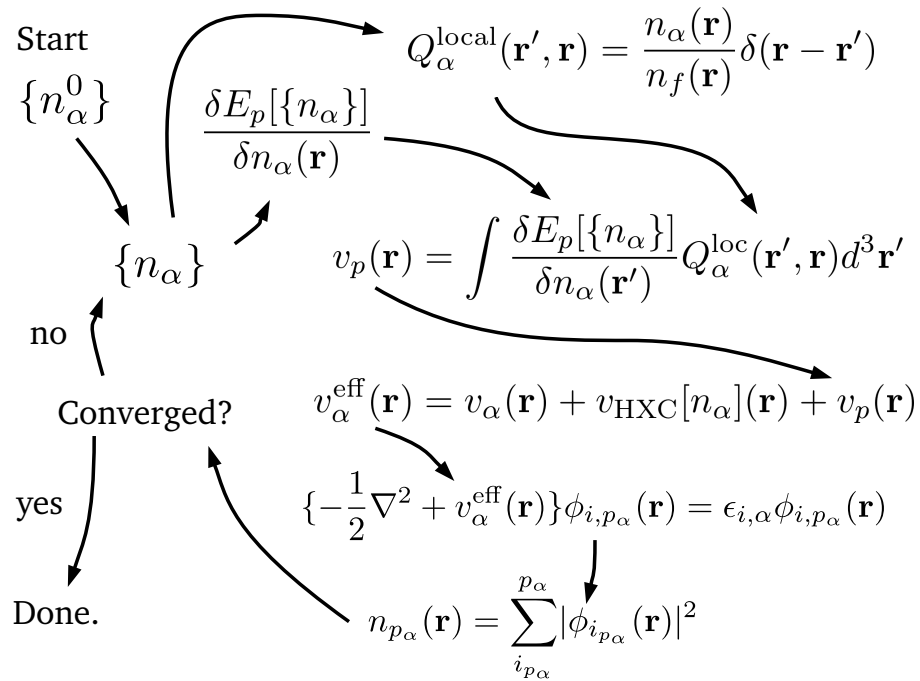


Figure 5.3. Flow diagram of PDFT SCF cycle with local-Q approximation and access to all functional derivatives of the partition energy.

6. Non-Additive Kinetic Energy

PDFT and other fragment based methods rely on explicit density-functionals for the non-additive non-interacting kinetic energy in order to improve computational efficiency as compared to standard KS-based methods. However, explicit density-functionals for the non-additive non-interacting kinetic energy come with many of the same problems as explicit density-functionals for the regular non-interacting kinetic energy. It is straightforward to write the kinetic energy as a functional of a set of orbitals, but it is much less clear how to write the kinetic energy as a functional of the density. This is in fact the reason for the success of the Kohn-Sham method in DFT as compared to the alternative computationally attractive orbital-free DFT. Nevertheless explicit density-functional modeling of non-additive kinetic energy hold some advantages over completely orbital-free methods. First, the non-additive kinetic energy is a smaller piece of the total energy and therefore a larger portion of the total energy expression is treated exactly. Second, as will be explored in the first section of this chapter, unlike the kinetic energy density, the non-additive kinetic energy density is unambiguously defined. Third, the fragments provide a new component with which to construct approximations. This idea will be explored in the final section of this chapter.

6.1 Unambiguous Non-Additive Kinetic Energy Density

There are several commonly used expressions which yield the kinetic energy of a set of orbitals. In general they may all be written as an integral over all points in space:

$$T_s = \int t_s(\mathbf{r}) d\mathbf{r} \quad (6.1)$$

While T_s is uniquely defined by the orbitals, there are actually an infinite number of expressions for $t_s(\mathbf{r})$ which will integrate to T_s . Two commonly used expressions are:

$$t_s^I(\mathbf{r}) = -\frac{1}{2} \sum_i^N \phi_i^*(\mathbf{r}) \nabla^2 \phi_i(\mathbf{r}) \quad (6.2)$$

and,

$$t_s^{II}(\mathbf{r}) = \frac{1}{2} \sum_i^N |\nabla \phi_i(\mathbf{r})|^2 \quad (6.3)$$

These expressions are related by adding a term of $\frac{1}{4} \nabla^2 n(\mathbf{r})$ to $t_s^I(\mathbf{r})$ [91]. An infinite number of expressions may be found by adding any arbitrary multiple of $\nabla^2 n(\mathbf{r})$ to equations 6.2 or 6.3. In general t_s^{II} has the advantage that it is positive definite, while t_s^I has the advantage of being closely related to the KS equations. In general, designers of density functionals need to pay attention to which of these two kinetic energy densities their approximation is trying to model [92].

The non-additive kinetic energy is typically expressed as a difference between functionals as in equation 4.4 however it may also be written as:

$$T_s^{\text{nad}} = \int t_s^{\text{nad}}(\mathbf{r}) d\mathbf{r} \quad (6.4)$$

This non-additive kinetic energy density may be written:

$$t_s^{\text{nad}}(\mathbf{r}) = t_s^m(\mathbf{r}) - \sum_{\alpha} t_s^{\alpha}(\mathbf{r}) \quad (6.5)$$

Where $t_s^m(\mathbf{r})$ is the kinetic energy density corresponding to the sum of fragment densities and $t_s^{\alpha}(\mathbf{r})$ is the kinetic energy density corresponding to the fragment α . As long as the same kinetic energy expression is used for both $t_s^m(\mathbf{r})$ and $t_s^{\alpha}(\mathbf{r})$ then $t_s^{\text{nad}}(\mathbf{r})$ will be the same. This is because $\nabla^2 n_f(\mathbf{r}) = \sum_{\alpha} \nabla^2 n_{\alpha}(\mathbf{r})$. Therefore differences between kinetic energy density expressions cancel out in the non-additive expression.

6.2 Implicit T_s^{nad} Functionals

The exact T_s may be formulated as an implicit density functional by performing a constrained search over wavefunctions yielding a particular density [89]:

$$T_s[n] = \min_{\Psi \rightarrow n} \langle \Psi | \hat{T} | \Psi \rangle \quad (6.6)$$

This expression can in turn be used to construct the non-additive kinetic energy. This constrained search is typically transformed into an unconstrained search with the addition of a lagrange multiplier:

$$T_s[n] = \min_{\Psi} [\langle \Psi | \hat{T} | \Psi \rangle + \int v_s(\mathbf{r}) (\langle \Psi | \hat{n}(\mathbf{r}) | \Psi \rangle - n(\mathbf{r})) d\mathbf{r}] \quad (6.7)$$

Here, $\hat{n}(\mathbf{r})$ is the density operator, which will yield the density of $|\Psi\rangle$ corresponding to the point \mathbf{r} . The lagrange multiplier, $v_s(\mathbf{r})$, can be identified as the KS potential. This optimization may then be performed numerically, by searching over potentials for v_s . $|\Psi\rangle$ may be represented as a single slater determinant and each orbital may be optimized by solving the euler equation 2.14. First and second derivatives may be used in the optimization of v_s as outlined in [89].

In order to calculate the functional derivatives of the kinetic energy, which is necessary for constructing the partition potential, we use the method mentioned by Jacob et al. [85] and implemented by both Fux et al. [61] and Goodpaster et al. [25]. This inversion yields the potential $v_s(\mathbf{r})$, and the corresponding chemical potential, μ_m . We can then use the euler equation 4.11 to find the functional derivative of the first term of Eq. 4.4. We can similarly use the potentials and chemical potentials corresponding to each n_p and n_{p+1} to obtain the functional derivative of the second term of equation 4.4. These potentials are available without the need for an inversion.

In the end we arrive at an expression for the functional derivative of the non-additive non-interacting kinetic energy with respect to one of the fragment densities.

$$\frac{\delta T_s^{\text{nad}}[\{n_\alpha\}]}{\delta n_\alpha(\mathbf{r})} = \mu_m - \mu_\alpha + v_s[n_\alpha](\mathbf{r}) - v_s[n_f](\mathbf{r}) \quad (6.8)$$

6.3 Two-Orbital approximation

In two orbital homonuclear diatomics one Kohn-Sham orbital will have gerade symmetry while the other orbital will have ungerade symmetry. By treating the fragment densities of these systems as somewhat like localized molecular orbitals we can construct approximations to these two orbitals. We first construct an approximation to the ungerade orbital:

$$\phi_{\text{ug}}(\mathbf{r}) = C(n_1(\mathbf{r})^{\frac{1}{2}} - n_2(\mathbf{r})^{\frac{1}{2}}) \quad (6.9)$$

This approximate orbital will have the correct symmetry and will be normalized by setting $C = \frac{1}{2}N/(\int(n_1(\mathbf{r})^{\frac{1}{2}} - n_2(\mathbf{r})^{\frac{1}{2}})^2 d^3\mathbf{r})^{\frac{1}{2}}$. After normalization we can construct the remaining gerade orbital from the remaining density.

$$\phi_{\text{g}}(\mathbf{r}) = \left(\frac{n_m(\mathbf{r})}{2} - \phi_{\text{ug}}^2(\mathbf{r}) \right)^{\frac{1}{2}} \quad (6.10)$$

Each approximate orbital will be normalized to half the total number of electrons.

For a simple visualization of how this approximation works we perform these calculations non-self consistently on a simple one-dimensional double-well system. We compare the approximated orbitals to orbitals obtained from inverting the sum of fragment densities as in 6.2. This comparison is made in figure 6.1. This approximation becomes exact as the separation goes to infinity, but still does quite well in the bonding region even at relatively short bond lengths.

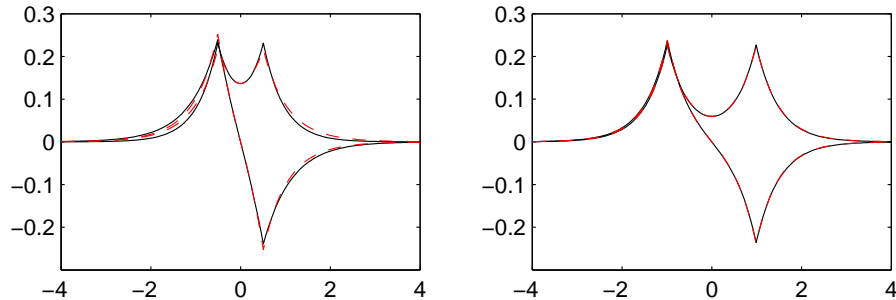


Figure 6.1. Approximated (dashed red) and Inverted (solid black) orbital comparison for two different bond separations. The top shows a bond separation of 1 atomic unit and the bottom shows a separation of 2 atomic units. The approximation gets significantly better with increasing bond separation, but even at smaller separation it does well in the bonding region between the two wells.

These approximated orbitals are then used to construct the non-additive kinetic energy:

$$T_{s,TO}^{\text{nad}} = \frac{M}{2} \int (|\nabla \phi_{\text{ug}}(\mathbf{r})|^2 + |\nabla \phi_{\text{g}}(\mathbf{r})|^2 - |\nabla n_1(\mathbf{r})^{\frac{1}{2}}|^2 - |\nabla n_2(\mathbf{r})^{\frac{1}{2}}|^2) d\mathbf{r} \quad (6.11)$$

We expect the optimal scale factor, M , should be a bit less than 1 for the Helium dimer. This is because the approximate orbitals are correctly normalized and do correspond to the sum of fragment densities. The kinetic energy follows a variational principle and therefore the correct kinetic energy for the two orbitals of the helium dimer must be less than the kinetic energy of our approximate orbitals. For other systems it is yet clear what an optimal choice for M should be.

6.4 Rare-Gas Dimers

The two orbital approximation is based on systems in which each fragment density is represented by a single orbital and the molecular density is represented by two orbitals, such as the Helium dimer. However, we can still apply the approximation

to any two fragment system. Figure 6.2 compares binding energy results for the smallest six rare-gas dimers for KS calculations, Thomas-Fermi T_s^{nad} and the Two-Orbital T_s^{nad} . These calculations are results of non-self-consistent calculations. In other words, isolated fragment densities are calculated and then superimposed in place at some fixed bond length. Then the partition energies are calculated for these frozen densities. This eliminates the need to calculate functional derivatives, and is equivalent to the method of Gordon and Kim [46].

It is clear that the $M = 1$ Two-Orbital T_s^{nad} by itself only works well in the case of the Helium dimer. However, we also plot a scaled version of the approximation where an optimal M is chosen for each system. When the optimal M value is chosen for each system there is nearly perfect agreement throughout the entire dissociation curve. These M values were chosen so that the depth of the binding energy matched the depth of the Kohn-Sham kinetic energy. Nevertheless the agreement between the scaled two-orbital approximation and the KS binding energies is impressive.

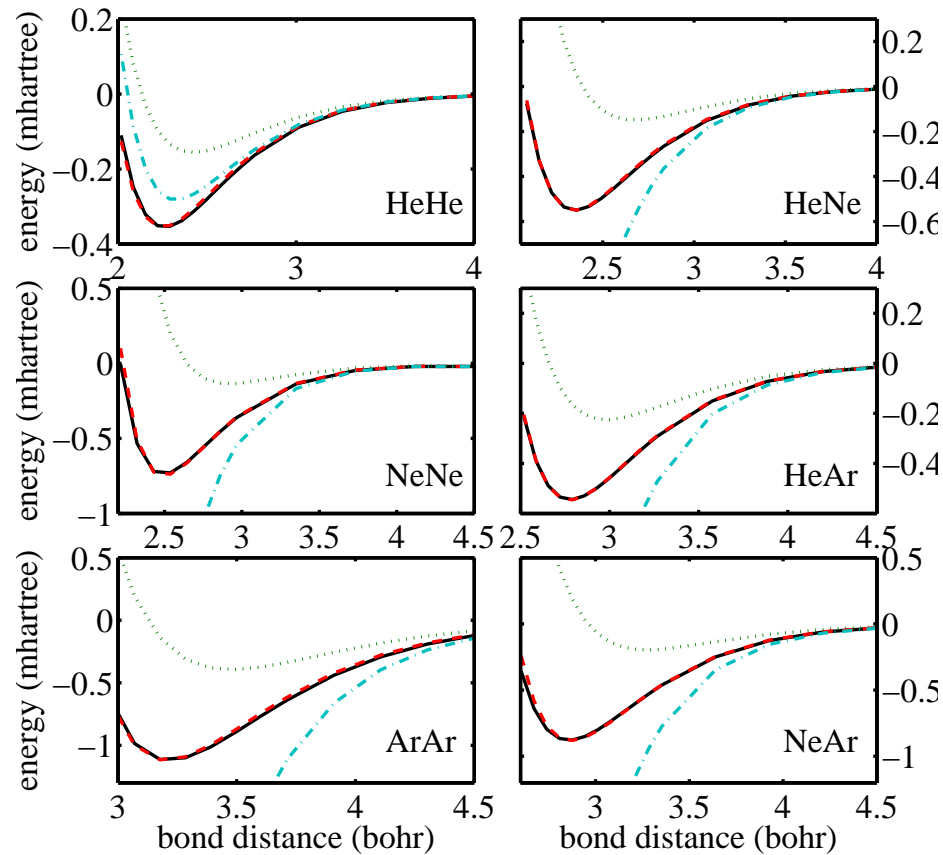


Figure 6.2. Binding energies for a variety of rare-gas dimers using the LDA. The solid black lines correspond to KS results. The other lines correspond to non-self consistent PDFT calculations performed on the isolated fragment densities fixed at various separations. The dotted and dashed lines correspond to using different non-additive kinetic energies. The dotted green line correspond to using the Thomas-Fermi kinetic energy functional. The cyan dot-dashed line corresponds to the two orbital approximation with $M = 1$. And the red dashed line corresponds to the two orbital approximation with optimally scaled M values. The optimal M values for each dimer are as follows: HeHe $M = 0.9249$, HeNe $M = 2.1187$, HeAr $M = 3.8641$, NeNe $M = 2.7930$, NeAr $M = 3.9959$, ArAr $M = 4.9287$

7. NWChem Implementation

This section contains work from an article entitled ‘Molecular binding energies from partition density functional theory’ written by the author, Qin Wu and Adam Wasserman, published in the Journal of Chemical Physics [2].

Approximate molecular calculations via standard Kohn-Sham Density Functional Theory are *exactly* reproduced by performing self-consistent calculations on isolated fragments via Partition Density Functional Theory [Phys. Rev. A **82**, 024501 (2010)]. We illustrate this with the binding curves of small diatomic molecules. We find that partition energies are in all cases qualitatively similar and numerically close to actual binding energies. We discuss qualitative features of the associated partition potentials.

In this work, by employing the Wu-Yang algorithm [89] for iterative inversion, we demonstrate convergence of the PDFT equations in small diatomic molecules using basis sets, and discuss qualitative features of partition potentials and partition-energy binding curves for He_2 , H_2 , and LiH . We show that the partition energies and potentials are interesting quantities in themselves, as they can be used as conceptual and interpretative tools.

First, we summarize the PDFT procedure in Sec.7.1, providing details of our implementation. Convergence of the PDFT equations is demonstrated in Sec.7.2 for the binding curves of He_2 , H_2 , and LiH , along with implications, qualitative features of partition potentials, and E_p -binding curves (in addition to actual binding curves). Concluding remarks are given in Sec.7.3.

7.1 Method

For the simplicity of discussion, we consider a compound with only two parts (A and B), but the method is equally applicable to any number of fragments. We also limit ourselves to fragments with fixed integer number of electrons, as in related recent work on embedding-DFT [25, 81, 82], only briefly discussing the issue of chemical potential equalization and fractional electron numbers.

In PDFT, the total energy is expressed as

$$E[n] = E_A[n_A] + E_B[n_B] + E_p[n_A, n_B] \quad (7.1)$$

where $n(\mathbf{r}) = n_A(\mathbf{r}) + n_B(\mathbf{r})$, and a common functional for E , E_A and E_B is assumed. As in standard DFT, the fragment energies E_α ($\alpha = A, B$) are given by:

$$E_\alpha[n_\alpha] = T_s[n_\alpha] + E_{\text{HXC}}[n_\alpha] + \int d\mathbf{r} v_\alpha(\mathbf{r}) n_\alpha(\mathbf{r}) \quad , \quad (7.2)$$

Where $v_\alpha(\mathbf{r})$ stands for the nuclear potential of fragment α (i.e. the fixed “external potential” for the electrons in the isolated fragment), the sum of which equals the molecular external potential $v(\mathbf{r}) = \sum_\alpha v_\alpha(\mathbf{r})$. In Eq.7.2, $T_s[n_\alpha]$ is the non-interacting kinetic energy, and $E_{\text{HXC}}[n_\alpha]$ is the sum of the Hartree and exchange-correlation energies for density n_α .

Equation 7.1 can be viewed as a formal and exact definition of E_p for the case of binary fragmentation. To minimize E by variations of fragments’ densities, which are built from their own sets of orbitals, we have the following Kohn-Sham equations:

$$\left[-\frac{1}{2} \nabla^2 + v_\alpha(\mathbf{r}) + v_p(\mathbf{r}) + v_{\text{HXC}}[n_\alpha](\mathbf{r}) \right] \phi_i^\alpha(\mathbf{r}) = \epsilon_i^\alpha \phi_i^\alpha(\mathbf{r}) \quad (7.3)$$

Here, α is a fragment index, i.e A or B in this work, for the sum of the Hartree and exchange-correlation potential corresponding to density n_α . The partition potential $v_p(\mathbf{r})$ is common to both fragments, thus has no α -index.

$v_p(\mathbf{r})$ could be derived explicitly if we knew the functional form of $E_p[\{n_\alpha\}]$ by taking its functional derivative with respect to variations of any fragment density: $v_p(\mathbf{r}) = \delta E_p[\{n_\alpha\}]/\delta n_\alpha$, to be evaluated at the densities that minimize $\sum_\alpha E_\alpha[n_\alpha]$. Without an expression for E_p as an explicit functional of the $\{n_\alpha\}$, it is also possible to derive $v_p(\mathbf{r})$ through an iterative procedure, which was first proposed in ref. [38] and we reiterate here.

Suppose that we are at the beginning of the k -th iteration. We obtain the fragment densities $n_\alpha^{(k)}$ by solving Eq. 7.3. We then construct a total pro-molecule density as $\tilde{n}^{(k)}(\mathbf{r}) = \sum n_\alpha^{(k)}(\mathbf{r})$. Because the effect of $v_p(\mathbf{r})$ is to make $\tilde{n}(\mathbf{r})$ the same as the true ground-state density of the whole system $n_s(\mathbf{r})$, the difference between $\tilde{n}^{(k)}(\mathbf{r})$ and $n_s(\mathbf{r})$ should be used as guidance to update $v_p^{(k)}(\mathbf{r})$. For that, we do a constrained search to find the energy of $\tilde{n}^{(k)}$, i.e.

$$E[\tilde{n}^{(k)}] = \min_{n \rightarrow \tilde{n}^{(k)}} E[n]. \quad (7.4)$$

This equation is to be interpreted together with an algorithm chosen to force an arbitrary density $n(\mathbf{r})$ to tend to a prescribed density $\tilde{n}^k(\mathbf{r})$. We employ the direct optimization algorithm of Wu and Yang [89], as used in calculating the frozen density energy in a recently-developed density based energy decomposition analysis [93]. Thus we rewrite the above equation as

$$E[\tilde{n}^{(k)}] = E_v[\tilde{n}^{(k)}] + E_{\text{HXC}}[\tilde{n}^{(k)}] + \min_{\Psi \rightarrow \tilde{n}^{(k)}} \{T_s[\Psi] + E_X[\Psi]\} \quad (7.5)$$

for a general hybrid functional, where $E_X[\Psi]$ represents a fraction of the HF exchange energy calculated from a Slater determinant Ψ that is constrained to yield $\tilde{n}^{(k)}$. At

the end of this minimization, the effective potential for the molecular Kohn-Sham orbitals is

$$v_{\text{eff}}(\mathbf{r}) = v_{\alpha}(\mathbf{r}) + v_{\text{HXC}}[\tilde{n}^{(k)}](\mathbf{r}) - v_{\lambda}(\mathbf{r}) \quad , \quad (7.6)$$

where $v_{\lambda}(\mathbf{r})$ is just the Lagrange multiplier corresponding to the density constraint and is expanded by a linear combination of atom-centered Gaussian functions. Because $v_{\lambda}(\mathbf{r})$ is used to force the density of the whole system to be $\tilde{n}^{(k)}$, its reverse should have the effect of making $\tilde{n}(\mathbf{r})$ more like $n_s(\mathbf{r})$. That is: we can set $v_p(\mathbf{r}) = -v_{\lambda}(\mathbf{r})$ and start the next iteration of fragment calculations. In practice, we update $v_p(\mathbf{r})$ as follows:

$$v_p^{(i)}(\mathbf{r}) = v_p^{(i-1)}(\mathbf{r}) - \theta * v_{\lambda}^{(i)}(\mathbf{r}) \quad , \quad (7.7)$$

where i is the iteration number, and θ is a damping factor between 0 and 1 used to control convergence. In our calculation, we have used $\theta = 1$ or $\theta = 0.25$. The convergence criterion we use is $|E[\tilde{n}_k] - E[n_s]| < \epsilon$, where $\epsilon = 10^{-6}$; this guarantees the converged energy is the same at the ground-state energy. The alternative choice of $|E[\tilde{n}_k] - E[\tilde{n}_{k-1}]| < \epsilon$ gives essentially the same results.

The partition potential obtained this way is given by [38]:

$$\begin{aligned} v_p(\mathbf{r}) = & \quad v(\mathbf{r}) + v_{\text{HXC}}[n](\mathbf{r}) - v_s[n](\mathbf{r}) \\ & - v_{\alpha}(\mathbf{r}) - v_{\text{HXC}}[n_{\alpha}](\mathbf{r}) + v_s[n_{\alpha}](\mathbf{r}) \quad , \end{aligned} \quad (7.8)$$

This expression is identical to the one derived by Wesolowski and Warshel for the orbital-free embedding potential in Frozen-Density Embedding [84], and to the ‘‘crystalline potential’’ introduced by Cortona [53]. At self-consistency, however, the potential obtained by those methods differs in general from our $v_p(\mathbf{r})$ because they are evaluated at different fragment densities: $v_p(\mathbf{r})$ results from a variational procedure that lies outside the domain of DFT: It is the Lagrange multiplier that relaxes the constraint that the sum of fragment densities be equal to the molecular density, while at the same time minimizing the sum of fragment energies. This minimization effectively

selects a unique $v_p(\mathbf{r})$ [22] out of the infinite set of acceptable orbital-free embedding potentials [84,94]. Furthermore, we emphasize that in our procedure we never fix the density of any part of our system, and all fragment densities are self-consistent with respect to one another.

We now mention a few differences with the numerical procedures employed in recent related work [25,61,79,81]. On the technical level, Fux et al. [61] used the same inversion algorithm we use in this work, whereas Goodpaster et al. [81] and Roncero et al. [79] employed the ZMP procedure [95]. The numerical problems associated with the use of a finite basis set are nicely explained in ref. [61], where a regularization procedure was used to smooth out the potentials. On the theoretical level, there is a difference on whether (and how) self-consistency is achieved. In refs. [79] and [61] the inversions are performed for a fixed density, since the main purpose in those works is to employ the resulting potentials for non-DFT calculations. Goodpaster et al. [81] perform the inversions self-consistently, as we do, but the self-consistency condition is different: Whereas we minimize the total energy calculated just like in usual DFT with chosen functionals (but under the density constraint), they minimize the kinetic energy by ZMP (Levy constrained search), and calculate E_{xc} with the resulting density on a grid.

7.2 Results

We demonstrate our calculations of $v_p(\mathbf{r})$ with three simple examples of diatomic systems: He_2 , H_2 , and LiH . In all calculations, Dunning’s aug-cc-pvTz basis set is used for molecular orbitals.

The counter-poise (CP) method is used to account for any Basis Set Superposition Error (BSSE). This approach is crucial in PDFT since $v_p(\mathbf{r})$ adds features to the fragment’s effective potential directly at the location of the other atom, precisely where the ghost basis functions are added [96].

The partition potential is expanded onto a set of basis functions. The size of the basis set for the partition potential determines how closely the KS molecular density is reproduced. In the limit of a complete basis set for the partition potential the sum of the fragments exactly matches the KS molecular density. We used five atom-centered Gaussian functions, and each center has five s-type functions, with even-tempered exponents of 2^n ; $n=0; \pm 2; \pm 4$.

In the following discussion, we will use several energy terms. Suppose E_A^0 and E_B^0 are the energies of the fragments with no influence of the partition potential; E_A^p and E_B^p are their energies with the converged partition potential; and E_{AB} is the energy of the compound. Therefore the binding energy is $E_{\text{bind}} = E_{AB} - (E_A^0 + E_B^0)$, and the partition energy is $E_p = E_{AB} - (E_A^p + E_B^p)$. We also define the preparation energy as $E_{\text{prep}} = (E_A^p + E_B^p) - (E_A^0 + E_B^0)$, which is the energy increase associated with the deformation of fragments. Clearly, $E_{\text{bind}} = E_{\text{prep}} + E_p$. We can also separate E_{prep} into the sum of fragment contributions, $E_{\text{prep}} = \sum_{\alpha} (E_{\text{prep}}^{\alpha}) = \sum_{\alpha} (E_{\alpha}^p - E_{\alpha}^0)$.

Table 7.1.

Comparison between molecular energies (a.u.) obtained from PDFT and from standard KS-DFT calculations using the same functional (B3LYP) and basis set (aug-cc-pvTz) for both.

	$E(\text{PDFT})$	$E(\text{DFT})$	Error
He ₂ ($R = 0.5$)	-5.569777622113	-5.569777624227	-3.80E-10
He ₂ ($R = 0.8$)	-5.709621657286	-5.709621657554	-4.69E-11
H ₂ (OSH)	-1.180048619032	-1.180048623628	-3.89E-09
H ₂ (CSH)	-1.180048619388	-1.180048623628	-3.59E-09

7.2.1 Helium Dimer

Rare-gas dimers are known to be weakly bound due to van der Waals interactions, which are not accurately captured by most density-functional approximations. However, because our procedure is general and independent of the exchange-correlation

functional, it is not critical to have the correct binding curve. Instead, for a clear demonstration, we use Hartree-Fock exchange only, which is known to be purely repulsive between nonpolar closed-shell systems. As shown in Fig. 7.1, the binding energy for He_2 is all positive and increases rapidly when the internuclear distance is shortened. It also shows that the preparation energy is very small, which means the deformation in He atoms is small, as expected in this system, though it starts to grow when the atoms are too close to each other. The repulsive nature of the interaction means that electron densities are pushed away from each other when the two He atoms are in close contact. Thus the internuclear region has a density decrease, as shown in Fig. 7.2. In PDFT, this density difference is achieved through deformation of each atom, due to the action of the partition potential. In Fig. 7.3 we plot v_p along the internuclear axis at a few representative internuclear distances. Clearly, v_p is most positive in the internuclear region, corresponding to the density deficiency. The magnitude of v_p decreases as the internuclear distance increases, until to a point that no v_p is needed.

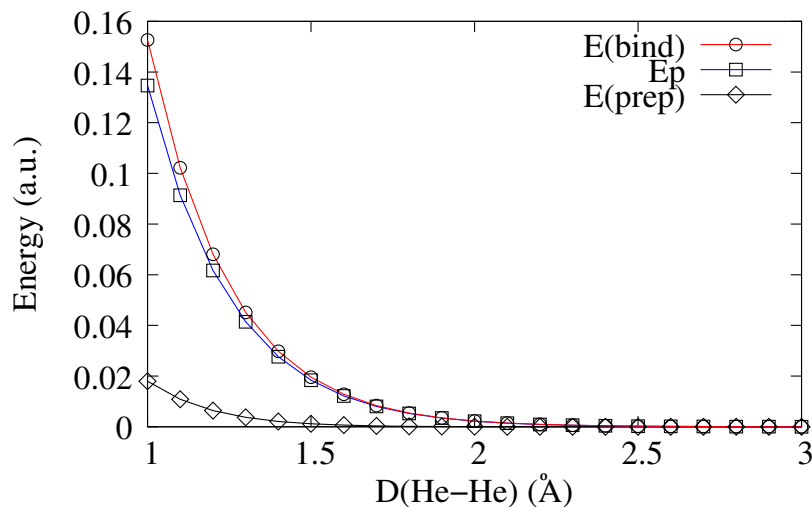


Figure 7.1. The Hartree-Fock energies for He_2 at different internuclear distances.

It is notable that there are significantly more oscillations in the partition potential than in the density differences. Some of the oscillations are physical. But there

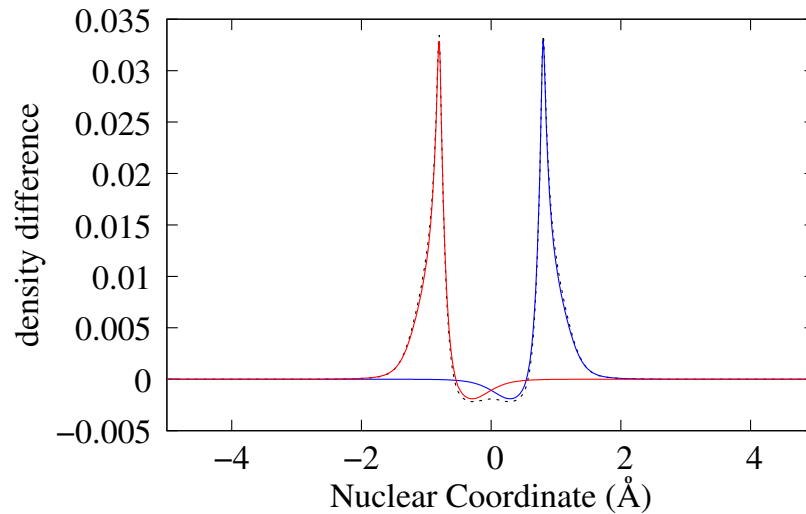


Figure 7.2. The density differences in He_2 as compared to the original atoms along the line through both nuclei. The total difference (dashed line) is the sum of the deformation in each atom (solid line). The nuclei coordinates are $R = \pm 0.8 \text{ \AA}$.

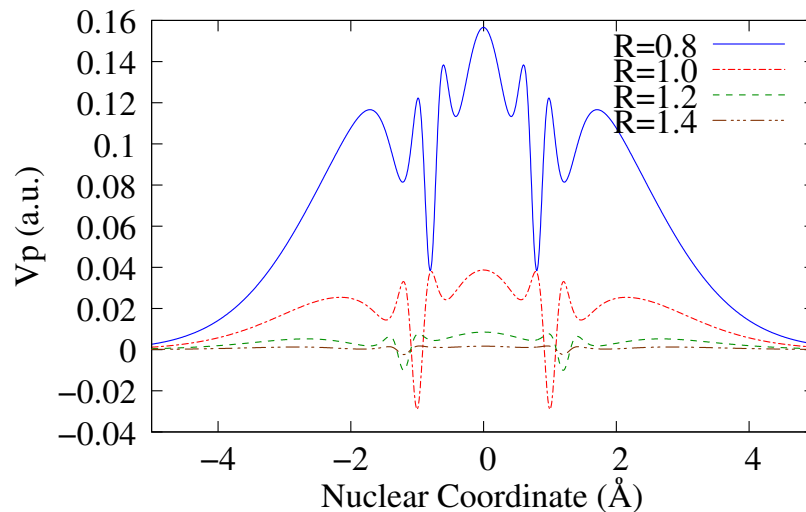


Figure 7.3. The partition potentials for He_2 at different internuclear distances. The nuclei are at $\pm R$.

are at least two other possible reasons contributing to the oscillations in v_p . One is pathological with gaussian densities, as nicely explained by Schipper, Gritsenko and Baerends [97]. The other is numerical and due to the fact that we expand v_p in a finite basis set [98]. We have used a small number of functions so as to limit the

oscillations caused by the expansion. However, we are unable to use non-gaussian densities yet, which makes it difficult to determine the nature of the oscillations.

Fig.7.4 demonstrates the agreement between the total density obtained via a direct molecular calculation, and the sum of fragments' densities obtained via PDFT. The numerical error can be made as small as desired by improving the quality of the basis set. Note that when the aug-cc-pvtz basis set is employed, the magnitude of the errors is no larger than 5% of the *difference* between the PDFT densities and isolated-atom densities, which amounts to error of less than 0.03% when compared to the actual molecular density. Table 7.1 gives the comparison between the molecular energies calculated via PDFT and those from a separate standard KS-DFT calculation.

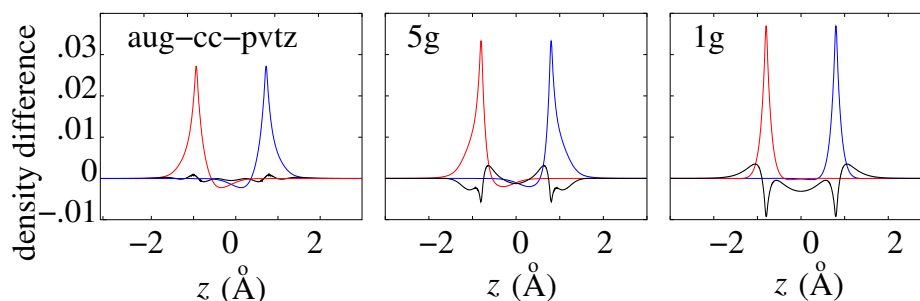


Figure 7.4. In each panel a different expansion is used for the partition potential of the Helium dimer (ng stands for n gaussians). The black curve is the difference between the sum of the densities and the molecular density from a standard DFT calculation (along the bond axis of the molecule). The red and blue curves are the differences between the PDFT fragments and the isolated fragments.

7.2.2 Hydrogen Molecule

For the covalently bonded molecule H_2 , the natural choice of partition is to use two open-shell H (OSH) atoms (spin up on the left, spin down on the right, or viceversa). Because the electronic ground-state of H_2 is a spin-singlet, we only consider the total charge density. Mathematically one could also use half-occupied closed-shell H atoms

(CSH) as the fragments (both left and right atoms having half spin-up, half spin down), thus without polarizing the spin. We study the energetics of both partitions as a function of the internuclear distance, using the B3LYP approximation to the exchange-correlation functional. For the H_2 molecule, we only consider restricted Kohn-Sham (RKS) calculations. It is well-known that a restricted calculation does poorly for large internuclear distances. The erroneous behavior is evident from the binding energy curve when the OSH atoms are used as the reference. As shown in figure 7.5, E_{bind} approaches a positive value instead of zero. On the other hand, when the CSH atoms are used as the reference, E_{bind} does go to zero. However, it becomes too large at the optimal bond length. The two binding curves are simply different by a constant shift, and this shift comes from the fact that OSH and CSH have different energies in the B3LYP approximation, while they should be degenerate with the exact functional [99].

In PDFT, the differences in the choice of fragments will not matter if the partition energy can compensate for the difference and yield identical total energy. In our case here, the two E_p are indeed quite different. However, the two E_p curves differ more than by a simple constant shift. The non-uniform difference can be appreciated by comparing the preparation energies. E_{prep} of OSH fragments is smaller at short internuclear distances than that of CSH fragments. However, the latter goes to zero at long distances while the former does not. At long distances, a restricted H_2 is essentially two half-occupied closed-shell H atoms, so the asymptotic behavior is not surprising. But it is interesting to see that at short distances, the OSH fragments pay less penalty to make their densities resemble that of the molecule.

7.2.3 Lithium Hydride

As another example, we consider the heteronuclear LiH. Within the formal partition theory, there is a unique choice of the fragments, with their chemical potentials equi-

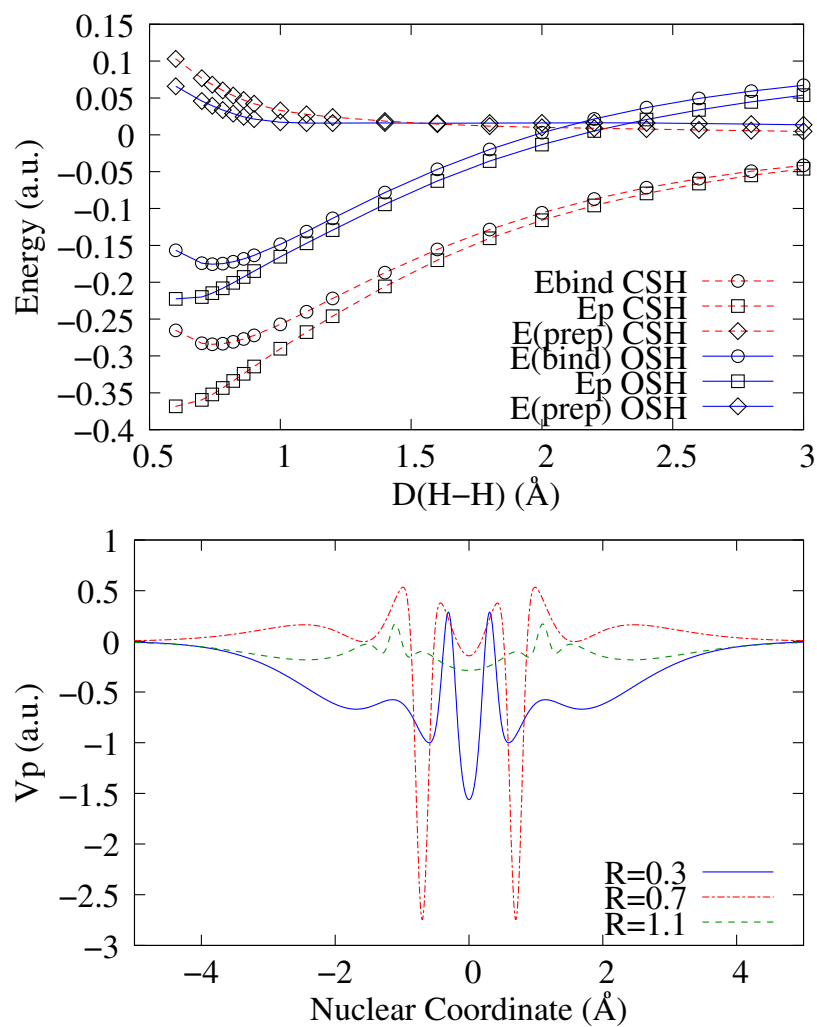


Figure 7.5. Top: The B3LYP energies for H_2 at different interatomic distances. The optimized bond length is $D = 0.743$ Å. Bottom: The partition potentials for H_2 at different internuclear distances.

librated. Achieving equilibration requires treating fragments with fractional number of electrons in the spirit of PPLB [21]. In that case, the number of electrons in a fragment is also a variable to be optimized. Because the partition potential will be different when the fragments change, the optimization of both the partition potential and the number of electrons is mutually dependent and has to be achieved simultaneously. We will treat this complexity in the future. In this work, we simply use fixed fragments and derive the corresponding partition potential, which we denote as $v_p^c(\mathbf{r})$ to indicate that the fragment occupations are constrained to integers.

Table 7.2.

Table of energies (in a.u.) for the two Lithium Hydride partitions. The molecular energy for LiH is -8.088129 and its HOMO is -0.1953916.

	Ionic		Neutral	
	Li ⁺	H ⁻	Li	H
E_α^p	-7.2847	-0.5033	-7.4450	-0.4968
E_α^0	-7.2859	-0.5364	-7.4927	-0.5023
E_{prep}^α	0.0013	0.0331	0.0477	0.0055
E_{prep}	0.0344		0.0533	
E_p	-0.3002		-0.1464	

Without the optimal fragments, we consider all possible partitions. For LiH, there are two possibilities. First, we use neutral atoms. Second, we use Li⁺ and H⁻. We do the partition at the optimized internuclear distance of 1.59 Å. Table 7.2 contains partition and preparation energies for both partition choices. The preparation energy of the ionic partition is lower than that of the neutral partition. This means it takes less energy to deform the ionic fragments so that they add to the molecular density than it does for the neutral fragments. This indicates that the correct partition is closer to the ionic case than the to neutral case. We also note that the partition energy is larger in the ionic case, which could be the result of Coulomb attraction. It is interesting that the hydrogen atom contributes the dominant portion of E_{prep} in the neutral case, whereas the lithium atom provides the dominant contribution in the ionic case.

Note that the ionic/neutral ratio of partition energies at the equilibrium bond length is close to two, and so is the inverse ratio of preparation energies. Assuming the fragment energy varies approximately linearly with occupation numbers, we speculate that the sum of fragment energies is minimized close to where the occupation number of the H atom is $5/3$ and the occupation number of the Li atom is about $7/3$ (this corresponds to $2/3$ of an electron transferred from Li to H). The correct answer can only be found by properly doing the calculation with the PPLB functional for the fragment energies. It will be very interesting to compare the resulting PDFT formal charges with the ones provided by other standard methods.

One surprising aspect of our results for integer numbers is that the partition potential for the ionic case is much stronger along the internuclear axis than the neutral one (Fig. 7.6), despite causing less distortion in fragments' energies.

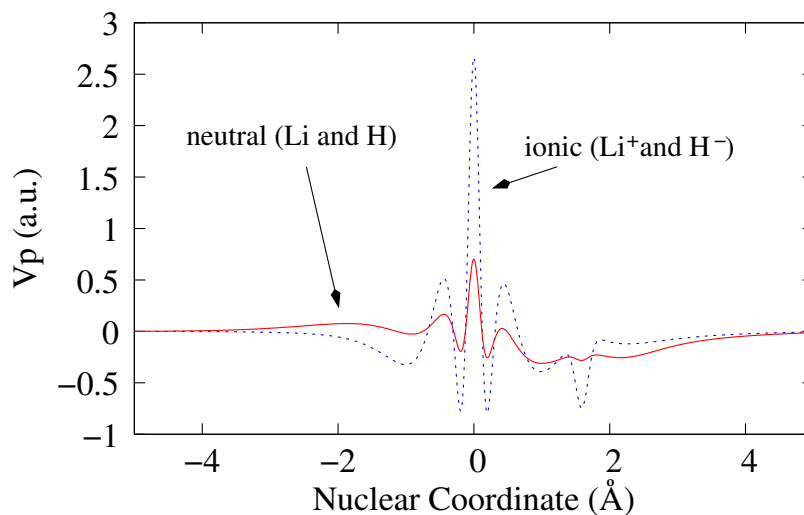


Figure 7.6. The B3LYP partition potentials for LiH (constrained to fixed integer occupation numbers). The Li atom is at $x = 0$ and H at $x = 1.59$ Å.

7.3 Concluding Remarks

Without having to solve directly the KS equations for the total external potential, we have shown how the PDFT algorithm of ref. [38] provides in practice the same answers via *fragment*-KS equations. In addition, this method yields fragment densities, fragment energies, and a partition potential that is shared by all fragments such that the sum of their densities reproduces the correct total density.

Although no physical meaning can be attached to a partition potential beyond the one implied by its definition (i.e. that it is the potential common to all fragments such that the sum of the fragment densities equals the total molecular density), some generic features of partition potentials seem to go in line with chemical intuition: they are positive when the interaction between fragments is repulsive (case of He_2 within Hartree-Fock), and their average magnitude is larger when the interaction between fragments is stronger. Similarly, the strength of the interaction between fragments is loosely measured by the magnitude of the partition energy. No such conclusion can be drawn for the preparation energy, however, as shown for the case of LiH where a somewhat larger preparation energy is associated with a much smaller partition potential (neutral vs. ionic partition). But the preparation energy can tell us about the *character* of the bond, an aspect that we plan to study further in future work.

It would also be useful to employ PDFT as a tool for the bond decomposition analysis suggested by Ruedenberg et al. [100–103] studied through the lens of variational reasoning. The difference between isolated and PDFT fragment densities encodes information about *contraction* and *polarization* and the energy associated with contraction and polarization is included in E_{prep} . Portions of the quasi-classical and electron-sharing shifts are included in E_p [100].

The case of LiH also highlights the need to go beyond integer numbers of electrons in our implementation of PDFT.

PDFT calculations also allow us to look at the dissociation problem from a different angle. For example, we found that open-shell fragments in H_2 are preferred at short inter-nuclear separations in the sense that they pay less penalty to make their densities resemble that of the molecule, but close-shell fragments are preferred at long separations. The respective preparation energies cross near the Coulson-Fischer point.

Finally, we point out that from weak (He_2) to relatively strong (H_2) chemical bonds, partition energies are qualitatively similar to actual binding energies, and numerically close to them (i.e. preparation energies are *small* in the cases studied). This similarity of E_p -curves to their corresponding binding curves suggests that approximations of $E_p[\{n_\alpha\}]$ as explicit functionals of the $\{n_\alpha\}$ might be very useful for practical computations. Not only would they provide a direct way to obtain the partition potentials by functional differentiation, circumventing the need of expensive inversion steps; sensible approximations would also lead to energies that are close to actual binding energies. This is analogous to what happens in KS-DFT, whose success is largely due to the fact that the sum of KS orbital energies is typically close to actual ground-state energies in chemical applications.

8. Near-Additivity and Non-Integer Occupations

This section contains work from an article entitled 'Fragment occupations in partition density functional theory', written by Rougang Tang, the author, and Adam Wasserman, published in Physical Chemistry Chemical Physics. [3]

In this chapter we investigate two interrelated aspects of PDFT: the connections between fragment densities obtained via different choices of fragmentation, for which we find “near-additivity”, and the nature of their corresponding fragment occupations. Whereas near-integer occupations arise for very large inter-fragment separations, strictly integer occupations appear for small inter-fragment separations. Cases where the fragment chemical potentials cannot be equalized lead to fragment occupations that lock into integers. These two interrelated aspects of PDFT that are critical to its further development both as a computational tool and as a conceptual tool in chemistry:

(1) In PDFT, a given choice of fragmentation yields a *unique* set of fragment densities [22]. Any choice of $\{v_\alpha(\mathbf{r})\}$ is allowed as long as equation 3.1 is satisfied. Different partitions lead to different partition potentials, but to the same total density $n(\mathbf{r})$, by construction. The question arises as to whether the set of fragment densities $\{n_\alpha^{\text{I}}(\mathbf{r})\}$ of one partition (partition I, with N_f^{I} fragments) is connected to the set $\{n_\alpha^{\text{II}}(\mathbf{r})\}$ of a different partition (partition II, with N_f^{II} fragments) in any way other than the obvious:

$$\sum_{\alpha}^{N_f^{\text{I}}} n_{\alpha}^{\text{I}}(\mathbf{r}) = \sum_{\alpha}^{N_f^{\text{II}}} n_{\alpha}^{\text{II}}(\mathbf{r}) \quad . \quad (8.1)$$

This is the question we explore in Sec.8.1. The importance of addressing it stems from the fact that, as in other fragment-based computational methods [25, 54, 61, 82, 104], PDFT might lead to electronic-structure algorithms that scale linearly with system-

size. It is thus desirable that the fragment densities be as transferable as possible, in the sense that once obtained for a given system, they can be used effectively as the starting point for electronic-structure calculations on other systems. It is also desirable that the fragment densities be additive, or near-additive, in the sense that when a molecule is partitioned in two different ways, I and II, the sum of fragment densities in a subset of partition I is close to the sum of the corresponding densities in partition II. We investigate when near-additivity holds, and when it does not.

(2) In order to demonstrate convergence of the algorithm to the *exact* molecular density and energy, the method has been applied in the past to one-dimensional model systems where the number of electrons per fragment did not exceed $N_\alpha = 2$ [38, 83], and to the homonuclear diatomic molecules H_2 , where $N_\alpha = 1$ (α labels the nuclei), and He_2 , where $N_\alpha = 2$ [2]. We demonstrate here convergence of the algorithm when $N_\alpha > 2$, and show that a difference in the number of occupied orbitals among fragments leads to the possibility of *cusps* in E_f as a function of occupation numbers, rather than minima. The number of electrons in each fragment may then lock into integers, an interesting result whose consequences we discuss. This is connected with point 1 above in that different choices of fragmentation lead naturally to different values of fragment occupations.

We focus on problem (1) in Section 8.1, and on problem (2) in Section 8.2. We summarize and conclude in Section 8.3.

8.1 Near-Additivity

We investigate how the fragment densities obtained via different choices of fragmentation (different choices for the set $\{v_\alpha(\mathbf{r})\}$) are related to each other. Since there is only one sensible way of partitioning a diatomic molecule (in two fragments), the smallest molecular systems necessary for addressing this problem require at least three atoms.

Triatomics: Consider a generic triatomic molecule ABC , and two possible partitions: Partition I: $A + B + C$ ($N_f^I = 3$), and partition II: $A + BC$ ($N_f^II = 2$). We ask: Could it ever be true that a fragment density for partition II exactly equals the sum of the corresponding fragment densities for partition I, i.e.,

$$n_{BC}^{II}(\mathbf{r}) = n_B^I(\mathbf{r}) + n_C^I(\mathbf{r}) \quad ? \quad (8.2)$$

We prove that this is *impossible*. If equation 8.2 were true, then it would also have to be true that $n_A^{II}(\mathbf{r}) = n_A^I(\mathbf{r})$ because equation 8.1 guarantees: $n_A^I(\mathbf{r}) + n_B^I(\mathbf{r}) + n_C^I(\mathbf{r}) = n_A^{II}(\mathbf{r}) + n_{BC}^{II}(\mathbf{r})$. This in turn would imply that $N_A^I = N_A^{II}$. Therefore, $n_A^I(\mathbf{r})$ would be the ground-state density of N_A^I electrons in $v_A(\mathbf{r}) + v_p^I(\mathbf{r})$ and $n_A^{II}(\mathbf{r})$ would be the ground-state density of the same number of electrons in $v_A(\mathbf{r}) + v_p^{II}(\mathbf{r})$. Since $v_A(\mathbf{r})$ is the same in both cases (the external potential due to nucleus A), the Hohenberg-Kohn theorem requires $v_p^I(\mathbf{r}) = v_p^{II}(\mathbf{r})$, but this is impossible because $v_p^I(\mathbf{r})$ must develop features between nuclei B and C that are absent from $v_p^{II}(\mathbf{r})$, since the latter treats BC as one entity. In the vicinity of atom A and the $A - B$ bond, however, it is natural to expect $v_p^I(\mathbf{r}) \approx v_p^{II}(\mathbf{r})$. This leads to

$$n_{BC}^{II}(\mathbf{r}) \approx n_B^I(\mathbf{r}) + n_C^I(\mathbf{r}) \quad , \quad (8.3)$$

i.e. *near-additivity* (see left panel of figure 8.1). From this perspective, near-additivity appears equivalent to Kohn's nearsightedness principle [105], but expressed in the framework of PDFT.

Figure 8.1 shows a simple numerical illustration of near-additivity for the case of one-dimensional linear chains. The fragment potentials v_α of equation 3.1 are given by inverse squared hyperbolic cosines of unit strength: $v_\alpha(x) = \cosh^{-2}(x + R_\alpha)$, where the separation $R = R_{\alpha+1} - R_\alpha$ between fragments is fixed at $R = 2\text{a.u.}$ The number of electrons is set equal to the number of sites (but they are kept non-interacting, so first two terms of equation 3.13 vanish). The thick solid line corresponds to the

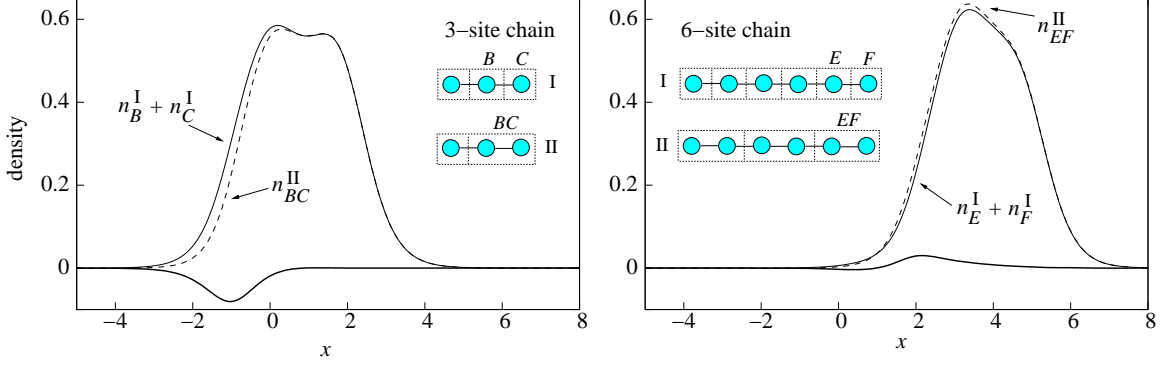


Figure 8.1. Comparison of the densities obtained for partitions I and II described in the text (Sec.8.1), for 3-site (left) and 6-site (right) linear chains, with 3 and 6 non-interacting electrons, respectively.

difference between $n_{BC}^{\text{II}}(x)$ and $n_B^{\text{I}}(x) + n_C^{\text{I}}(x)$. The difference is small, but clearly not zero. This *near-additivity* becomes more pronounced as the number of sites increases, as illustrated in the right panel of figure 8.1 for a 6-site chain. The difference between the two densities is smaller in magnitude (and of opposite sign) than that of the 3-site chain.

Returning to the 3-site chain, figure 8.2 shows how the fragment occupations change when $N = 2$ as the separation between the left and central wells is varied from zero to $R = 5\text{a.u.}$ while the separation between the two rightmost wells (B and C) is kept constant at $R = 3\text{a.u.}$ Near-additivity can be observed by comparing the occupation of fragment A from both partitioning schemes (N_A^{I} and N_A^{II}). They are essentially equal for all $R > 2$, so only at small separations $N_B^{\text{I}} + N_C^{\text{I}} \neq N_{BC}^{\text{II}}$. The R -dependence of occupation numbers is consistent with the one discussed in ref. [106] for heteronuclear diatomics. Four regions can be distinguished. Significant charge transfer from A to B (or to BC) is observed at large R , where the $A - B$ bond could be called ionic (region 1). The covalent character increases as R decreases down to a value where a plateau is observed (region 2), and further decreasing R leads to a rapid decrease of N_A^{I} and N_A^{II} down to zero, indicating a new ionic state (region 3). It is interesting that for unphysically small separations, the occupation numbers are

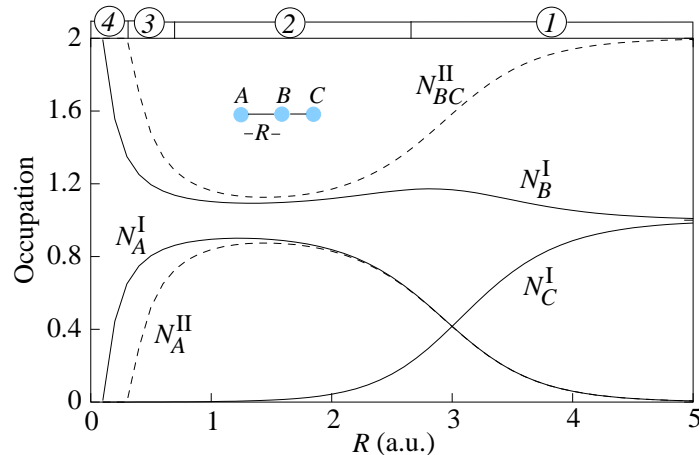


Figure 8.2. Change in the fragment occupations when one well of a two-electron triatomic system is separated from the other two. The variable R is the distance between the left well (A) and the central well (B). The distance between the center and right wells is 3.0a.u. The labels I and II indicate two different ways of partitioning. In I, each well has its own fragment, and in II the two rightmost wells share a fragment. The numbers 1→4 on the top horizontal axis correspond to the regions described in the text. Near-additivity can be observed by comparing the occupation of the first fragment from both partitioning schemes.

strictly integers, with $N_A^I = N_A^{II} = 0$ (united-atom region 4), and that this region is smaller for partition I than for partition II. We return to this point in Sec.8.2. We note that the value of R that determines the boundary between regions 1 and 2, where the electronic-structure of the molecule changes from being covalent to mixed ionic-covalent, coincides with that separation above which near-additivity holds.

Tetratomics: Consider a general tetratomic molecule $ABCD$, and two possible partitions: Partition I: $A + B + C + D$ ($N_f^I = 4$), and partition II: $AB + CD$ ($N_f^{II} = 2$). Any partitioning is allowed, even one with fragments whose atoms are not chemically bonded to each other. We ask the same question as before, equation 8.2: Could it be that $n_{CD}^{II}(\mathbf{r}) = n_C^I(\mathbf{r}) + n_D^I(\mathbf{r})$? This time, that possibility cannot be ruled out. The proof given above for triatomics does not hold anymore, as that proof required partitions I and II to share an identical fragment potential, which is not the case anymore. Interestingly, our numerical results in 4-site 1D chains would seem to suggest

that n_{CD}^{II} is indeed *identical* to $n_C^{\text{I}} + n_D^{\text{I}}$ (see figure 8.3), but a formal proof has not been found.

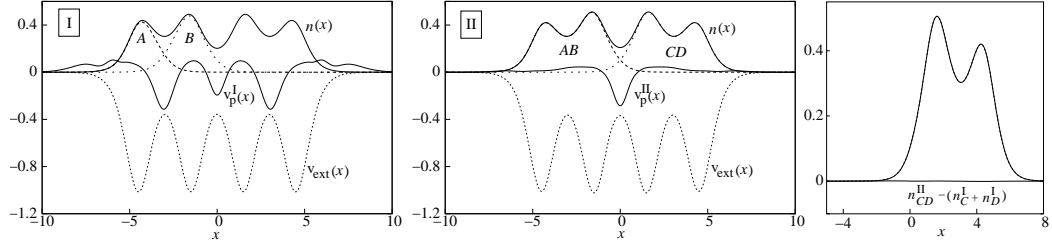


Figure 8.3. Two ways of fragmenting a 4-atom chain. *Left*: complete atomic fragmentation (partition I); *Center*: Binary fragmentation (partition II), where one fragment potential equals the sum of the two leftmost wells, and the other fragment potential equals the sum of the two wells on the right. The corresponding partition potentials are shown by thin solid lines; *Right*: Comparison of $n_C^{\text{I}}(x) + n_D^{\text{I}}(x)$ and $n_{CD}^{\text{II}}(x)$. They are identical within numerical accuracy.

For a third partition of the type $ABC + D$ it is again true that $n_{ABC}^{\text{III}}(\mathbf{r})$ is different from but nearly equal to $n_A^{\text{I}}(\mathbf{r}) + n_B^{\text{I}}(\mathbf{r}) + n_C^{\text{I}}(\mathbf{r})$ (not shown). These results suggest that there is a rich structure of interconnections between different choices of fragmentation, and further investigation in real systems with interacting electrons is worthwhile. Specifically, how general is the exact additivity result of figure 8.3? Is this due to the conservation of symmetry of $v_p(\mathbf{r})$ when going from partition I to partition II ?

8.2 Integers vs. Non-integers

Physically meaningful fractional occupations are obtained by treating the fragments in PDF-T as open systems that can exchange electrons with an infinite and distant reservoir [22]. Each fragment energy $E_\alpha[n_\alpha]$ is thus the *ensemble* ground-state energy of N_α electrons in the external potential $v_\alpha(\mathbf{r})$, given by [21, 107]:

$$E_\alpha[n_\alpha] = (2 - \nu_\alpha)E_\alpha[n_{p_\alpha}] + \nu_\alpha E_\alpha[n_{p_\alpha+2}] \quad , \quad (8.4)$$

where $0 < \nu_\alpha < 2$, and p_α and $p_\alpha+2$ are the even bordering integers of $N_\alpha = \int d\mathbf{r} n_\alpha(\mathbf{r})$. PDFT finds the set $\{\nu_\alpha\}$ that minimizes $E_f = \sum_\alpha E_\alpha[n_\alpha]$ for preselected sets of $\{p_\alpha\}$, to be varied as well. The resulting fragment densities are ensemble ground state densities of $N_\alpha = p_\alpha + \nu_\alpha$ electrons in $v_\alpha(\mathbf{r}) + v_p(\mathbf{r})$. For fixed potentials, the fragment energies have a piece-wise linear dependence on ν_α yielding constant fragment chemical potentials as dictated by PPLB [21]. However, for small changes in constrained occupation numbers, $v_p(\mathbf{r})$ may be allowed to change to ensure satisfaction of equation 3.5. This change in $v_p(\mathbf{r})$ has the effect of introducing small non-linearities in the dependence of E_f on the constrained occupation numbers. However, as long as these changes in $v_p(\mathbf{r})$ are small compared with the fragment potentials, $v_\alpha(\mathbf{r})$, the ν_α -dependence of $E_\alpha[n_\alpha]$ remains close to piece-wise linear, and the ν_α -dependence of fragment chemical potentials remain close to piecewise constant.

The minimum of E_f is to be found with respect to variations of the $\{n_\alpha\}$ and the $\{N_\alpha\}$. At that minimum, achieved in general for non-integer numbers, all fragments have the same HOMO energy, and electronegativity equalization holds throughout the molecule [37]. There are cases, however, where electronegativity equalization cannot be established, and the fragment occupation numbers lock into integers.

Cusps in E_f vs. $\{N_\alpha\}$: Start with a case where we know in advance the optimum set of $\{N_\alpha\}$. For example, for a homonuclear diatomic molecule with 4 electrons, we know in advance that a partition in two atomic fragments will place 2 electrons per fragment. The left panel in figure 8.4 shows the behavior of E_f along with the individual fragment contributions for all fragment occupations between 0 and 4. Since no more than 2 electrons are allowed in the same orbital, and the energy spectrum of each fragment is discrete, the cusp at $N_\alpha = 2$ appears because the chemical potential of both fragments jumps discontinuously at $N_\alpha = 2$ (bottom right panel of figure 8.4), and the transfer of even $\nu_\alpha \rightarrow 0^+$ electrons from left to right (or viceversa) raises E_f . But what happens with this cusp as the fragments become inequivalent? The right panels of figure 8.4 show analogous plots for the 1d-model of a heteronuclear diatomic

molecule: 4 electrons are placed in the double-well potential $v(x) = -Z_A \cosh^{-2}(x - 1.5) - Z_B \cosh^{-2}(x + 1.5)$, with $Z_A = 3 > Z_B = 1$. Although the chemical-potential discontinuities persist at $N_\alpha = 2$, E_f reaches a true minimum, rather than an infimum, when the two fragment chemical potentials cross at $N_A = 1.018$ and $N_B = 2.982$. For the parameters chosen in figure 8.4, approximately 1 electron transfers from B to A , minimizing E_f . The cusp remains an infimum as long as Z_A is not more than about one unit of charge higher than Z_B . But as Z_A becomes larger than $\sim 2Z_B$, the infimum becomes a minimum at non-integer occupations, and this minimum shifts smoothly from $N_A \approx 2$ to $N_A \approx 4$ as Z_A increases from about 2 to 4 (figure 8.5).

We may also be interested in the chemical quality of the fragments in the integer versus non-integer regions. Do the fragments still behave as expected while they are in this integer region? figure 8.5 compares the fragment densities for three different values of Z_A . In each case we can see that the fragment densities are well localized and decay monotonically from their maxima.

We also observed the appearance of cusps in E_f for a family of 1-d chains such as those discussed in Sec.8.1. We report results for 1-d chains with inverse $\cosh^2(x)$ potentials of unit strength, separated by a distance of 2.0a.u. Each chain has as many electrons as potential wells (non-interacting, but satisfying Pauli's principle). For a 3-site chain, within the $A - BC$ partition, the infimum of E_f is not a minimum but a cusp that appears clearly when fragment A has exactly one electron, and fragment BC has two. The discontinuity of E_f vs. $\{N_\alpha\}$ arises again from the impossibility to equalize the two HOMOs. The BC fragment has a fully occupied HOMO whereas the A -fragment has a singly occupied HOMO that lies in between the BC -HOMO and the BC -LUMO. Because the BC -HOMO is fully occupied, the transfer of even a small fraction of an electron from the A -HOMO would have to move into the BC -LUMO raising E_f . The transfer of a fraction of an electron from the BC -HOMO would go into the higher-lying A -HOMO, also raising E_f . The partition potential at the cusp is able to reproduce the exact molecular density, but not to level the HOMOS.

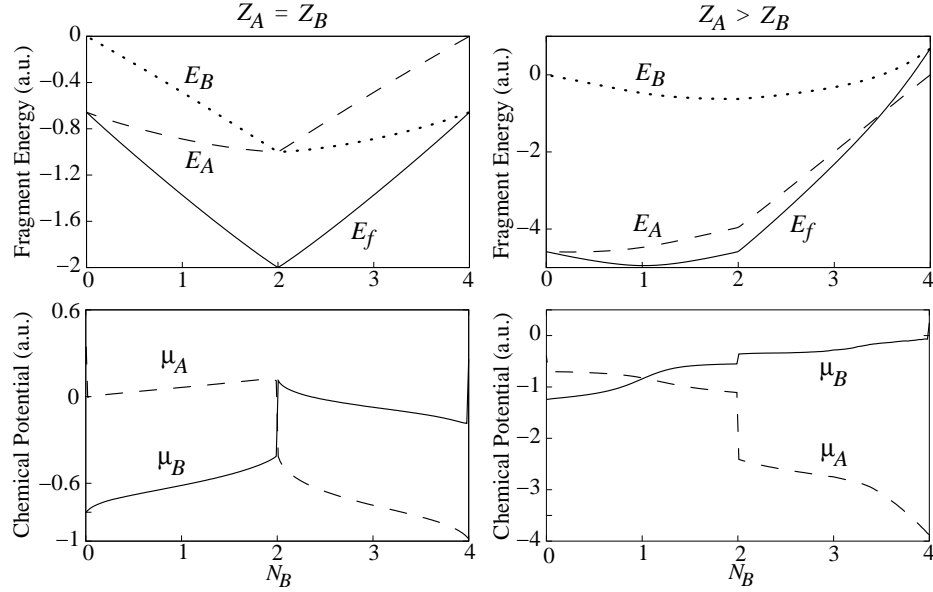


Figure 8.4. *Top left:* Fragment energies and their sum versus constrained occupation number of fragment 1 for a homonuclear double-well potential with 4 non-interacting electrons. The correct PDFT occupation numbers are the ones which minimize the sum of the fragment energies. The cusp at $N_1 = 2$ forces the occupation numbers to be integers. *Bottom left:* Fragment chemical potentials versus constrained occupation number of fragment 1. The correct PDFT occupation numbers are the ones which equalize the fragment chemical potentials. The discontinuities in the chemical potentials for the homonuclear case are such that equalization can not be obtained, and instead the occupation numbers are forced to be integers. *Top right:* Same as top-left, but for a heteronuclear double-well, $v(x) = -Z_A \cosh^{-2}(x-1.5) - Z_B \cosh^{-2}(x+1.5)$, with $Z_A = 3$ and $Z_B = 1$. *Left:* The infimum is no longer a cusp, but a minimum near $N_B = 1.0$. *Bottom right:* The two chemical potentials cross near $N_B = 1.0$, where E_f is minimized.

Partitioning a 6-site chain (with 6 non-interacting electrons) into 3 equivalent fragments also shows a cusp at $N_\alpha = 2$. The partition potential lowers the HOMO of the central fragment relative to the HOMO of the two side fragments. Fractions of electrons would tend to flow from the sides into the central fragment, but its HOMO is fully occupied, and occupying the LUMO would raise E_f . On the other hand, when a 5-site chain with 5 non-interacting electrons is partitioned into a 4-site and a 1-site fragment, there is no cusp in E_f , which gets minimized when the occupation of the

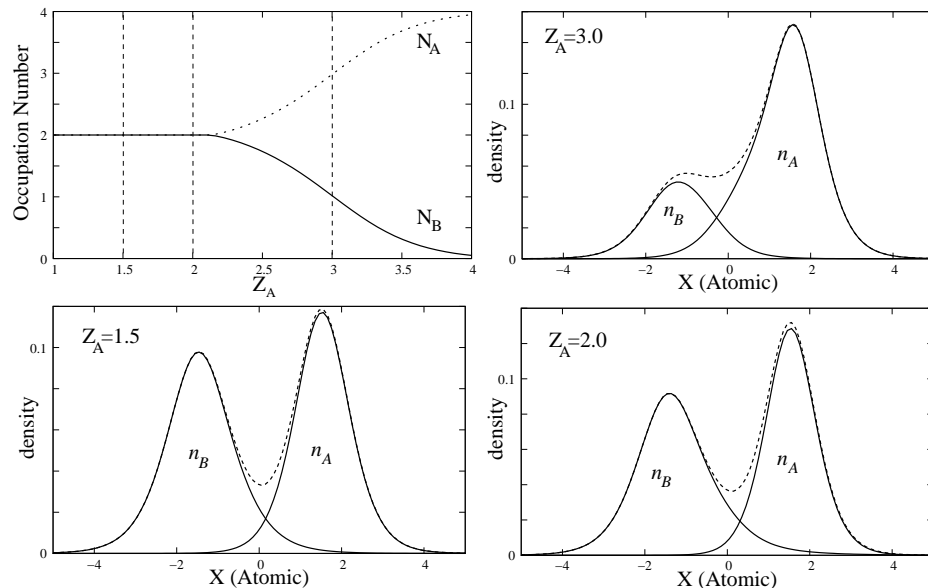


Figure 8.5. The top right panel shows fragment occupations versus Z_A , for $v(x) = -Z_A \cosh^{-2}(x - 1.5) - \cosh^{-2}(x + 1.5)$. For $Z_A < 2$, the cusp in E_f forces the occupation numbers into integer values as seen in the upper left panel of figure 8.4. Above this value the occupation numbers take on non-integer values as seen in the top right panel of figure 8.4. The other panels show the fragment densities at the various Z_A values indicated in the top right panel.

1-site fragment is close to 0.9. The partition potential pulls the 4-site LUMO down enough so that 0.1 electron flows into it from the 1-site HOMO, minimizing E_f while equalizing the chemical potentials.

Finally, we return to the case of a heteronuclear diatomic molecule and point out a connection between fragment occupations and inter-fragment separations:

Small separations lead to integer occupations: As noted in relation to figure 8.2, very small separations between neighboring fragments lead to the occupation numbers which are locked into integers. The left panel of figure 8.6 shows the occupation of the weaker fragment in a 1D hetero-nuclear double well with 2 non-interacting electrons. The horizontal axis is the separation between the wells. Each curve corresponds to a different value of ΔZ , the difference in strength between the two wells. When

the separation goes below some finite value (which decreases as ΔZ decreases), the electron ends up 100% in the fragment with the deeper well. In these cases with integer fragment occupations the two fragment chemical potentials never cross and the partition potential is exactly equal to the potential for the unoccupied fragment.

New qualitative features appear with the possibility of occupying different number of orbitals in different fragments. For example, with 4 non-interacting electrons in the same external potential as before, the covalent character of the bond may return at very small separations, leaving only a range of separations for which the chemical potentials cannot be equalized. For our model system, when $\Delta Z = 1.4$, the fragment occupations are integers only within the range $0.6 < R < 1.2$. For smaller values of ΔZ there is no covalent bond formation at small separations; for larger values of ΔZ there are no separations for which the fragments have strictly integer occupations.

At intermediate separations (region 2 in figure 8.2), the two chemical potentials cross at a fractional number that remains approximately constant for a relatively large range of separations. The smaller the value of ΔZ , the larger the extent of this plateau, and the smaller the range of separations for which chemical potential equalization cannot be achieved.

Large separations lead to near-integer occupations: As the separation grows to infinity, the crossing of the two chemical potentials occurs at fractional occupations that approach the integers asymptotically, becoming strictly integers only at $R = \infty$.

An alternative method for treating non-integer occupations was very recently proposed in the context of embedding theory [24]. It would be interesting to see if that method leads to the same conclusions reported here.

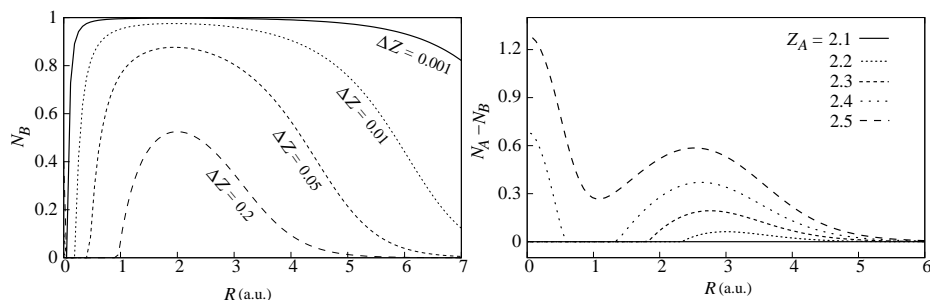


Figure 8.6. Occupation number of the shallower well versus separation (R) for a heteronuclear double well $v(x) = -Z_A \cosh^{-2}(x - R/2) - Z_B \cosh^{-2}(x + R/2)$ populated with 2 electrons (left panel), and 4 electrons (right panel). Various values of $\Delta Z = Z_A - Z_B$ are shown. *Left:* As the separation grows to infinity, the occupation numbers approach integers and for certain ΔZ at close separations the occupations are strictly integers. *Right:* The vertical axis on the right panel corresponds to the occupation of the deeper well (A) minus the occupation of the shallower well (B). The shallower well is fixed at a strength of 1.0 and the deeper well has a strength of Z_A which varies from 2.1 to 2.5. We can again observe that as the separation goes to infinity the occupation numbers approach integers and for certain ΔZ at close separations the occupations are integers. We also note that compared to the 2-electron case, the occupation numbers are much stiffer and require much larger heteronuclear differences to cause transfer.

8.3 Concluding Remarks

Even though PDFT provides an unambiguous prescription for obtaining a set of fragment densities for a given choice of fragmentation, the formalism itself does not tell us how to optimize that choice. It should be possible to establish principles or rules to determine an optimal choice of fragmentation according to pre-defined criteria. Maximization of the *near-additivity* discussed in this work could be one such criterion. If near-additivity holds, then the vast empirical knowledge encompassed by many rules of organic chemistry, for example, could be phrased in a simple but rigorous way in the language of PDFT [37].

To summarize, we have found that the sum of fragment densities belonging to a subset of the PDFT densities obtained for a given partition can be exactly equal (case of tetratomics) or nearly equal (case of triatomics) to elements of the set of densities corresponding to a different partition. As a function of separation between fragments, the onset of near-additivity coincides with a change of character in the relevant chemical bonds, at least in the 1d-models studied in this work.

As a function of fragment occupations, we observed the appearance of cusps in the sum of fragment energies, causing the fragments to accept only integer numbers of electrons. The cusps disappear when the fragment chemical potentials are equalized at non-integer fragment occupations. These cusps are connected with other discontinuity problems in ground-state DFT [21, 99], a topic we will explore in future work.

Future work also includes determining the performance of PDFT for prototype covalent, ionic, and metallic bonds. We plan to test the transferability of atomic properties and compare with other popular density-partitioning schemes. Our results on model systems [43] indicate that the fragment dipoles obtained by PDFT are more adjusted to chemical intuition and more transferable than those obtained by the partitioning schemes of Bader, Voronoi, and Hirschfeld. To establish the generality of these statements, it is critical to carry out more extensive studies.

This work is also a step towards a larger goal that should provide new opportunities for QM/MM applications and linear-scaling algorithms for efficient electronic-structure calculations of large systems.

9. CADMium

9.1 Benchmark PDFT calculations for Homo-nuclear Diatomic Molecules

This section contains work from the review article entitled ‘Density-Based Partitioning Methods for Ground-State Molecular Calculations’, written by the author and Adam Wasserman published in the Journal of Physical Chemistry A. [1]

In order to obtain benchmark PDFT results free of basis-set errors, we use our own all-electron real-space code (CADMium, for “Chemical Atoms in Diatomic Molecules”). Following the work of many others [108–112] we use prolate spheroidal coordinates to create a two-dimensional mesh. We then solve the Kohn Sham equations on this mesh, treating the cylindrical problem analytically. We used the Libxc package to evaluate XC-functionals [113].

Table 9.1 displays energies for several diatomic molecules along with the sum of fragment energies, the partition energy, and its components. The partition energy is strictly electronic and does not include contributions from non-additive nuclear-nuclear repulsion V_{nn}^{nad} . However, it is interesting to note that the magnitude of the electronic partition energy is consistently close to, but not equal to, V_{nn}^{nad} . The classical electrostatic terms: V_{nn}^{nad} , V_{nuc}^{nad} , and E_H^{nad} sum to approximately zero.

Also, in Figures 9.1 - 9.2, the partition potentials for several diatomics are compared along with the density difference between one of the two fragments and the corresponding isolated fragment density. The isolated fragment and the fragment in the molecule share the same potential except for the partition potential which deforms the fragment in the molecule. In general, we can see that the partition potential typically has an attractive well in between the two fragments, pulling some of the fragment

Table 9.1.

Energies and components of E_p , in atomic units. The LDA is used in all calculations (except in the first line corresponding to H_2^+ , where the exact functional for H_2^+ is used). Calculations are performed at equilibrium geometries, except for He_2 .

	D	E_f	E_p	V_{nn}^{nad}	V_{ext}^{nad}	T_s^{nad}	E_H^{nad}	E_{XC}^{nad}
$H_2^+(ex)$	2.0	-0.4470	-0.6556	0.5	-0.5704	-0.0852	-0.0421	0.0421
H_2^+	2.0	-0.4250	-0.6589	0.5	-0.5654	-0.0818	-0.0457	0.0341
H_2	1.446	-0.9119	-0.9173	0.6916	-1.3476	-0.1521	0.5842	-0.0019
He_2	6	-5.6689	-0.6668	0.6667	-1.3334	0.00004	0.6668	-0.0001
Li_2	5.122	-14.6750	-1.8068	1.7571	-3.6781	0.0049	1.8866	-0.0201
Be_2	4.522	-28.8749	-3.5770	3.5383	-7.1230	0.0604	3.5338	-0.0001

density into the bonding region. It also contains features closer to the nuclei, where it reshapes the spherical isolated fragments into fragments that fit into the molecule.

Figure 3.4 displays these same partition potentials but only along the bond axis, to compare v_p for the different molecules. The singularities in the partition potentials of H_2^+ and H_2 are clearly visible, and are also visible but smaller for Li_2 and Be_2 . We note that the partition potentials for H_2^+ and H_2 are the largest, followed by Be_2 and then Li_2 . He_2 has the smallest partition potential.

To analyze $v_p(\mathbf{r})$, it is useful to split it into components, in the same way as the energy. These components are compared in Figure 9.3. The Hartree and the external potential components are larger in magnitude than the other components, but they have opposite sign so their sum is plotted for better comparison. We may compare the relative sizes of the components in each partition potential. For H_2 , the Hartree plus external contribution plays a dominant role, while in the molecules with larger bond lengths the kinetic component plays an increasingly important role. In He_2 , the exchange-correlation and kinetic components play comparable roles, while the Hartree plus external potential term is relatively small.

For the case of H_2^+ we can compare results using LDA with exact PDFT results. Figure 9.4 displays the components of the partition potential for H_2^+ using LDA. In

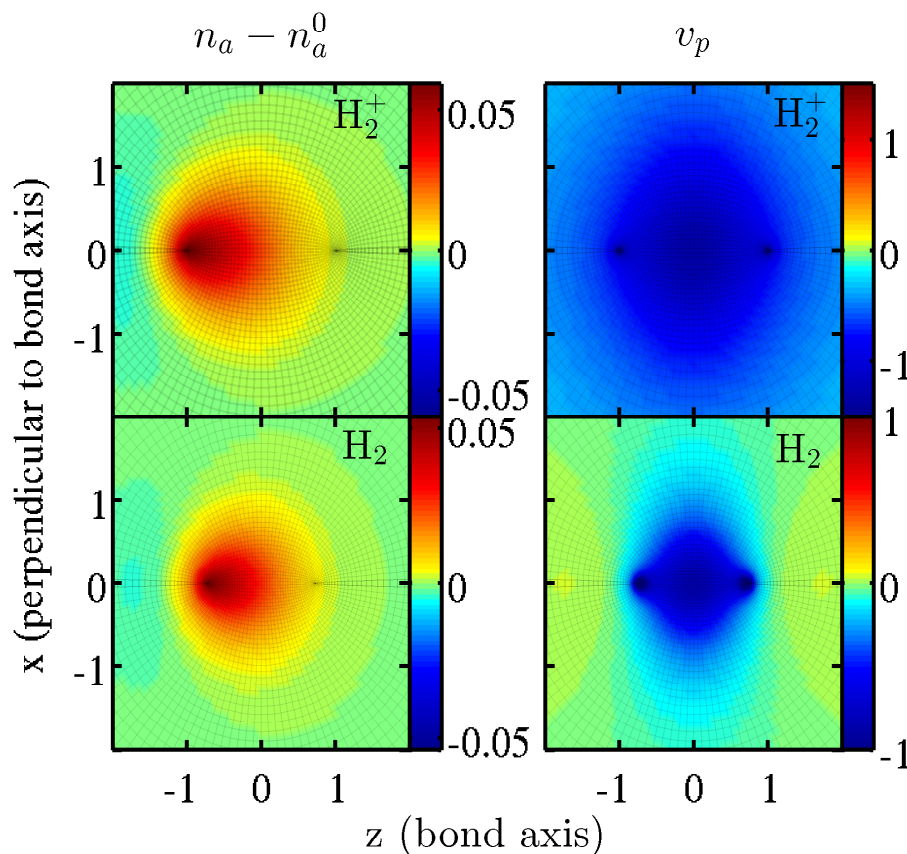


Figure 9.1. PDFT(LDA) calculations on H_2^+ and H_2 . The left column displays the difference between the left fragment density and the isolated atomic density while the right column displays the corresponding partition potential. The density for the fragment in the molecule sits in the same potential but with the addition of the partition potential. Thus, the partition potential is responsible for deformations of the isolated density into the fragment density in the molecule. In both plots, the partition potential is depressed in the bonding region (see also Figure 3.4), increasing the density in that region.

the exact case, the Hartree term exactly cancels with the exchange term leaving a total HXC contribution of zero. We can see that while the LDA XC component is close to canceling the Hartree contribution, it does not completely succeed.

Spin decomposition is tricky, as usual. Consider the case of Li_2 , shown in Figure 9.5. Each of the Li fragments has 3 electrons. Since the ground state of the molecule

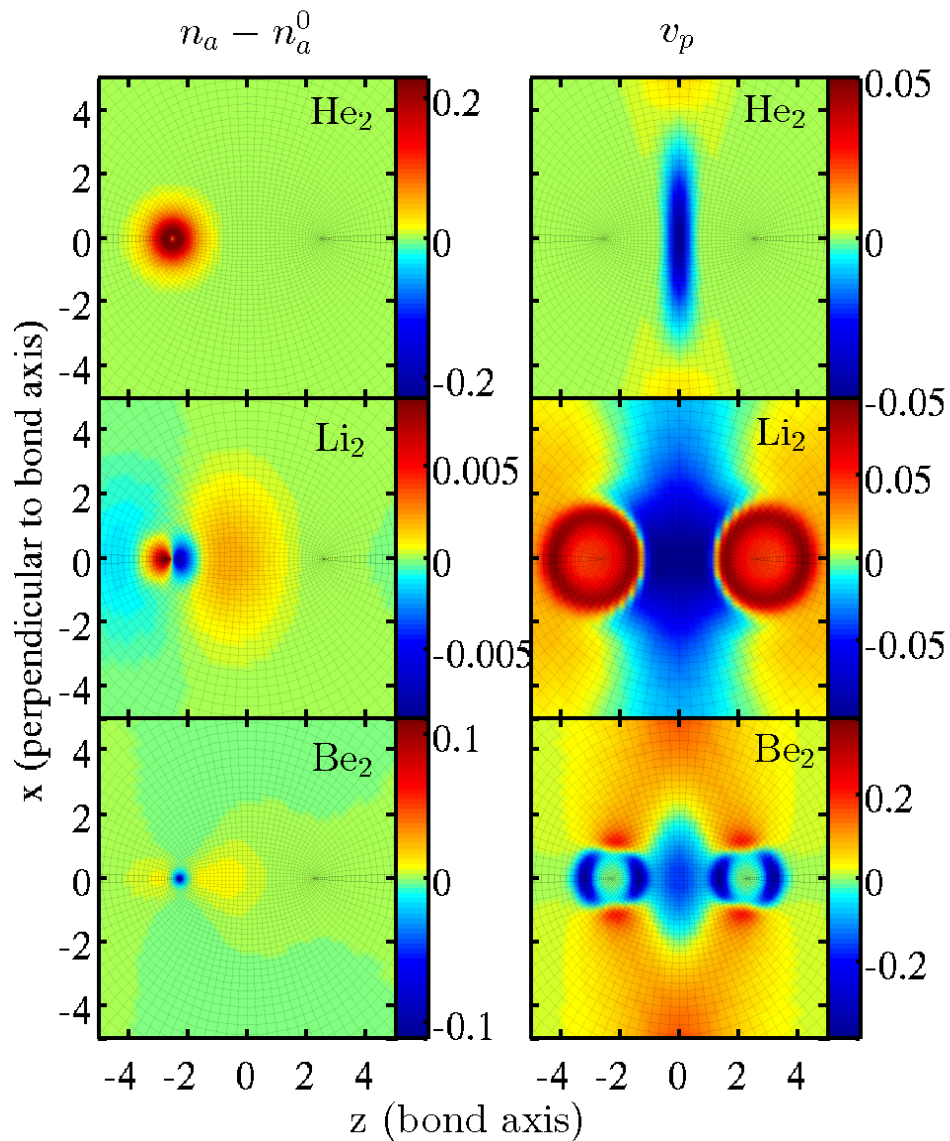


Figure 9.2. PDFT(LDA) calculations on He_2 , Li_2 , and Be_2 . The left column displays the difference between the left fragment density and the isolated atomic density while the right column displays the corresponding partition potential. In all three plots, the partition potential is depressed in the bonding region (see also Figure 3.4), increasing the density in that region. In the case of Be_2 , the partition potential squeezes each fragment and elongates it along the bond axis. In the case of Li_2 , the partition potential displays distinct plateau structures surrounding both nuclei. The edges of this plateau correspond to the transition between regions where the lowest occupied orbital contributes the most density and regions where the HOMO contributes the most density.

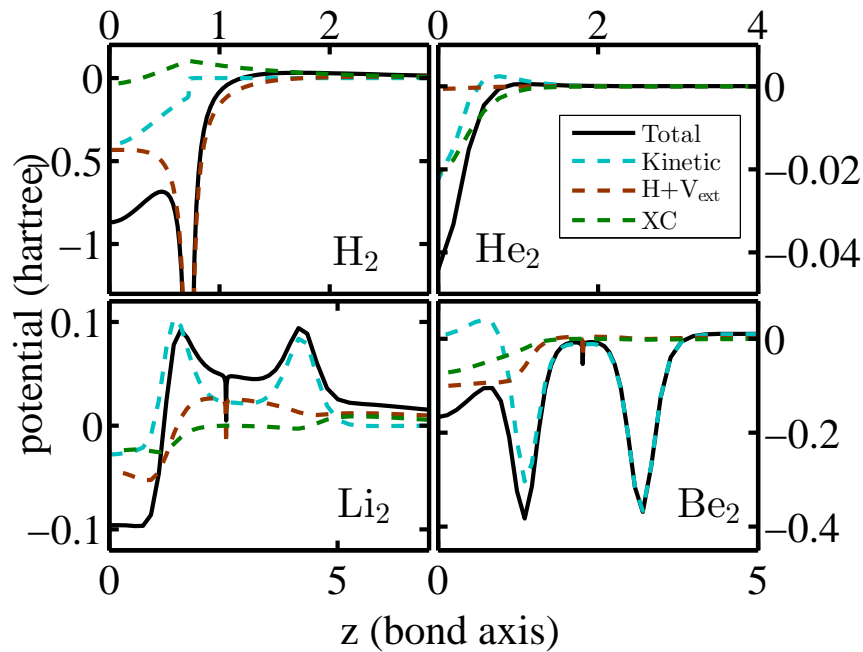


Figure 9.3. Components of the partition potential for H_2 , He_2 , Li_2 and Be_2 using the LDA. The total partition potential is solid black, the Hartree plus external potential component is in brown, the kinetic energy component is in blue and the XC component is in green.

is spin-unpolarized, each of the fragment densities is calculated as an ensemble of two oppositely spin-polarized systems: One system has two spin-up electrons and one spin-down electron while the other has two spin-down electrons and one spin-up electron. These component densities are averaged together to form a closed-shell density. The up-spin densities of the two ensemble components are shown on a log-scale in the right panel of Figure 9.5. These spin densities are averaged together to obtain the ensemble spin density for the fragment, shown in the left panel, where it is also compared with an isolated Li-atom density.

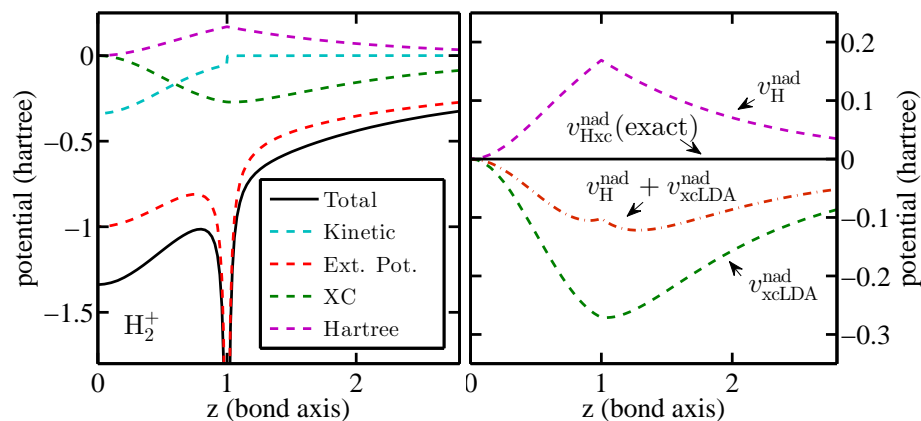


Figure 9.4. Left: Components of the partition potential for H_2^+ using the LDA. Right: The hartree and XC components of the partition potential, along with their sum. In the exact case, the XC component precisely cancels with the hartree component, which is shown in solid black. However, the LDA XC component does not exactly cancel with the hartree component.

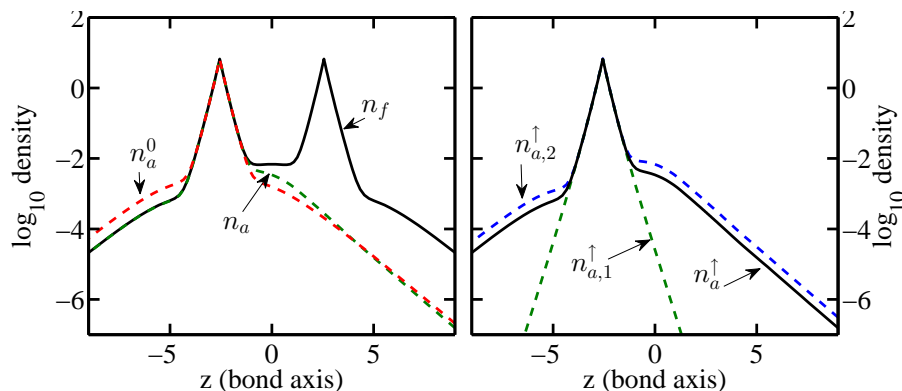


Figure 9.5. Left: One of the Li fragments within a Li_2 molecule as compared to an isolated Li atom and the density for the Li_2 molecule. Right: Each Li fragment has 3 electrons and come from an open shell calculation, however the Li_2 molecule is closed shell. This figure displays the ensemble spin up component with one electron and the ensemble spin up component with two electrons which combine to give a fragment density corresponding to a fractional spin up density.

9.2 Fractional Charges and Spins

Various fragment-based methods formulated for wavefunction-in-DFT embedding do not admit fractional numbers of electrons in the fragments. While wavefunction

methods could in principle be defined for fractional numbers of electrons through ensembles, this would require additional calculation using already expensive methods [24]. In these cases, it is simpler to fix the fragments to have integer values. However, as was demonstrated in Figure 3.3, there are certainly cases where chemical intuition and practicality indicate that a fragment contain fractional numbers of electrons.

As mentioned in the first Section, it is difficult to assign physical meaning to fragments within a molecule. However, to the extent that it is possible, PDFT seeks to treat these fragments as physical systems. These fragments represent open systems and therefore, in the case of non-integer occupations, the correct representation is achieved through ensembles [21]. Other authors [24] have favored an alternative option for treating fractional numbers of electrons, in which the density is constructed by simply fractionally occupying the HOMO:

$$n(\mathbf{r}) = \sum_{i_\alpha} f_{i_\alpha} |\phi_{i_\alpha}|^2 \quad (9.1)$$

Here the f_{i_α} will be 1 when its eigenvalue is less than the chemical potential, 0 when its eigenvalue is greater than the chemical potential. However, when the HOMO eigenvalue is equal to the chemical potential, the corresponding occupation number can take on a value in between 0 and 1. We refer to this method for constructing densities with fractional numbers of electrons as fractional orbital occupation (FOO).

Table 9.2.

Table of PDFT energies in atomic units comparing ensemble (ENS) vs FOO treatment of fractional charges and spins. All calculations used the LDA.

	D	E_{iso}	E_f	E_p	V_{nn}	E_{tot}
H_2^+ (ENS)	2	-0.4787	-0.4250	-0.6589	0.5	-0.5839
H_2^+ (FOO)	2	-0.5787	-0.5438	-0.5401	0.5	-0.5839
H_2 (ENS)	1.446	-0.9574	-0.9119	-0.9173	0.6916	-1.1377
H_2 (FOO)	1.446	-0.8913	-0.8293	-1	0.6916	-1.1377
Li_2 (ENS)	5.122	-14.6867	-14.6750	-1.8068	1.7571	-14.7246
Li_2 (FOO)	5.122	-14.6693	-14.6553	-1.8264	1.7571	-14.7246

We use our **CADMium** code to illustrate the differences between these two methods of handling fractional numbers of electrons. Table 9.2 displays results for a few diatomic molecules using both our ensemble method (ENS) and FOO. These calculations were performed using LDA exchange and correlation. Both calculations use exact expressions for the partition energy, in the sense that they exactly reproduce a molecular LDA KS-DFT calculation. Thus, the total energy is not affected by the choice of ENS vs FOO. However, this choice affects both the sum of fragment energies, E_f , and the partition energy, E_p , even when their sum is not affected.

For the case of ensembles, the partition energy is given by:

$$E_p^{\text{ENS}}[\{n_\alpha\}] = E[n_f] - \sum_\alpha ((1 - \nu_\alpha)E_\alpha[n_{p_\alpha}] + \nu_\alpha E_\alpha[n_{p_\alpha+1}]) , \quad (9.2)$$

whereas with FOO, the partition energy is:

$$E_p^{\text{FOO}}[\{n_\alpha\}] = E[n_f] - \sum_\alpha (E_\alpha[n_\alpha]) \quad (9.3)$$

The key difference between the two options is that the n_{p_α} always integrate to integer values, while the n_α may integrate to non-integer values. In the ensemble case, this means that the fragment energy functionals are never evaluated with fragment densities with fractional charges and spins. This difference is important due to the well known problems associated with approximate density functionals and fractional spins and charges. For a recent overview of these issues of XC functionals, see the work of Cohen, Mori-Sanchez and Yang [99,114–116]. The dependence of the energy on particle number is known for the exact case due to the work of Perdew, Parr, Levy, and Balduz using ensembles [21], and independently via arguments based on size-consistency and translational invariance [107].

The errors incurred in by local and semi-local XC functionals are illustrated in Figure 9.6 for the simple case of a hydrogen atom with a fractional number of electrons. The errors that are due to approximate non-interacting kinetic energy functionals are

illustrated in Figure 9.7. In these cases, the functionals perform best for densities closest to the integers, and perform poorly for densities corresponding to a fractional number of electrons.

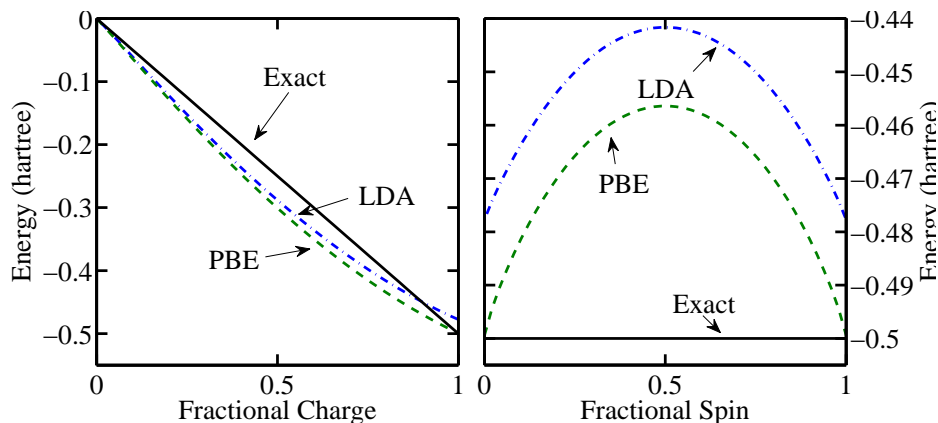


Figure 9.6. Energies of the hydrogen atom with fractional charge (left) and fractional spin(right). In both cases the exact is linear and is shown in solid black. PBE is shown in the dashed line and the LDA is shown in dot dashed line.

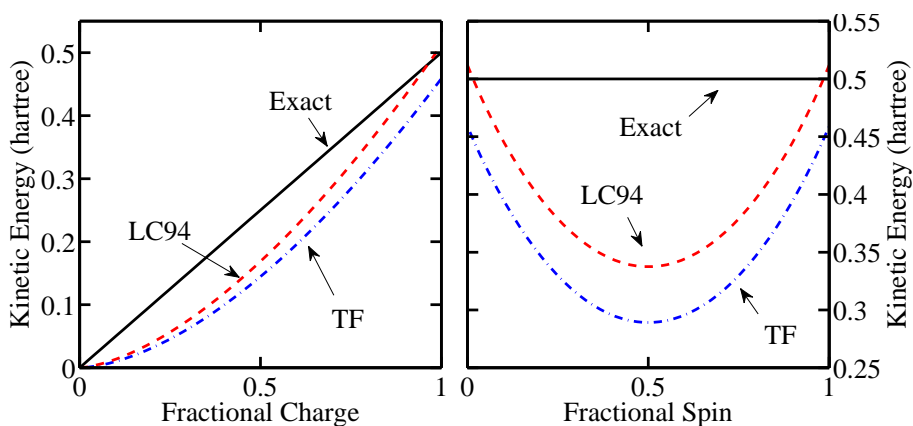


Figure 9.7. Kinetic energies of the hydrogen atom with fractional charge (left) and fractional spin(right). In both cases the exact is linear and is shown in black. Thomas Fermi is shown in the dot dashed line and the LC94 (PW91k) is shown in dashed line. These energies were evaluated for the exact densities.

Clearly, these errors need to be addressed in any fragment-based method that allows for fractional charges and spins, but the inability of standard density functionals to

correctly handle these densities also causes well-known issues in standard Kohn-Sham calculations with integer numbers of electrons. In particular, dissociation curves are strongly affected. The two paradigmatic systems exhibiting such errors are the hydrogen molecule and its ion in the case where their bonds are stretched. When a closed-shell molecule, such as H_2 , dissociates into open-shell fragments, unless symmetry is broken, there will be regions with fractional spins. The associated error caused by incorrect treatment of these fractional spins is known as static-correlation error. Similarly, in cases such as H_2^+ , where a charge is shared between two distant nuclear centers, incorrect treatment of the fractional charges on each center leads to delocalization error. The question of how to best correct these shortcomings remains largely open in DFT, in spite of recent progress on the development of explicit density functionals that yield the correct behavior [117, 118].

Part of the difficulty in addressing this issue is that it is not enough for functionals to be able to treat a whole system with fractional numbers of electrons, but the functional must also be able to recognize when a system with an integer number of electrons contains *regions* with fractional numbers of electrons or spins (e.g. stretched H_2^+ and stretched H_2). It is not possible for standard local or semi-local functionals to properly describe the delocalized electron of stretched H_2^+ . On the other hand, many standard density-functional approximations do quite well for localized densities that integrate to an integer number of electrons. The use of ensembles within PDFT suggests a possible solution. The fragments of PDFT have always been found to be well localized, and if a fragment does contain a fractional number of electrons or spins, then it is calculated as an ensemble of two systems with integer numbers of electrons and spins, and therefore the fragment energy will have the correct linear behavior for fractional numbers. Thus, if we look at the behavior of the energy for a fragment with arbitrary fractional spin and fractional charge within a molecule for fixed partition potential, it will exhibit precisely the “flat-plane behavior” required by the exact functional [114]. It will have linear dependence on fractional charge and spin even when using the LDA. This flat-plane behavior will remain even as the

molecule is stretched, so in the case of stretched H_2 and H_2^+ the sum of fragment energies will be very close to the correct molecular energy. The partition energy, on the other hand, might ruin the correct behavior, restoring the errors of LDA. Clearly, we “simply” need to correct the behavior of the partition energy in order to improve molecular dissociation within DFT. In this way, PDFT provides a different framework for addressing the issue. The goal is to develop improved functionals for the XC components of the partition energy rather than the XC functional itself. The partition energy is a functional of the fragment densities, and thus contains information about how overlapped or dissociated the fragments in a system may be. Exact conditions for the partition energy can aid in this process of functional development. This idea is explored further in reference [4].

10. Static-Correlation and Delocalization Errors

This work may also be found on the arxiv. [4]

Two open problems in DFT are the delocalization and static correlation errors of approximate functionals, arising from improper treatment of fractional charges and spins, respectively [99,114–116]. Delocalization error causes underestimation of energies in dissociating molecular ions, chemical reaction barrier heights, charge-transfer excitations, band-gaps of semiconductors, as well as overestimation of binding energies of charge-transfer complexes and response to electric fields. Static correlation error is responsible for the problems with degenerate and near-degenerate states, incorrect dissociation limit of neutral diatomics and poor treatment of strongly correlated systems. The simplest systems that display these errors are stretched H_2^+ and H_2 . Local and semi-local approximations to the exchange-correlation energy (E_{xc}) severely underestimate the dissociation energy of H_2^+ due to delocalization, and overestimate the dissociation energy of H_2 due to static correlation (See Table 10.1).

In this work we demonstrate that partition density-functional theory (PDFT) [38] is a suitable framework to solve these problems. The *partition energy* of PDFT (denoted E_p , to be defined below) is amenable to simple approximations which can handle delocalized and statically correlated electrons, greatly improving dissociation energies in both cases. For example, Table 10.1 reports on the results we obtained by applying PDFT with the Local Density Approximation (LDA) and a simple “Overlap Approximation” (OA) for E_p (defined in Eq.10.2). We are not aware of approximate XC-functionals that yield similar accuracy for both H_2^+ and H_2 within standard KS-DFT.

Table 10.1.
Dissociation energies for H_2^+ and H_2 in units of milihartrees.

	KS-DFT (LDA)	PDFT (OA-LDA)	exact
H_2^+	18.1	102.0	102.6
H_2	246.1	180.0	174.5

10.1 Ensembles in PDFT

Within PDFT each individual fragment calculation is a standard DFT calculation for the ensemble ground-state density of N_α electrons in an effective potential. We denote the α^{th} fragment density as n_α and the sum of fragment densities as n_f . The number of electrons in each fragment, N_α , is determined from the principle of chemical potential equalization [22] and is not necessarily an integer number. The effective external potential for each fragment is the sum of the fragment’s potential, v_α , and the partition potential, v_p . The latter is a *global* quantity ensuring that all of the fragment calculations produce densities that sum to yield the correct molecular density while minimizing the sum of the fragment energies, E_f . The partition potential enters formally as a lagrange multiplier, but can be calculated as the functional derivative of E_p with respect to the total density [23].

The partition energy, E_p , central to our work, is the difference between the total molecular energy, $E[n]$, and the sum of the fragment energies, $E_f = \sum_\alpha E_\alpha[n_\alpha]$. Each fragment energy, $E_\alpha[n_\alpha]$, is the total electronic energy for N_α electrons in the fragment potential $v_\alpha(\mathbf{r})$ (the partition potential does not contribute to E_α). If N_α is not an integer then $E_\alpha[n_\alpha]$ is the energy of an ensemble of two systems, one with $p = \lfloor N_\alpha \rfloor$ electrons and another one with $p + 1 = \lceil N_\alpha \rceil$ electrons. As argued in ref. [23], the minimum value of E_f with respect to variations of the n_α ’s is a functional of the total density. Subtracting this quantity from the true ground-state energy yields $E_p[n] = E[n] - E_f[n]$, an implicit functional of the molecular density. We may also write E_p

as an explicit functional of the fragment densities: $E_p[\{n_\alpha\}] = E[n_f] - E_f[\{n_\alpha\}]$. In the two-fragment case, E_p can be divided into components and written out explicitly in terms of fragment densities:

$$E_p[n_1, n_2] = \Delta T_s[n_1, n_2] + \Delta V_{\text{ext}}[n_1, n_2] + \Delta E_{\text{H}}[n_1, n_2] + \Delta E_{\text{XC}}[n_1, n_2] \quad (10.1)$$

where $\Delta F \equiv F[n_f] - \sum_\alpha F_\alpha[n_\alpha]$. This is similar to the non-additive functionals of embedding theory [24, 53, 54] except that the functional values for each fragment are calculated from ensembles, as noted previously. In practice, a choice of density-functional approximation (DFA) must be made for E_{XC} and ΔE_{XC} . In addition, the ΔT_s term requires writing the non-interacting kinetic energy as a functional of the density. Approximate kinetic energy functionals may be used [119], although ΔT_s can also be obtained from an inversion of the sum of fragment densities as in ref. [25]. (We use von Weizsäcker inversion here, since both of our illustrative systems, H_2^+ and H_2 , have a single occupied orbital).

For a given choice of XC functional, we may *exactly* reproduce the corresponding KS-DFT calculation as long as the same DFA is employed for ΔE_{XC} and E_f [2]. We can also trivially reproduce a KS-DFT calculation by setting the number of fragments equal to one. In these ways PDFT subsumes KS-DFT.

However, PDFT also goes beyond KS-DFT. For example, the following ‘‘Overlap Approximation’’ produces the results reported on the 2nd column of Table 10.1 (when used with LDA):

$$E_p^{\text{OA}} = \Delta T_s + \Delta V_{\text{ext}} + f(N_s, S) \Delta E_{\text{H}} + S \Delta E_{\text{XC}} , \quad (10.2)$$

where $S[n_1, n_2] = N_s^{-1} \int d\mathbf{r} \sqrt{n_1(\mathbf{r})n_2(\mathbf{r})}$, $N_s = \sqrt{N_1 N_2}$, and $f(N_s, S) = (\lfloor N_s \rfloor + S(1 - \lfloor N_s \rfloor))$. The overlap measure, S , is designed to go to zero at infinite fragment separation and to one at the united-fragment limit (reminiscent of the work of [120]). Why this works will be made clear later on. We note that although E_p^{OA} produces accurate

dissociation energies for the paradigm systems H_2^+ and H_2 , the actual binding curves are inaccurate at intermediate separations. Nevertheless, Table 10.1 suggests that the route is promising. One strategy for improving upon OA is to investigate different choices for the overlap S and for $f(N_s, S)$. Another promising route that we explore here is choosing one XC functional for the fragment calculations and another for the ΔE_{XC} term, thus producing a molecular density and energy different from those of a KS-DFT calculation performed using either XC functional. The separation of $E_p[n]$ and $E_f[n]$ opens opportunities for new approximations within a self-consistent framework. In particular, when the error of a DFT calculation is due to fragmentation, as in bond-stretching, expressing $E_p[n]$ as a functional of the set of fragment densities has the potential of fixing the error from its root. The physics of *inter*-fragment interactions is contained in E_p while the *intra*-fragment interactions are contained in E_f .

This is the main idea we wish to explore in the remainder of this chapter. We first discuss a consequence of using different levels of approximation for E_p and E_f . As shown in ref. [23], the partition potential is determined from the chain rule: $v_p(\mathbf{r}) = \sum_{\alpha} \int d\mathbf{r}' v_{p,\alpha}(\mathbf{r}') Q_{\alpha}(\mathbf{r}', \mathbf{r})$, where the α^{th} -partition potential is given by $v_{p,\alpha}(\mathbf{r}) = \delta E_p / \delta n_{\alpha}(\mathbf{r})$ and $Q_{\alpha}(\mathbf{r}', \mathbf{r}) = \delta n_{\alpha}(\mathbf{r}') / \delta n(\mathbf{r})$ satisfies the sum-rule: $\sum_{\alpha} Q_{\alpha}(\mathbf{r}', \mathbf{r}) = \delta(\mathbf{r}' - \mathbf{r})$. As long as the same level of approximation is employed for E_p and E_f , then at convergence $v_{p,\alpha}(\mathbf{r}) = v_{p,\beta}(\mathbf{r}) \forall \alpha, \beta$ so the choice of Q_{α} is inconsequential provided the sum-rule is satisfied. When different levels of approximation are used for E_p and E_f , however, the $v_{p,\alpha}(\mathbf{r})$ are not necessarily identical at convergence, and it becomes critical to specify the approximation being used for the Q_{α} . Future work will need to establish the effect of different approximations for Q on final energies and densities. Throughout the present work, we employ the Local-Q approximation suggested in ref. [23], which directly leads to an expression for the two-fragment partition potential:

$$v_p(\mathbf{r}) = \frac{n_1(\mathbf{r})}{n(\mathbf{r})} v_{p,1}(\mathbf{r}) + \frac{n_2(\mathbf{r})}{n(\mathbf{r})} v_{p,2}(\mathbf{r}) \quad (10.3)$$

We now have all of the necessary tools to perform PDFT calculations with separate approximations for E_f and E_p . We implemented these calculations on a real-space prolate spheroidal grid, following the work of Becke and other workers [108–112], and found XC potentials and energies through use of the Libxc library [113]. We validated the code through calculations on H_2^+ and H_2 at equilibrium geometries for both PDFT and standard KS-DFT calculations where our code yields the same energies to within 10^{-7} hartrees for all calculations (see table 10.2 for comparison to the literature). We now look at the delocalization and static-correlation errors from the point of view of PDFT, and demonstrate our proposed solutions.

Table 10.2.

Comparison of total energies in hartree, for our PDFT code, and from benchmark KS-DFT calculations.

	H_2 PW91	H_2 LDA	H_2^+ Exact
R (bohr)	1.414	1.446	2.0
KS-DFT (hartree)	-1.170693 ¹	-1.137692 ¹	-0.6026342144(7) ²
PDFT (hartree)	-1.17071	-1.1376923	-0.60263425

10.2 Delocalization Error

We first consider the accuracy of E_f in H_2^+ . Since the Hamiltonian has inversion symmetry, the correct ground-state density has “half an electron” on the left and “half an electron” on the right, but the correct ground-state energy at infinite separation is that of an isolated hydrogen atom (-0.5 hartree). A correct size-consistent electronic-structure method must therefore assign an energy of -0.25 hartree to a hydrogen atom with *half* an electron. This same argument may be extended to dissociating hydrogen chains, resulting in the conclusion that the energy is a piecewise-linear function of electron number [107]. This is of course accomplished by the exact grand-canonical

¹Reference [111]

²Reference [112]

ensemble functional [21], but it is *not* accomplished by most approximate functionals, as can be seen in Fig.10.1 for PBE [20] and LDA [121, 122]. While PBE yields an excellent value for the energy of a single electron in a hydrogen atom, the self-interaction error $\text{SIE} = E_{\text{H}}[n] + E_{\text{xc}}[n]$ is a convex function of electron number N . As a consequence, PBE underestimates the energy for *half* an electron in a hydrogen atom by 53mH. Two times this error is precisely $\Delta E_{\text{H}}(\infty) + \Delta E_{\text{xc}}(\infty)$ in Eq.(10.1), the PBE delocalization error of H_2^+ at infinite separation. The OA of Eq.10.2 works by suppressing this error as $S(\infty) = 0$ and happens to be accurate at the equilibrium separation as well, but is inadequate at intermediate separations.

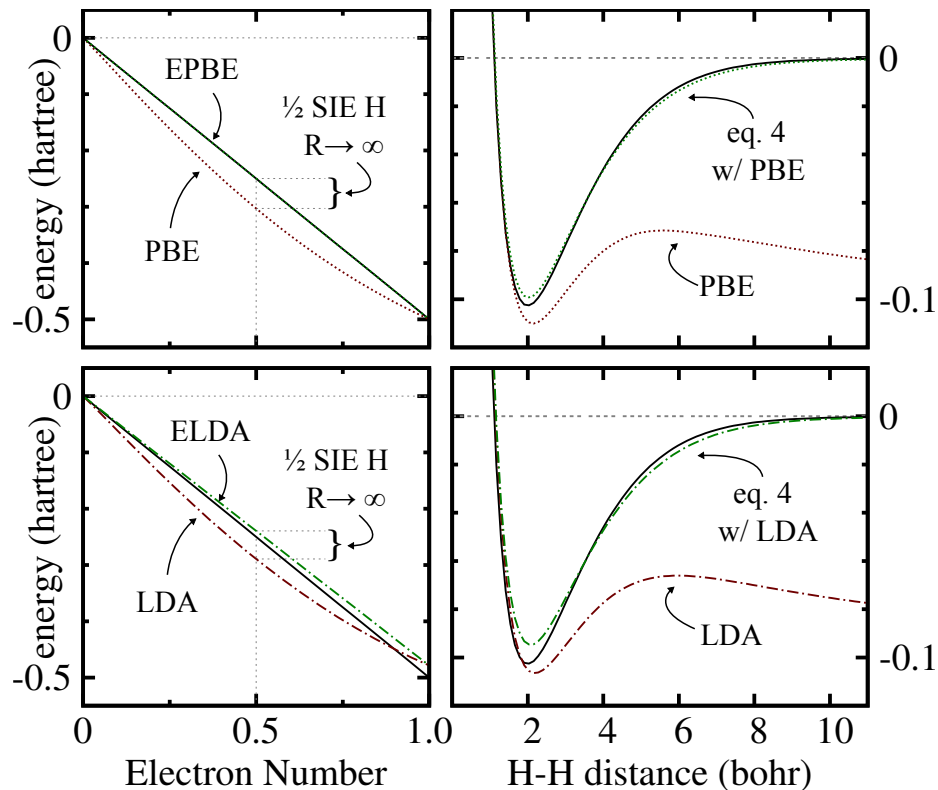


Figure 10.1. Plots on the left: Energies of a hydrogen atom with fractional number of electron. Exact energies are plotted in solid black along with DFA and ensemble-DFA results. Note that ensemble-PBE and the exact curve are indistinguishable. The origin of the self interaction error of stretched H_2^+ is indicated in both frames. Plots on the right: The exact dissociation energy of H_2^+ is plotted in solid black along with standard KS-DFT results and PDFT results using Eq.(10.4).

Because PDFT treats each fragment using an ensemble, the fragment calculation for the left or right half of stretched H_2^+ is a linear interpolation between calculations for zero and one electron. We call this interpolation ensemble-PBE (EPBE) for PBE or ensemble-LDA (ELDA) for LDA, and plot the resulting curves in Fig. 10.1. Note that the EPBE curve is indistinguishable from the exact curve leading us to the conclusion that our calculation of E_f is reasonably accurate.

We therefore focus on improvements to the E_p functional and look to range-separated hybrid (RSH) functionals for inspiration [123]. In RSH functionals a larger portion of exact exchange is included in long-range interactions to improve accuracy. The distinction between long-range and short-range is made by a tunable parameter. In our case the distinction between long and short range is the distinction between E_f and E_p . This suggests inclusion of exact exchange in E_p should improve its long-range behavior.

We explore this idea by using exact-exchange for the ΔE_{xc} term of Eq.10.1:

$$\Delta E_{\text{xc}}[n_1, n_2] \approx \Delta E_{\text{x}}^{\text{EXX}}[n_1, n_2] \quad (10.4)$$

For single-orbital systems, exact exchange can be calculated directly from the density. For larger systems it could be obtained via inversion along with the kinetic energy. The results of a self-consistent PDFT calculation with this functional are shown in Fig.10.1. $\Delta E_{\text{x}}^{\text{EXX}}$ exactly cancels ΔE_{H} , making E_p exact for H_2^+ . The remaining error is due to $E_f[n]$. PBE and even LDA provide good approximations for $E_f[n]$ because each fragment calculation is done for a well-localized density with an integer number of electrons. The ensemble formulation then gives us the correct scaling for the energy of each half-electron fragment.

10.3 Static Correlation Error

We next see how this idea might be applied to handle static correlation, taking H_2 as an example. As in the H_2^+ case, we first consider the dissociation products of H_2 : two isolated hydrogen atoms, with a total energy of -1.0 hartree. However, the molecular calculation is spin-neutral, and it remains spin-neutral throughout dissociation due to inversion symmetry. Therefore each dissociating hydrogen atom has an electron which is “half spin up” and “half spin down”. The exact functional assigns an energy to this fragment equal to that of a spin-up electron in a hydrogen atom. This is known as the constancy condition [114]. However, approximate functionals do not show this behavior and typically overestimate the energy of a system with fractional spins. This overestimation exactly matches the static correlation error of dissociated H_2 , and is given by $\Delta E_{xc}(\infty)$. Once again Eq.10.2 works by suppressing this error as $S(\infty) = 0$ and is accurate at the equilibrium separation as well, but is inadequate at intermediate separations.

Each fragment in an H_2 PDFT calculation contains one electron, but the energies and spin-densities are considered to be ensembles of a spin-up and a spin-down electron. The energies and densities are then linear interpolations between a spin-up calculation and a spin-down calculation. These two cases are degenerate so the fragment energies satisfy the constancy condition. Once again, E_f is accurate with standard DFA’s and we simply need to improve E_p .

We may at first consider a similar approach to what we used for H_2^+ :

$$\Delta E_{xc}[n_1, n_2] \approx \Delta E_x^{EXX}[n_1, n_2] + \Delta E_C^{DFA}[n_1, n_2] \quad , \quad (10.5)$$

where ΔE_C^{DFA} is the non-additive correlation energy from the DFA used in fragment calculations. The results using both PBE and LDA are plotted in the top frame of Fig.10.2 along with the exact E_p for both PBE and LDA. We see that inclusion of exact exchange actually worsens the dissociation behavior.

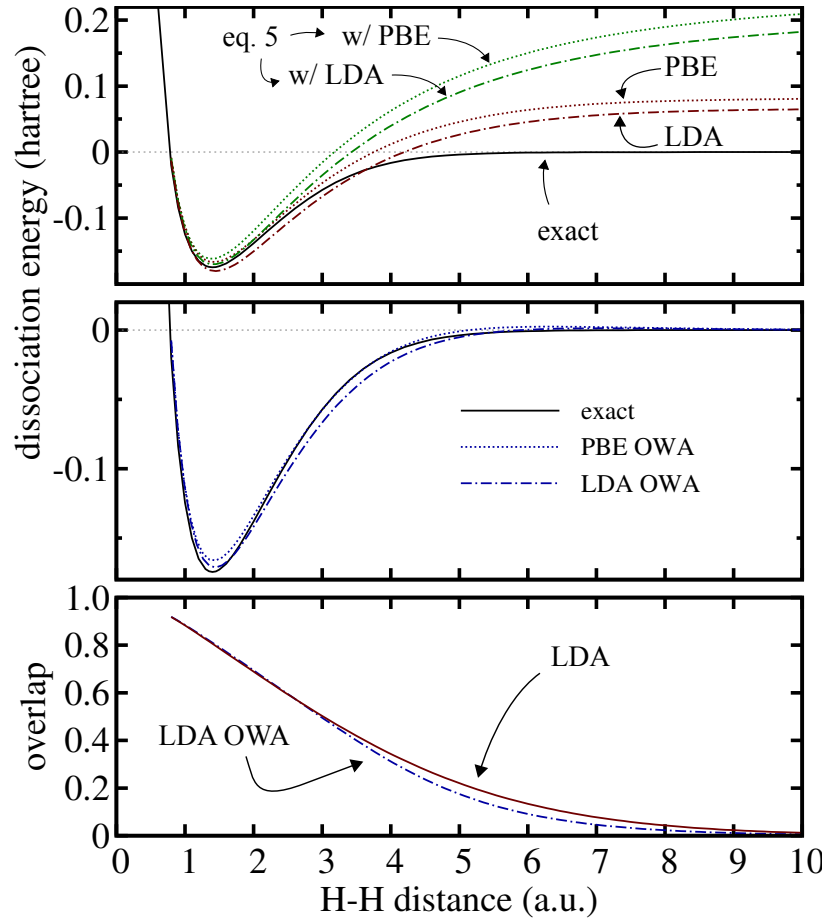


Figure 10.2. Top: H_2 Dissociation energies for: standard functionals (red), eq.10.5 with standard functionals for E_f (green) and exact [124] (solid black) Middle: H_2 Dissociation energies for OWA functionals and exact [124] (solid black) Bottom: The H_2 overlap, S , for a PDFT-LDA calculation in comparison to an OWA-LDA calculation. We see that the OWA slightly suppresses the overlap.

However, size-consistency imposes another constraint on the partition energy: at infinite separation E_p must go to zero. For H_2 the only part of E_p which does not go to zero is the ΔE_{xc} term. We propose the following overlap-weighted approximation (OWA):

$$\Delta E_{xc} \approx \Delta E_{xc}^{OWA} = S(\Delta E_x^{EXX} + \Delta E_c^{DFA}) \quad , \quad (10.6)$$

where S is the same overlap measure introduced in Eq.10.2. It is plotted in the bottom frame of Fig.10.2. Clearly, the OWA only slightly suppresses the overlap.

The middle frame of figure 10.2 shows OWA results using PBE and LDA for ΔE_C^{DFA} . We see that both OWA-PBE and OWA-LDA follow the exact curve closely and approach the correct dissociation limit.

10.4 Peak and Step in XC potential

To understand the success of OWA we go further and examine the molecular XC potential that yields the same molecular density as our PDFT calculations. This can be done in the present case through von Weizsäcker inversion:

$$v_{\text{xc}}(\mathbf{r}) = \frac{1}{2} \frac{\nabla^2 \sqrt{n_f(\mathbf{r})}}{\sqrt{n_f(\mathbf{r})}} + \epsilon - v_{\text{ext}}(\mathbf{r}) - v_{\text{H}}[n_f](\mathbf{r}) \quad (10.7)$$

ϵ is the KS eigenvalue and $v_{\text{H}}[n_f]$ is the Hartree potential due to the sum of fragment densities.

Fig.10.3 compares the effective XC potential from two PDFT calculations on stretched H_2 (internuclear separation of 10 bohrs). For the first we use the LDA in both E_f and E_p . For the second we use LDA in E_f and OWA-LDA for ΔE_{xc} in E_p .

There has been significant previous work on *exact* Kohn-Sham potentials and it is well known that stretched H_2 develops a peak at the bond midplane [125–131]. This exact feature of $v_s(\mathbf{r})$, essential for the correct description of dissociation and electron dynamics [132, 133], is absent from most approximate DFA's but is nicely captured by our OWA, motivating further development of time-dependent PDFT [74].

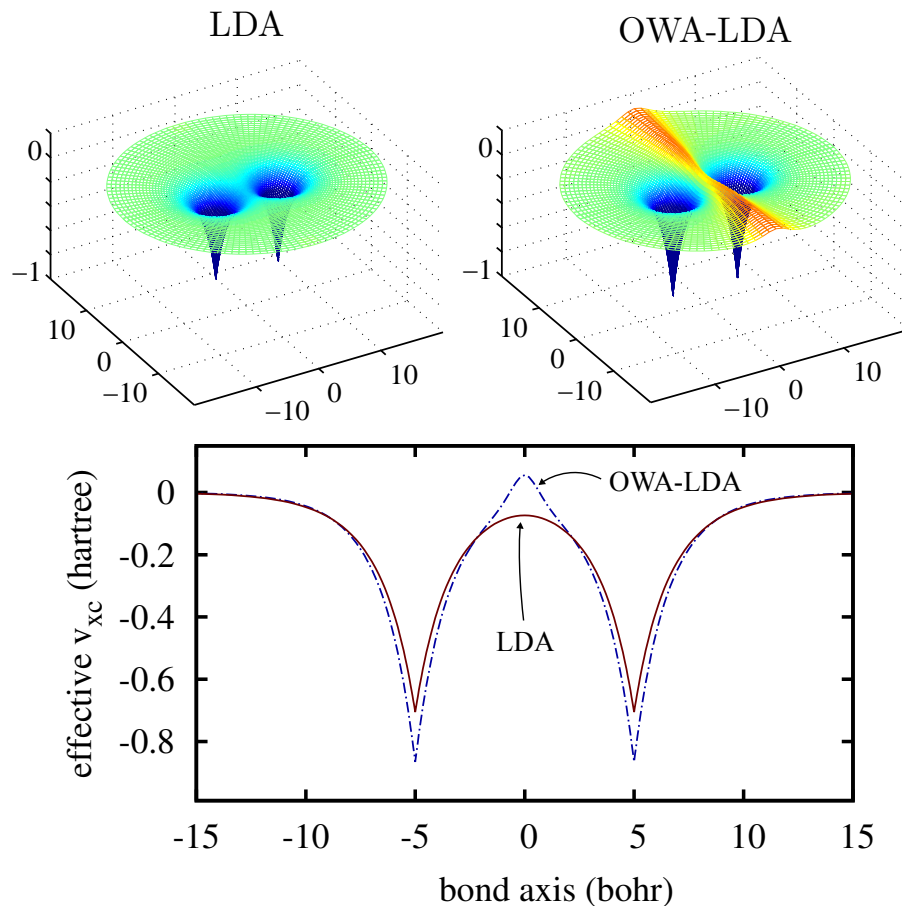


Figure 10.3. Effective XC-potentials for two PDFT H_2 calculations with $R = 10$ bohr. The top two plots show an entire 2D plane along the bonding axis while the bottom plot compares the effective XC-potential in a 1D slice along the bond axis. Nuclei are at $+5$ and -5 on the bond axis.

10.5 Concluding Remarks

The techniques described thus far are specific to homonuclear diatomics, but work is ongoing to extend these ideas to more general multifragment systems. Our results suggest that local and semi-local density-functional approximations already do well for the localized fragments involved in the calculation of E_f and attention needs to be placed on developing general approximations for E_p . This chapter indicates that the path is worth taking, as even simple approximations for E_p can achieve via frag-

ment calculations what sophisticated XC-functionals cannot via standard molecular calculations.

REFERENCES

REFERENCES

- [1] Jonathan Nafziger and Adam Wasserman. Density-based partitioning methods for ground-state molecular calculations. *The Journal of Physical Chemistry A*, 118(36):7623–7639, 2014.
- [2] Jonathan Nafziger, Qin Wu, and Adam Wasserman. Molecular binding energies from partition density functional theory. *J. Chem. Phys*, 135(23):234101–234101–6, 2011.
- [3] Rougang Tang, Jonathan Nafziger, and Adam Wasserman. Fragment occupations in partition density functional theory. *Phys. Chem. Chem. Phys.*, 14(21):7780–7786, 2012.
- [4] J. Nafziger and A. Wasserman. Fragment-based Treatment of Delocalization and Static Correlation Errors in Density-Functional Theory. *ArXiv e-prints*, May 2013.
- [5] Paul Adrien Maurice Dirac. Quantum mechanics of many-electron systems. *Proc. R. Soc. A*, 123(729):714–733, 1929.
- [6] P. Hohenberg and W. Kohn. Inhomogeneous electron gas. *Phys. Rev.*, 136(3B):B864–B871, 1964.
- [7] Klaus Capelle. A bird’s-eye view of density-functional theory. *Brazilian Journal of Physics*, 36(4A):1318–1343, 2006.
- [8] M. A. L. Marques and E. K. U. Gross. A primer in density functional theory. *Lecture Notes in Physics*, 620:144–184, 2003.
- [9] Reiner M Dreizler and Cora S Lüdde. A safari through density functional theory. In *Exciting Interdisciplinary Physics*, pages 465–478. Springer, 2013.
- [10] Robert Parr and Weitao Yang. *Density-Functional Theory of Atoms and Molecules*. Oxford University Press, 1989.
- [11] Kieron Burke and Lucas O. Wagner. Dft in a nutshell. *Int. J. Quantum Chem.*, 113(2):96–101, 2013.
- [12] T. L. Gilbert. Hohenberg-kohn theorem for nonlocal external potentials. *Phys. Rev. B*, 12:2111–2120, Sep 1975.
- [13] J.T. Chayes, L. Chayes, and MaryBeth Ruskai. Density functional approach to quantum lattice systems. *Journal of Statistical Physics*, 38(3-4):497–518, 1985.
- [14] C. A. Ullrich and W. Kohn. Kohn-sham theory for ground-state ensembles. *Phys. Rev. Lett.*, 87:093001, Aug 2001.
- [15] Mel Levy. Electron densities in search of hamiltonians. *Phys. Rev. A*, 26:1200–1208, Sep 1982.

- [16] Elliott H. Lieb. Density functionals for coulomb systems. In Reiner M. Dreizler and João da Providência, editors, *Density Functional Methods In Physics*, volume 123 of *NATO ASI Series*, pages 31–80. Springer US, 1985.
- [17] L. H. Thomas. The calculation of atomic fields. *Mathematical Proceedings of the Cambridge Philosophical Society*, 23(05):542–548, 1927.
- [18] Enrico Fermi. Un metodo statistico per la determinazione di alcune priorietà dell’atome. *Rend. Accad. Naz. Lincei*, 6(602-607):32, 1927.
- [19] W. Kohn and L. J. Sham. Self-consistent equations including exchange and correlation effects. *Phys. Rev.*, 140(4A):A1133–A1138, 1965.
- [20] John P. Perdew, Kieron Burke, and Matthias Ernzerhof. Generalized gradient approximation made simple. *Phys. Rev. Lett.*, 77(18):3865–3868, 1996.
- [21] John P. Perdew, Robert G. Parr, Mel Levy, and Jose L. Balduz Jr. Density-functional theory for fractional particle number: Derivative discontinuities of the energy. *Phys. Rev. Lett.*, 49(23):1691–1694, 1982.
- [22] Morrel H. Cohen and Adam Wasserman. On hardness and electronegativity equalization in chemical reactivity theory. *Journal of statistical physics*, 125(5-6):1121–1139, 2006.
- [23] Martín A. Mosquera and Adam Wasserman. Partition density functional theory and its extension to the spin-polarized case. *Mol. Phys.*, 111(4):505–515, 2013.
- [24] Chen Huang and Emily A. Carter. Potential-functional embedding theory for molecules and materials. *J. Chem. Phys*, 135(19):194104–194104, 2011.
- [25] Jason D. Goodpaster, Nandini Ananth, Frederick R. Manby, and Thomas F. Miller III. Exact nonadditive kinetic potentials for embedded density functional theory. *J. Chem. Phys*, 133:–, 2010.
- [26] O. V. Gritsenko. On the principal difference between the exact and approximate frozen-density embedding theory. volume 6, pages 355–365. WORLD SCIENTIFIC, 2013.
- [27] Eduardo Fabiano, Savio Laricchia, and Fabio Della Sala. Frozen density embedding with non-integer subsystems particle numbers. *J. Chem. Phys*, 140(11):–, 2014.
- [28] Robert G. Parr, Robert A. Donnelly, Mel Levy, and William E. Palke. Electronegativity: The density functional viewpoint. *J. Chem. Phys*, 68(8):3801–3807, 1978.
- [29] Robert G. Parr and Libero J. Bartolotti. Some remarks on the density functional theory of few-electron systems. *J. Phys. Chem.*, 87(15):2810–2815, 1983.
- [30] Peter Elliott, Daniel Jensen, Adam Wasserman, and Kieron Burke. Comment on application of partition density-functional theory to one-dimensional models. *Phys. Rev. A*, 89(2):–, 2014.
- [31] Andreas W. Gotz, S. Maya Beyhan, and Lucas Visscher. Performance of kinetic energy functionals for interaction energies in a subsystem formulation of density functional theory. *J. Chem. Theory Comput.*, 5(12):3161–3174, 2009.
- [32] Tosio Kato. On the eigenfunctions of many-particle systems in quantum mechanics. *Commun. Pure Appl. Math.*, 10(2):151–177, 1957.

- [33] Robert G. Parr, Paul W. Ayers, and Roman F. Nalewajski. What is an atom in a molecule? *J. Phys. Chem. A*, 109(17):3957–3959, 2005.
- [34] F. L. Hirshfeld. Bonded-atom fragments for describing molecular charge densities. *Theoretica chimica acta*, 44(2):129–138, 1977.
- [35] Roman F. Nalewajski and Robert G. Parr. Information theory, atoms in molecules, and molecular similarity. *Proc. Nat. Acad. Sci. U. S. A.*, 97(16):8879–8882, 2000.
- [36] Robert G. Parr. Remarks on the concept of an atom in a molecule and on charge transfer between atoms on molecule formation. *Int. J. Quantum Chem.*, 26(5):687–692, 1984.
- [37] Morrel H. Cohen and Adam Wasserman. On the foundations of chemical reactivity theory. *J. Phys. Chem. A*, 111(11):2229–2242, 2007.
- [38] Peter Elliott, Kieron Burke, Morrel H. Cohen, and Adam Wasserman. Partition density-functional theory. *PHYSICAL REVIEW A Phys Rev A*, 82:–, 2010.
- [39] William E. Palke. The electronic chemical potential and the h atom in the h2 molecule. *J. Chem. Phys*, 72(4):2511–2514, 1980.
- [40] Michael P. Guse. An atoms in molecules approach to density functional theory. *J. Chem. Phys*, 75(2):828–833, 1981.
- [41] Richard F. W. Bader, Yoram Tal, Steven G. Anderson, and T. Tung Nguyen-Dang. Quantum topology: Theory of molecular structure and its change. *Isr. J. Chem.*, 19(1-4):8–29, 1980.
- [42] Richard F. W. Bader. Everyman’s derivation of the theory of atoms in molecules. *J. Phys. Chem. A*, 111(32):7966–7972, 2007.
- [43] Yu Zhang and Adam Wasserman. Transferability of atomic properties in molecular partitioning: A comparison. *J. Chem. Theory Comput.*, 6(11):3312–3318, 2010.
- [44] R. F. W. Bader. Reply to comments of li and parr on baders definition of an atom. *J. Chem. Phys*, 85(5):3133–3134, 1986.
- [45] Robert G. Parr. Atoms in molecules: Reply to baders comment. *J. Chem. Phys*, 85(5):3135–3135, 1986.
- [46] Roy G. Gordon and Yung Sik Kim. Theory for the forces between closedshell atoms and molecules. *J. Chem. Phys*, 56(6):3122–3133, 1972.
- [47] A.I.M. Rae. A theory for the interactions between closed shell systems. *Chem. Phys. Lett.*, 18(4):574–577, 1973.
- [48] C.P. Wood and N.C. Pyper. Electron gas predictions of interatomic potentials tested by ab initio calculations. *Mol. Phys.*, 43(6):1371–1383, 1981.
- [49] Robert A. Harris. Induction and dispersion forces in the electron gas theory of interacting closed shell systems. *J. Chem. Phys*, 81(5):2403–2405, 1984.
- [50] M.J. Clugston. The calculation of intermolecular forces. a critical examination of the gordon-kim model. *Advances in Physics*, 27(6):893–912, 1978.

- [51] Alberto Vela, Andrés Cedillo, and José L. Gázquez. Interatomic interactions in density functional theory. *Int. J. Quantum Chem.*, 29(4):937–948, 1986.
- [52] G. Senatore and K. R. Subbaswamy. Density dependence of the dielectric constant of rare-gas crystals. *Phys. Rev. B*, 34(8):5754–5757, 1986.
- [53] Pietro Cortona. Self-consistently determined properties of solids without band-structure calculations. *Phys. Rev. B*, 44(16):–, 1991.
- [54] Tomasz Adam Wesolowski and Arieh Warshel. Frozen density functional approach for ab initio calculations of solvated molecules. *J. Phys. Chem.*, 97(30):8050–8053, 1993.
- [55] L. L. Boyer and M. J. Mehl. A self consistent atomic deformation model for total energy calculations: Application to ferroelectrics. *Ferroelectrics*, 150(1):13–24, 1993.
- [56] Christoph R. Jacob and Johannes Neugebauer. Subsystem density-functional theory. *Wiley Interdisciplinary Reviews: Computational Molecular Science*, pages n/a–n/a, 2013.
- [57] Johannes Neugebauer. Chromophore-specific theoretical spectroscopy: From subsystem density functional theory to mode-specific vibrational spectroscopy. *Phys. Rep.*, 489(1-3):1–87, 2010.
- [58] Johannes Neugebauer, Manuel J. Louwerse, Evert Jan Baerends, and Tomasz A. Wesolowski. The merits of the frozen-density embedding scheme to model solvatochromic shifts. *J. Chem. Phys*, 122(9):–, 2005.
- [59] Xiuwen Zhou, Jakub W. Kaminski, and Tomasz A. Wesolowski. Multi-scale modelling of solvatochromic shifts from frozen-density embedding theory with non-uniform continuum model of the solvent: the coumarin 153 case. *Phys. Chem. Chem. Phys.*, 13(22):10565–10576, 2011.
- [60] Sebastian Höfener, André Severo Pereira Gomes, and Lucas Visscher. Solvatochromic shifts from coupled-cluster theory embedded in density functional theory. *J. Chem. Phys*, 139(10):–, 2013.
- [61] Samuel Fux, Christoph R. Jacob, Johannes Neugebauer, Lucas Visscher, and Markus Reiher. Accurate frozen-density embedding potentials as a first step towards a subsystem description of covalent bonds. *J. Chem. Phys*, 132(16):–, 2010.
- [62] André Severo Pereira Gomes and Christoph R. Jacob. Quantum-chemical embedding methods for treating local electronic excitations in complex chemical systems. *Annual Reports Section "C" (Physical Chemistry)*, 108(1):222–277, 2012.
- [63] N. Govind, Y.A. Wang, A.J.R. da Silva, and E.A. Carter. Accurate ab initio energetics of extended systems via explicit correlation embedded in a density functional environment. *Chem. Phys. Lett.*, 295(1-2):129–134, 1998.
- [64] Patrick Huang and Emily A. Carter. Advances in correlated electronic structure methods for solids, surfaces, and nanostructures. *Annu. Rev. Phys. Chem.*, 59(1):261–290, 2008.

- [65] L. L. Boyer, H. T. Stokes, and M. J. Mehl. Application of a kohn-sham-like formulation of the self-consistent atomic deformation model. *Ferroelectrics*, 194(1):173–186, 1997.
- [66] L. L. Boyer, H. T. Stokes, and M. J. Mehl. Calculation of polarization using a density functional method with localized charge. *Phys. Rev. Lett.*, 84(4):709–712, 2000.
- [67] M.J. Mehl, H.T. Stokes, and L.L. Boyer. Development of a kohn-sham like potential in the self-consistent atomic deformation model. *J. Phys. Chem. Solids*, 57(10):1405–1407, 1996.
- [68] M. M. Ossowski, L. L. Boyer, M. J. Mehl, and M. R. Pederson. Water molecule by the self-consistent atomic deformation method. *Phys. Rev. B*, 68(24):–, 2003.
- [69] L. L. Boyer, H. T. Stokes, M. M. Ossowski, and M. J. Mehl. Self-consistent atomic deformation method for application of density functional theory. *Phys. Rev. B*, 78(4):–, 2008.
- [70] Mark E. Casida and Tomasz A. Wesowski. Generalization of the kohn-sham equations with constrained electron density formalism and its time-dependent response theory formulation. *Int. J. Quantum Chem.*, 96(6):577–588, 2004.
- [71] Johannes Neugebauer. Couplings between electronic transitions in a subsystem formulation of time-dependent density functional theory. *J. Chem. Phys*, 126(13):–, 2007.
- [72] Johannes Neugebauer. On the calculation of general response properties in subsystem density functional theory. *J. Chem. Phys*, 131(8):–, 2009.
- [73] Michele Pavanello. On the subsystem formulation of linear-response time-dependent dft. *J. Chem. Phys*, 138(20):204118–204118–8, 2013.
- [74] Martín A. Mosquera, Daniel Jensen, and Adam Wasserman. Fragment-based time-dependent density functional theory. *Phys. Rev. Lett.*, 111(2):–, 2013.
- [75] Chen Huang, Florian Libisch, Qing Peng, and Emily A Carter. Time-dependent potential-functional embedding theory. *The Journal of chemical physics*, 140(12):124113, 2014.
- [76] Tomasz Adam Wesolowski and Jacques Weber. Kohn-sham equations with constrained electron density: an iterative evaluation of the ground-state electron density of interacting molecules. *Chem. Phys. Lett.*, 248(1-2):71–76, 1996.
- [77] Yves A. Bernard, Marcin Duak, Jakub W. Kamiski, and Tomasz A. Wesowski. The energy-differences based exact criterion for testing approximations to the functional for the kinetic energy of non-interacting electrons. *Journal of Physics A: Mathematical and Theoretical*, 41(5):–, 2008.
- [78] Marie Humbert-Droz, Xiuwen Zhou, Sapana V. Shedge, and Tomasz A. Wesolowski. How to choose the frozen density in frozen-density embedding theory-based numerical simulations of local excitations? *Theor. Chem. Acc.*, 133(1):1–20, 2014.
- [79] O. Roncero, M. P. de Lara-Castells, P. Villarreal, F. Flores, J. Ortega, M. Paniagua, and A. Aguado. An inversion technique for the calculation of embedding potentials. *J. Chem. Phys*, 129(18):–, 2008.

- [80] O. Roncero, A. Zanchet, P. Villarreal, and A. Aguado. A density-division embedding potential inversion technique. *J. Chem. Phys*, 131(23):–, 2009.
- [81] Jason D. Goodpaster, Taylor A. Barnes, and Thomas F. Miller III. Embedded density functional theory for covalently bonded and strongly interacting subsystems. *J. Chem. Phys*, 134(16):–, 2011.
- [82] Chen Huang, Michele Pavone, and Emily A. Carter. Quantum mechanical embedding theory based on a unique embedding potential. *J. Chem. Phys*, 134(15):–, 2011.
- [83] Peter Elliott, Morrel H. Cohen, Adam Wasserman, and Kieron Burke. Density functional partition theory with fractional occupations. *J. Chem. Theory Comput.*, 5(4):827–833, 2009.
- [84] Tomasz A. Wesolowski. One-electron equations for embedded electron density: Challenge for theory and practical payoffs in multi-level modelling of complex polyatomic systems. *Computational Chemistry: Reviews of Current Trends*, edited by J. Leszczynski, 10:–, 2006.
- [85] Christoph R. Jacob, S. Maya Beyhan, and Lucas Visscher. Exact functional derivative of the nonadditive kinetic-energy bifunctional in the long-distance limit. *J. Chem. Phys*, 126(23):–, 2007.
- [86] Marcin Duak and Tomasz A. Wesolowski. On the electron leak problem in orbital-free embedding calculations. *J. Chem. Phys*, 124(16):–, 2006.
- [87] Juan Maria Garcia Lastra, Jakub W. Kaminski, and Tomasz A. Wesolowski. Orbital-free effective embedding potential at nuclear cusps. *J. Chem. Phys*, 129(7):–, 2008.
- [88] Samuel Fux, Karin Kiewisch, Christoph R. Jacob, Johannes Neugebauer, and Markus Reiher. Analysis of electron density distributions from subsystem density functional theory applied to coordination bonds. *Chem. Phys. Lett.*, 461(4-6):353–359, 2008.
- [89] Qin Wu and Weitao Yang. A direct optimization method for calculating density functionals and exchange-correlation potentials from electron densities. *J. Chem. Phys*, 118(6):2498–2509, 2003.
- [90] Christoph R. Jacob. Unambiguous optimization of effective potentials in finite basis sets. *J. Chem. Phys*, 135(24):–, 2011.
- [91] Eunji Sim, Joe Larkin, Kieron Burke, and Charles W. Bock. Testing the kinetic energy functional: Kinetic energy density as a density functional. *J. Chem. Phys*, 118(18):8140–8148, 2003.
- [92] David Garcia-Aldea and JE Alvarellos. Kinetic energy density study of some representative semilocal kinetic energy functionals. *The Journal of chemical physics*, 127(14):144109, 2007.
- [93] Qin Wu, Paul W Ayers, and Yingkai Zhang. Density-based energy decomposition analysis for intermolecular interactions with variationally determined intermediate state energies. *The Journal of chemical physics*, 131(16):164112, 2009.

- [94] Andreas Savin and Tomasz A Wesolowski. Orbital-free embedding effective potential in analytically solvable cases. In *Advances in the Theory of Atomic and Molecular Systems*, pages 311–326. Springer, 2009.
- [95] Qingsheng Zhao, Robert C Morrison, and Robert G Parr. From electron densities to kohn-sham kinetic energies, orbital energies, exchange-correlation potentials, and exchange-correlation energies. *Physical Review A*, 50(3):2138, 1994.
- [96] Frank Jensen. *Introduction to computational chemistry*. John Wiley & Sons, 2013.
- [97] PRT Schipper, OV Gritsenko, and EJ Baerends. Kohn-sham potentials corresponding to slater and gaussian basis set densities. *Theoretical Chemistry Accounts*, 98(1):16–24, 1997.
- [98] Tim Heaton-Burgess, Felipe A Bulat, and Weitao Yang. Optimized effective potentials in finite basis sets. *Physical review letters*, 98(25):256401, 2007.
- [99] Aron J. Cohen, Paula Mori-Sánchez, and Weitao Yang. Fractional spins and static correlation error in density functional theory. *J. Chem. Phys*, 129:–, 2008.
- [100] Klaus Ruedenberg and Michael W. Schmidt. Why does electron sharing lead to covalent bonding? A variational analysis. *Journal of computational chemistry*, 28(1):391–410, 2007.
- [101] Klaus Ruedenberg and Michael W. Schmidt. Physical Understanding through Variational Reasoning: Electron Sharing and Covalent Bonding. *The Journal of Physical Chemistry A*, 113(10):1954–1968, 2009.
- [102] Th Bitter, K. Ruedenberg, and W. H. E. Schwarz. Toward a physical understanding of electron-sharing two-center bonds. I. General aspects. *Journal of computational chemistry*, 28(1):411–422, 2007.
- [103] T. Bitter, S. G. Wang, K. Ruedenberg, and W. H. E. Schwarz. Toward a physical understanding of electron-sharing two-center bonds. II. Pseudo-potential based analysis of diatomic molecules. *Theoretical Chemistry Accounts*, 127(3):237–257, 2010.
- [104] Patrick Huang and Emily A Carter. Self-consistent embedding theory for locally correlated configuration interaction wave functions in condensed matter. *The Journal of chemical physics*, 125(8):084102, 2006.
- [105] Walter Kohn. Density functional and density matrix method scaling linearly with the number of atoms. *Physical Review Letters*, 76(17):3168, 1996.
- [106] Morrel H Cohen, Adam Wasserman, Roberto Car, and Kieron Burke. Charge transfer in partition theory. *The Journal of Physical Chemistry A*, 113(10):2183–2192, 2009.
- [107] Weitao Yang, Yingkai Zhang, and Paul W. Ayers. Degenerate ground states and a fractional number of electrons in density and reduced density matrix functional theory. *Phys. Rev. Lett.*, 84(22):5172–5175, 2000.
- [108] Axel Dieter Becke. Numerical hartree-fock-slater calculations on diatomic molecules. *J. Chem. Phys*, 76:–, 1982.

- [109] Leif Laaksonen, Pekka Pyykkö, and Dage Sundholm. Two-dimensional fully numerical solutions of molecular schrödinger equations. i. one-electron molecules. *Int. J. Quantum Chem.*, 23(1):309–317, 1983.
- [110] Jacek Kobus, Leif Laaksonen, and Dage Sundholm. A numerical hartree-fock program for diatomic molecules. *Comput. Phys. Commun.*, 98(3):346–358, 1996.
- [111] T. Grabo, T. Kreibich, and E. K. U. Gross. Optimized effective potential for atoms and molecules. *Molecular Engineering*, 7(1-2):27–50, 1997.
- [112] Adi Makmal, Stephan Kummel, and Leeor Kronik. Fully numerical all-electron solutions of the optimized effective potential equation for diatomic molecules. *J. Chem. Theory Comput.*, 5(7):1731–1740, 2009.
- [113] Miguel AL Marques, Micael JT Oliveira, and Tobias Burnus. Libxc: a library of exchange and correlation functionals for density functional theory. *Comput. Phys. Commun.*, pages –, 2012.
- [114] Aron J. Cohen, Paula Mori-Sánchez, and Weitao Yang. Insights into current limitations of density functional theory. *Science*, 321(5890):792–794, 2008.
- [115] Paula Mori-Sánchez, Aron J. Cohen, and Weitao Yang. Localization and delocalization errors in density functional theory and implications for band-gap prediction. *Phys. Rev. Lett.*, 100(14):–, 2008.
- [116] Paula Mori-Sánchez, Aron J. Cohen, and Weitao Yang. Discontinuous nature of the exchange-correlation functional in strongly correlated systems. *Phys. Rev. Lett.*, 102(6):–, 2009.
- [117] Eli Kraisler and Leeor Kronik. Piecewise linearity of approximate density functionals revisited: Implications for frontier orbital energies. *Phys. Rev. Lett.*, 110(12):–, 2013.
- [118] Erin R. Johnson. A density functional for strong correlation in atoms. *J. Chem. Phys*, 139(7):–, 2013.
- [119] T. A. Wesolowski, Yves Ellinger, and Jacques Weber. Density functional theory with an approximate kinetic energy functional applied to study structure and stability of weak van der waals complexes. *J. Chem. Phys*, 108:–, 1998.
- [120] Jorge Morales and Todd J. Martínez. A new approach to reactive potentials with fluctuating charges: quadratic valence-bond model. *J. Phys. Chem. A*, 108(15):3076–3084, 2004.
- [121] P. a. M. Dirac. Note on exchange phenomena in the thomas atom. *Mathematical Proceedings of the Cambridge Philosophical Society*, 26(03):376–385, 1930.
- [122] John P. Perdew and Yue Wang. Accurate and simple analytic representation of the electron-gas correlation energy. *Phys. Rev. B*, 45(23):13244–13249, 1992.
- [123] Roi Baer, Ester Livshits, and Ulrike Salzner. Tuned range-separated hybrids in density functional theory. *Annu. Rev. Phys. Chem.*, 61:85–109, 2010.
- [124] L. Wolniewicz. Relativistic energies of the ground state of the hydrogen molecule. *J. Chem. Phys*, 99:–, 1993.
- [125] Marten A. Buijse, Evert Jan Baerends, and Jaap G. Snijders. Analysis of correlation in terms of exact local potentials: Applications to two-electron systems. *Phys. Rev. A*, 40(8):–, 1989.

- [126] Robert Van Leeuwen and Evert Jan Baerends. An analysis of nonlocal density functionals in chemical bonding. *Int. J. Quantum Chem.*, 52(4):711–730, 1994.
- [127] Robert Van Leeuwen, Oleg Gritsenko, and Evert Jan Baerends. Step structure in the atomic kohn-sham potential. *Zeitschrift für Physik D Atoms, Molecules and Clusters*, 33(4):229–238, 1995.
- [128] Oleg V. Gritsenko and Evert Jan Baerends. Effect of molecular dissociation on the exchange-correlation kohn-sham potential. *Phys. Rev. A*, 54(3):–, 1996.
- [129] Oleg V. Gritsenko and Evert Jan Baerends. Electron correlation effects on the shape of the kohn-sham molecular orbital. *Theor. Chem. Acc.*, 96(1):44–50, 1997.
- [130] N. Helbig, I. V. Tokatly, and A. Rubio. Exact kohn-sham potential of strongly correlated finite systems. *J. Chem. Phys.*, 131:–, 2009.
- [131] David G. Tempel, Todd J. Martinez, and Neepa T. Maitra. Revisiting molecular dissociation in density functional theory: a simple model. *J. Chem. Theory Comput.*, 5(4):770–780, 2009.
- [132] P. Elliott, J. I. Fuks, A. Rubio, and N. T. Maitra. Universal dynamical steps in the exact time-dependent exchange-correlation potential. *Phys. Rev. Lett.*, 109(26):–, 2012.
- [133] J. I. Fuks, P. Elliott, A. Rubio, and N. T. Maitra. Dynamics of charge-transfer processes with time-dependent density functional theory. *The Journal of Physical Chemistry Letters*, 4(5):735–739, 2013.

VITA

VITA

Jonathan NAFZIGER

PERSONAL DATA

PLACE AND DATE OF BIRTH: United States — 29 October 1985

ADDRESS: 215 East Pine Ave., West Lafayette, IN, USA

PHONE: +765 430 8354

EMAIL: jnafziger@gmail.com

EDUCATION

MAY 2015 PhD in PHYSICS, **Purdue University**,

Advisor: Prof. Adam WASSERMAN

GPA: 3.92/4.0

MAY 2008 Undergraduate Degree in PHYSICS, **Goshen College**,

Minor: Mathematics Advisor: John Ross BUSCHERT

Overall GPA: 3.82/4.0 GPA in Major: 3.98/4.0

RESEARCH EXPERIENCE

2010-Present **Partition Density-Functional Theory (PDFT)**,

Research with Prof. Adam Wasserman:

*PDFT is a formally exact method for breaking a molecular electronic structure calculation into a collection of fragment calculations.*2007-2008 **Acoustics of Handbells**,

Research with Prof. John Ross Buschert:

Studied the behavior of nearly degenerate modes of vibration in handbells using holographic interferometry and an anechoic chamber.

PUBLICATIONS

1. JN, Qin Wu, and Adam Wasserman. "Molecular Binding Energies from Partition Density Functional Theory." *J. Chem. Phys.* 135, no. 23 (2011): 234101-234107.
2. Rougang Tang, JN, and Adam Wasserman. "Fragment Occupations in Partition Density Functional Theory." *Phys. Chem. Chem. Phys.* 14, no. 21 (2012): 7780-7786.
3. JN, and Adam Wasserman. "Delocalization and Static Correlation in Partition Density Functional Theory." *arXiv preprint* arXiv:1305.4966 (2013)
4. JN, and Adam Wasserman. "Density-based partitioning methods for ground-state molecular calculations." *J. Phys. Chem. A* 118.36 (2014): 7623-7639.

PRESENTATIONS

- Molecular Binding Energies from Partition Density-Functional Theory
 - Poster at 2011 CECAM conference on Density-Functional Theory in Dublin, Ireland. (Received MCC travel award to attend.)
- Finding Partition Potentials.
 - Talk at the 2012 March Meeting of the APS in Boston.
- Weakness of the F₂ Bond: A Perspective from PDFT
 - Poster at the 44th Midwest Theoretical Chemistry Conference at the University of Wisconsin-Madison
- Delocalization and Static Correlation in PDFT.
 - Talk at the 2013 Computational Science and Engineering Student Conference at Purdue.
 - Talk at the 45th Midwest Theoretical Chemistry Conference at the Urbana-Champaign campus of University of Illinois
 - Poster at the 2013 Gordon Research Conference on Time-Dependent Density-Functional Theory in Biddeford, Maine
 - Talk at the 246th National Meeting of the ACS in Indianapolis
 - Poster at the 2014 School and Workshop on Time-Dependent Density-Functional Theory in Benasque, Spain (Received MCC travel award to attend)
- Ensemble treatment of fragments within a molecule.
 - Talk at the 2014 March Meeting of the APS in Denver.

- Partition Density-Functional Theory: Uniqueness and Ensembles
 - Invited talk at the 2014 CECAM conference on “Density-based embedding for multiscale simulations” in Lausanne, Switzerland
- Benchmark Partition Density Functional Theory Calculations for Diatomic Molecules
 - Poster at the 2014 Midwest Theoretical Chemistry Conference at Northwestern University (Received Outstanding Poster Award)
- Introduction to Partition Density-Functional Theory
 - Talk for the Purdue Physics Graduate Student Seminar Series 2014
 - Invited talk at the Physics Department Colloquium of Universidad de Antioquia, Medellín, Colombia, 2015

TEACHING EXPERIENCE

- Adjunct Professor at Goshen College (2013)
 - Taught a semester of Analytical Mechanics
- Teaching assistant at Purdue University (2009-2010)
 - Recitation for Phys 241: Electricity and Magnetism
 - Lab for Phys 221: Electricity and Magnetism
- Teaching assistant at Goshen College (2007-2008)
 - Lab for General Physics and Electronics